

**APPLICATION OF SELF ASSEMBLED  
MONOLAYER TECHNIQUE TO IMPROVE HOLE  
TRANSPORT IN ORGANIC LEDS**

**A Thesis Submitted to  
the Graduate School of Engineering and Sciences of  
İzmir Institute of Technology  
in Partial Fulfillment of the Requirements for the Degree of**

**MASTER OF SCIENCE**

**in Physics**

**by**

**Maviş ŞEKER**

**July 2011  
İZMİR**

We approve the thesis of **MaviŖe ŖEKER**

---

**Assoc. Prof. Salih OKUR**

Supervisor

---

**Assist. Prof. Enver TARHAN**

Committee Member

---

**Assist. Prof. Ŗmer MERMER**

Committee Member

05 July 2011

---

**Prof. Dr.Nejat BULUT**

Head of the Department of Physics

---

**Prof. Dr. DurmuŖ Ali DEMİR**

Dean of the Graduate School of  
Engineering and Sciences

## ACKNOWLEDGEMENTS

I would like to thank to my advisor Assoc. Prof. Salih Okur for teaching me many valuable things during the master program, for his continuous support and encouragement in the lab. His wide knowledge and logical way of thinking have been of great value for me. I cannot thank him enough. It has been an honor to work with him for me.

I would like to acknowledge Asst. Prof. Şerafettin Demić and his PhD student Mustafa Can from Ege University. Their ideals and concepts have had a remarkable influence on my understanding in the field of Chemistry. Moreover, I am also thankful to Asst. Prof. Kasım Ocakođlu for providing us Ru complexes.

Furthermore, I would like to thank also other members of my thesis defense committee Asst. Prof. Ömer Mermer, Asst. Prof. Enver Tarhan and Asst. Prof. Hadi M. Zareie for helpful comments and suggestions.

I thankfully acknowledge TUBITAK for master scholarship. This research was partially supported by TUBITAK project number 108T718.

I would like to give my special thanks to my lab mates Nesli Yađmurcukardeş, Hasan Aydın, Ali Kemal Havare, Fevzi Sümer, Cebrail Özbek, Ufuk Yücel and Evren Çulcular for their warm friendship and help.

I would like to express my sincere gratitude to each of my friends at Izmir Institute of Technology for providing a great atmosphere and a wonderful work place. We have unforgettable memories at the end of two years and now each of them is very important for me. Especially Hilal Sađlam, Fulya Türkođlu and Hasan Köseođlu have always been by my side and shared my all feelings.

Last, but most importantly, I would like to thank my precious family: my mother Sebat Şeker, my father Ahmet Şeker, my brother Tunahan Şeker and my fiance Sıtkı Yaman for their ceaseless support, motivation, love in all my life and believing in me. Whatever I say is still very much short for the love they have conferred upon me.

# ABSTRACT

## APPLICATION OF SELF ASSEMBLED MONOLAYER TECHNIQUE TO IMPROVE HOLE TRANSPORT IN ORGANIC LEDS

This thesis concentrates on the fabrication and characterization of highly efficient Organic Light-Emitting Diode (OLED) with surface modification of indium tin oxide (ITO) anodes by using self-assembled monolayer (SAM) technique. ITO has been commonly used as an anode for OLEDs, because of the combination of high optical transparency and good electrical conductivity. That is why, ITO substrate is used in this study. On the other hand, the ITO film has often a rough surface, relatively low work function compared with the adjacent organic layer and its surface energy is not well matched to nonpolar organic film. For this purpose, in this work, eleven different SAM molecules were examined to modify ITO surface. Clearly, we aim to reduce the barrier of hole injection, lower the turn-on voltage and improve charge transfer characteristic at the anode-organic film interface using SAM molecules.

The ITO work function with the SAM molecules was measured using Kelvin Probe Force Microscopy (KPFM). KPFM measurements were carried out to investigate if there is any increase in ITO work function. Atomic Force Microscopy (AFM) via semi-contact mode was examined the surface morphology of modified ITO. The transmittances of the ITOs with SAM were measured using an UV spectrometer. In addition to these surface analyses, the device performances were characterized by Keithley 236 and High-Resolution Spectrometer. Moreover, Space-Charge-Limited Current (SCLC) and Schottky models were used to analyze the I-V characteristics to calculate hole mobility and barrier heights, respectively.

## ÖZET

### ORGANİK LED'LERDE DEŞİK İLETİMİNİ ARTIRMAYA YÖNELİK ORGANİZE TEK KATMAN TEKNİĞİNİN UYGULANMASI

Bu tez, kendiliğinden organize tek katman kaplama tekniğı (KOT) kullanılarak, indiyum kalay oksit (ITO) anot yüzey modifikasyonu ile yüksek verimli organik ışık yayan diyot (OLED) üretimi ve karakterizasyonu üzerine yoğunlaşmaktadır. ITO, yüksek optik geçirgenlik ve iyi elektriksel iletkenlik kombinasyonundan dolayı OLED'lerde anot olarak yaygın kullanılır. Bu nedenle, bu çalışmada ITO alttaş kullanılmıştır. Öte yandan, ITO filmi genellikle pürüzlü bir yüzey, bitişik organik katman ile karşılaştırıldığında nispeten düşük çalışma fonksiyonlu ve yüzey enerjisinde apolar organik filmle uyumlu değildir. Bu amaçla, bu çalışmada on bir farklı SAM molekülü ITO yüzeyini modifiye etmek için incelenmiştir. Açıkça, SAM moleküllerini kullanarak deşik iletim bariyerini azaltmayı, çalışma potansiyelini düşürmeyi ve anot-organik film arayüzünde yük transfer karakteristiğini geliştirmeyi hedefledik.

SAM molekülleri ile ITO çalışma fonksiyonu Kelvin Probe Kuvvet Mikroskobu (KPFM) kullanılarak ölçülmüştür. KPFM ölçümleri ITO çalışma fonksiyonunda herhangi bir artış olup olmadığını araştırmak için yapılmıştır. Atomik Kuvvet Mikroskobu (AKM) yarı-kontakt modu ile modifiye edilmiş ITO yüzey morfolojisi incelenmiştir. SAM'li ITO'ların transmittansları UV spektrometre kullanılarak ölçülmüştür. Bu yüzey analizlerinin yanı sıra, cihaz performansları Keithley 236 ve yüksek çözünürlüklü spektrometre ile karakterize edilmiştir. Ayrıca, Space-Charge-Limited Current (SCLC) ve Schottky modelleri I-V datalarını analiz ederek, mobility ve bariyer hesapları için kullanılmıştır.

*To my Lovely Family*

# TABLE OF CONTENTS

LIST OF FIGURES .....	x
LIST OF TABLES .....	xiv
CHAPTER 1. INTRODUCTION .....	1
1.1. Introduction to Organic Light-Emitting Diodes .....	1
1.2. Advantages of OLEDs .....	2
1.3. Background .....	3
1.4. Objectives of the Dissertation .....	5
1.5. Dissertation Organization .....	6
CHAPTER 2. ORGANIC SEMICONDUCTORS AND ORGANIC LIGHT- EMITTING DIODES .....	7
2.1. Organic Semiconductors .....	7
2.1.1. Atomic Orbitals .....	8
2.1.2. Chemical Bonds .....	9
2.1.3. Molecular Energy Levels and Energy Bands .....	10
2.1.4. Charge Transport Mechanism in Organic Semiconductor .....	12
2.2. Organic Light-Emitting Diodes: Structure and Operation .....	13
2.2.1. Basic Cell Configuration .....	13
2.2.2. Materials .....	14
2.2.2.1. Anode Material .....	14
2.2.2.2. Cathode Material .....	15
2.2.2.3. Organic Layers (Small Molecules) .....	15
2.2.3. OLED Fabrication Procedure .....	17
2.2.3.1. Vacuum Thermal Evaporation System .....	17
2.2.3.2. Spin-Coating System .....	18
2.2.4. Principle of Operation of OLEDs .....	19
2.2.5. Charge Transport Phenomenon in OLEDs .....	21
2.2.5.1. Charge Injection .....	21
2.2.5.2. Charge Transport .....	24

2.2.5.3. Hole-Electron Recombination and Exciton Formation .....	25
2.2.5.4. Light Emission .....	27
2.2.6. Device Efficiency .....	27
2.2.6.1. Quantum Efficiency .....	28
2.2.6.2. Power Efficiency .....	29
2.2.6.3. Luminous Efficiency .....	29
CHAPTER 3. SELF-ASSEMBLED MONOLAYER .....	30
3.1. Introduction to Self-assembled Monolayer .....	31
3.2. Formation and Utilization of SAMs .....	33
3.3. Parameters Affecting on SAM Formation .....	34
3.4. SAM-HTL .....	37
3.5. Application of SAMs .....	38
3.6. Characterization Techniques of SAMs .....	39
CHAPTER 4. EXPERIMENTAL DETAILS .....	40
4.1. Device Fabrication .....	40
4.1.1. Etching of ITO Substrates .....	40
4.1.2. Cleaning Procedure of ITO Substrates .....	42
4.1.3. Oxygen Plasma Treatment .....	43
4.1.4. SAM Formation .....	44
4.1.5. Organic Layer and Cathode Deposition .....	48
4.2. Device Characterization Techniques .....	51
4.2.1. Electrical Characterization .....	51
4.2.2. Optical Characterization .....	53
4.2.3. Surface Characterization .....	54
CHAPTER 5. RESULTS AND DISCUSSION .....	57
5.1. Optical Characterization Results .....	57
5.2. Surface Characterization Results .....	58
5.2.1. Atomic Force Microscopy Results .....	58
5.2.2. Kelvin Probe Force Microscopy Results .....	66
5.3. Electrical Characterization Results .....	71



5.3.1. Space Charge Limited Current Results.....	71
5.3.2. Schottky Thermal Injection Results .....	80
5.3.3. Current-Voltage and Electroluminescence Characteristics .....	86
CHAPTER 6. CONCLUSION .....	93
REFERENCES .....	101

# LIST OF FIGURES

<b>Figure</b>	<b>Page</b>
Figure 1.1. Basic OLED device structure .....	2
Figure 1.2. Qualitative comparison of displays .....	3
Figure 1.3. Prototype Electroluminescent cell proposed by Tang and Van Slyke.....	4
Figure 1.4. OLED progress over the last three decades .....	5
Figure 2.1. Illustration of the hybrid orbitals for carbon atom.....	9
Figure 2.2. Schematic representation of $\sigma$ and $\pi$ bond in organic materials .....	9
Figure 2.3. Illustration of bond energy diagram and creation of lower energy $\pi$ bonding orbital. ....	11
Figure 2.4. Schematic of charge transport by hopping. ....	12
Figure 2.5. Simplest OLED device construction. ....	13
Figure 2.6. Chemical structures of TPD, NPB and Alq3.....	17
Figure 2.7. Schematic of Vacuum Thermal Evaporator for small molecules.....	18
Figure 2.8. Schematic illustration of spin-coating system. ....	19
Figure 2.9. a)OLED device structure under applied bias b) Simplified energy band diagram representing the basic steps of EL; (1) charge carrier injection (2) charge carrier transport (3) exciton formation and (4) radiative decay.....	19
Figure 2.10. a)Schottky type carrier injection at metal-organic interface.b)Fowler-Nordheim tunneling carrier injection under the influence of a local high electric field.....	23
Figure 2.11. Diagram for possible singlet and triplet exciton formation .....	26
Figure 3.1. An array of molecules self-assembled on a flat substrate surface .....	32
Figure 3.2. Formation of SAM by immersing a substrate in appropriate solution .....	33
Figure 3.3. Shematic illustration of the SAMs of surfactant molecules on substrate ...	34
Figure 3.4. Schematic illustration of the formation of SAMs of surfactant molecules on a solid surface with its principle components of time.....	36
Figure 4.1. The etching process on ITO coated glasses.....	41
Figure 4.2. Picture of etched ITO.....	41
Figure 4.3. Cleaning procedure of etched ITO.....	42
Figure 4.4. Schematic of oxygen plasma treatment mechanism.....	43
Figure 4.5. The schematic representation of ITO surface after oxygen plasma.....	44

Figure 4.6. The picture of oxygen plasma cleaning in our thermal evaporation system.....	44
Figure 4.7. Preparation procedure for self-assembled monolayer .....	47
Figure 4.8. The picture of organic solvents (SAM solvents).....	48
Figure 4.9. Picture of our thermal evaporation system for organic molecules .....	49
Figure 4.10. Picture of our thermal evaporation system for metals .....	49
Figure 4.11. Thermal evaporation of material by joule heating from applying bias to a)heating coil or b) source boat.....	50
Figure 4.12. Mask pattern used for aluminum evaporation .....	50
Figure 4.13. The final measurement configuration of OLED.....	51
Figure 4.14. The experimental setup of I-V characterizaiton and spectrometer.....	52
Figure 4.15. I-V program created with LabView <sup>TM</sup> .....	52
Figure 4.16. UV/VIS/NIR Spectrometer.....	53
Figure 4.17. The program of EL spectrum.....	54
Figure 4.18. Representation of the basic principle of AFM.....	55
Figure 4.19. The picture of our AFM system.....	55
Figure 5.1. UV-VIS spectra result of non-treated ITO and ITO with various SAM ..	57
Figure 5.2. Surface topography image of a) bare ITO, b) ITO/NPB, c) ITO/K-27, d)ITO/K-27/NPB, e) ITO/K-28, f) ITO/K-28/NPB, g) ITO/K-30 and h)ITO/K-30/NPB surface with 2 $\mu\text{m}$ $\times$ 2 $\mu\text{m}$ scan area .....	59
Figure 5.3. Surface topography image of a) bare ITO, b) ITO/MHDA and c) ITO/MDA surface with 2 $\mu\text{m}$ $\times$ 2 $\mu\text{m}$ scan area.....	60
Figure 5.4. Surface topography image of a) bare ITO, b) ITO/DDA and c) ITO/TDA surface with 2 $\mu\text{m}$ $\times$ 2 $\mu\text{m}$ scan area .....	61
Figure 5.5. Surface topography image of a) bare ITO, b) ITO/NPB, c) ITO/ODA-HCl-ETOH, d) ITO/ODA-HCl-ETOH/NPB, e) ITO/ODA-HCl-MEOH, f) ITO/ODA-HCl-MEOH/NPB, g) ITO/TDA-1 and h) ITO/TDA-1/NPB, i) ITO/ODT-Cl-Si and j) ITO/ODT-Cl-Si/NPB surface with 2 $\mu\text{m}$ $\times$ 2 $\mu\text{m}$ scan area .....	62
Figure 5.6. The local contact potential difference of bare ITO and SAM modified ITO a) K-27, b) K-28 and c) K-30.....	67
Figure 5.7. The local contact potential difference of bare ITO and SAM modified ITO a) MHDA and b) MDA.....	67
Figure 5.8. The local contact potential difference of bare ITO and SAM modified ITO a) DDA and b)TDA .....	68
Figure 5.9. The local contact potential difference of bare ITO and SAM modified ITO a) ODA-HCl-ETOH , b) ODA-HCl-MEOH, c) TDA-1 and d) ODT-Cl-Si .....	68

Figure 5.10. Current density vs voltage (J-V) characteristics for the devices: ITO/K-27/NPB/Al, ITO/K-28/NPB/Al, ITO/K-30/NPB/Al and ITO/NPB/Al .....	73
Figure 5.11. Current density vs voltage (J-V) characteristics for diodes with the configuration of: ITO/MDA/NPB/Al, ITO/MHDA/NPB/Al and ITO/NPB/Al .....	74
Figure 5.12. Current density vs voltage (J-V) characteristics for diodes with the configuration of: ITO/DDA/NPB/Al, ITO/TDA/NPB/Al and ITO/NPB/Al .....	74
Figure 5.13. Current density vs voltage (J-V) characteristics for the devices: ITO/ODA-HCl-ETOH/NPB/Al, ITO/ODA-HCl-MEOH/NPB/Al, ITO/ODT-Cl-Si/NPB/Al, ITO/TDA-1/NPB/Al and ITO/NPB/Al .....	75
Figure 5.14. The logarithm of $J/E^2$ versus the square root of the applied electric field for ITO/K-27/NPB/Al, ITO/K-28/NPB/Al, ITO/K-30/NPB/Al and ITO/NPB/Al diodes .....	75
Figure 5.15. The logarithm of $J/E^2$ versus the square root of the applied electric field for ITO/MDA/NPB/Al, ITO/MHDA/NPB/Al and ITO/NPB/Al diodes .....	76
Figure 5.16. The logarithm of $J/E^2$ versus the square root of the applied electric field for ITO/DDA/NPB/Al, ITO/TDA/NPB/Al and ITO/NPB/Al diodes .....	76
Figure 5.17. The logarithm of $J/E^2$ versus the square root of the applied electric field for ITO/TDA-1/NPB/Al, ITO/ODA-HCl-ETOH/NPB/Al, ITO/ODA-HCl-MEOH/NPB/Al, ITO/ODT-Cl-Si/NPB/Al and ITO/NPB/Al diodes .....	77
Figure 5.18. The carrier mobility $\mu$ of ITO/K-27/NPB/Al, ITO/K-28/NPB/Al, ITO/K-30/NPB/Al and ITO/NPB/Al diodes with varying electric field.....	78
Figure 5.19. The carrier mobility $\mu$ of ITO/MDA/NPB/Al, ITO/MHDA/NPB/Al and ITO/NPB/Al diodes with varying electric field .....	78
Figure 5.20. The carrier mobility $\mu$ of ITO/DDA/NPB/Al, ITO/TDA/NPB/Al and ITO/NPB/Al diodes with varying electric field.....	79
Figure 5.21. The carrier mobility $\mu$ of ITO/ODA-HCl-ETOH/NPB/Al, ITO/ODA-HCl-MEOH/NPB/Al, ITO/TDA-1/NPB/Al, ITO/ODT-Cl-Si/NPB/Al and ITO/NPB/Al diodes with varying electric field.....	79
Figure 5.22. I-V characteristics of the ITO/K-27/NPB/Al, ITO/K-28/NPB/Al, ITO/K-30/NPB/Al, ITO/NPB/Al and ITO/Al Schottky diodes .....	81
Figure 5.23. I-V characteristics of the ITO/MDA/NPB/Al, ITO/MHDA/NPB/Al, ITO/NPB/Al and ITO/Al Schottky diodes .....	82

Figure 5.24. I-V characteristics of the ITO/DDA/NPB/Al, ITO/TDA/NPB/Al, ITO/NPB/Al and ITO/Al Schottky diodes .....	82
Figure 5.25. I-V characteristics of the ITO/ODA-HCl-ETOH/NPB/Al, ITO/ODA-HCl-MEOH/NPB/Al, ITO/TDA-1/NPB/Al, ITO/ODT-Cl-Si/NPB/Al, ITO/NPB/Al and ITO/Al Schottky diodes .....	83
Figure 5.26. I-V characteristics for the OLED devices: ITO/K-27/NPB/Alq <sub>3</sub> /Al, ITO/K-28/NPB/Alq <sub>3</sub> /Al, ITO/K-30/NPB/Alq <sub>3</sub> /Al and ITO/NPB/Alq <sub>3</sub> /Al .....	86
Figure 5.27. I-V characteristics for the OLED devices: ITO/MDA/NPB/Alq <sub>3</sub> /Al, ITO/MHDA/NPB/Alq <sub>3</sub> /Al and ITO/NPB/Alq <sub>3</sub> /Al.....	87
Figure 5.28. I-V characteristics for the OLED devices: ITO/DDA/NPB/Alq <sub>3</sub> /Al, ITO/TDA/NPB/Alq <sub>3</sub> /Al and ITO/NPB/Alq <sub>3</sub> /Al.....	87
Figure 5.29. I-V characteristics for the OLED devices: ITO/ODA-HCl-ETOH/NPB/Alq <sub>3</sub> /Al, ITO/ODA-HCl-MEOH/NPB/Alq <sub>3</sub> /Al, ITO/TDA-1/NPB/Alq <sub>3</sub> /Al, ITO/ODT-Cl-Si/NPB/Alq <sub>3</sub> /Al and ITO/NPB/Alq <sub>3</sub> /Al .....	88
Figure 5.30. EL spectrum of the ITO/SAM (K-27, K-28 and K-30) modified or unmodified/NPB/Alq <sub>3</sub> /Al OLED devices .....	90
Figure 5.31. EL spectrum of the ITO/SAM (MDA and MHDA) modified or unmodified/NPB/Alq <sub>3</sub> /Al OLED devices .....	90
Figure 5.32. EL spectrum of the ITO/SAM (DDA and TDA) modified or unmodified/NPB/Alq <sub>3</sub> /Al OLED devices .....	91
Figure 5.33. EL spectrum of the ITO/SAM (ODA-HCl-ETOH, ODA-HCl-MEOH, TDA-1 and ODT-Cl-Si) modified or unmodified/NPB/Alq <sub>3</sub> /Al OLED devices .....	91
Figure 5.34. Pictures of green OLEDs in operation under the same voltages: a) ITO/NPB/Alq <sub>3</sub> /Al and b) ITO/ODT-Cl-Si/NPB/Alq <sub>3</sub> /Al .....	92

## LIST OF TABLES

<b><u>Table</u></b>	<b><u>Page</u></b>
Table 4.1. Organics of SAM used in the experiments with chemical structures and the preparation conditions.....	45
Table 5.1. Roughness values of bare ITO, ITO/K-27, ITO/K-28, ITO/K-30, ITO/NPB, ITO/K-27/NPB, ITO/K-28/NPB and ITO/K-30/NPB .....	64
Table 5.2. Roughness values of bare ITO, ITO/MHDA and ITO/MDA.....	64
Table 5.3. Roughness values of bare ITO, ITO/DDA and ITO/TDA .....	65
Table 5.4. Roughness values of bare ITO, ITO/ODA-HCl-ETOH, ITO/ODA-HCl-MEOH, ITO/TDA-1, ITO/ODT-Cl-Si, ITO/NPB, ITO/ODA-HCl-ETOH/NPB, ITO/ODA-HCl-MEOH/NPB, ITO/TDA-1/NPB and ITO/ODT-Cl-Si/NPB .....	65
Table 5.5. The measured surface potentials of bare ITO and K-27, K-28 and K-30 modified ITOs .....	69
Table 5.6. The measured surface potentials of bare ITO and MHDA and MDA modified ITOs .....	69
Table 5.7. The measured surface potentials of bare ITO and DDA and TDA modified ITOs .....	70
Table 5.8. The measured surface potentials of bare ITO and ODA-HCl-ETOH, ODA-HCl-MEOH, TDA-1 and ODT-Cl-Si modified ITOs.....	70
Table 5.9. Barrier height values of the ITO/K-27/NPB/Al, ITO/K-28/NPB/Al, ITO/K-30/NPB/Al and ITO/NPB/Al Schottky diodes.....	84
Table 5.10. Barrier height values of the ITO/MDA/NPB/Al, ITO/MHDA/NPB/Al and ITO/NPB/Al Schottky diodes .....	84
Table 5.11. Barrier height values of the ITO/DDA/NPB/Al, ITO/TDA/NPB/Al and ITO/NPB/Al Schottky diodes.....	84
Table 5.12. Barrier height values of the ITO/ODA-HCl-ETOH/NPB/Al, ITO/ODA-HCl-MEOH/NPB/Al, ITO/TDA-1/NPB/Al, ITO/ODT-Cl-Si/NPB/Al and ITO/NPB/Al Schottky diodes .....	85
Table 5.13. Summary of electrical characterization results of first group with Ru complex .....	94
Table 5.14. Summary of electrical characterization results of second group .....	95
Table 5.15. Summary of electrical characterization results of third group.....	96
Table 5.16. Summary of electrical characterization results of fourth group .....	97

# CHAPTER 1

## INTRODUCTION

### 1.1. Introduction to Organic Light-Emitting Diodes

Organic light-emitting devices (OLEDs) have been one of the most interesting and attractive research community which include synthetic and physical chemistry, device physics and electrical engineering constitute targeting flat panel displays and solid-state lighting applications around the world. Over the last two decades, much research focused on OLEDs which promise the properties of being self emitting, consuming low power, having broader viewing angle and faster switching speed. The subject transformation of electricity into light is attractive for various scientific disciplines and brought to wide public attention (Wong, 2009). Conversely, even using organic materials for light emitting devices entered the markets, continuing challenges in improving the efficiency and long-term degradation process of OLEDs remain. These are essentially contingent upon to the dynamics of the basic electroluminescence (EL) process in these materials and devices, namely charge transfer excitons formation and relaxation process. The full understanding of the dynamics of EL process and charge carrier of organic materials will supply a solid base for the future optimization of the OLEDs features and performance.

OLED structure consists of a thin film of an organic compound layers sandwiched between two electrodes. Anode in most cases is transparent. The basic working principle can be explained as following: By applying an appropriate bias to the electrodes, charges get injected into the organic material where they form excited states that recombine and result in light emission as shown in Figure 1.1. In chapter 2, a basic structure of OLED as well as discussion of its principle and charge transport phenomenon is given in detail.

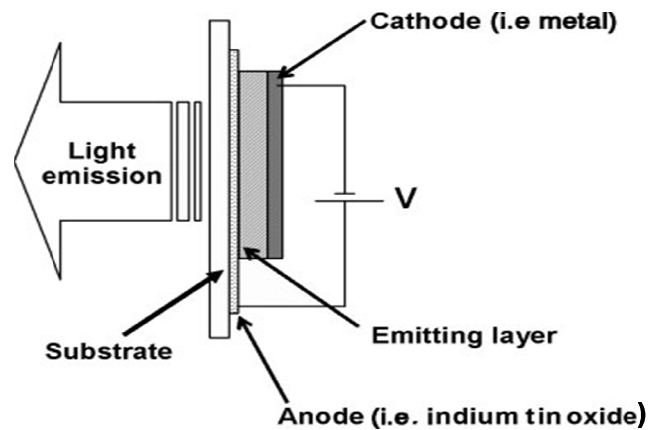


Figure 1.1. Basic OLED device structure  
 (Source: (Geffroy et al., 2006))

## 1.2. Advantages of OLEDs

Over the last decade, many flat panel displays such as liquid crystal display (LCD), plasma display panel (PDP) and organic light emitting diode display (OLED) etc. has been developed and studied intensively. OLED displays have become commercially available in portable small electronic applications such as mobile phones, digital cameras, car radios, PDAs, GPS devices, some laptop cameras, MP3 players, TVs, keyboards, watches, low-coast organic lasers and so on with limited size for nine years.

OLEDs have many advantages over other display technologies such as low operating voltages down to 3-5 V, very wide dynamic range, current-driven devices, tuning color of light emission, depositing on any substrates, low coast, easy fabrication and self-luminous (Bardsley, 2004). Also, they are used as pixels in a flat panel displays and available commercially. Enormous energy saving is the most important impact of OLEDs. Moreover, it is possible to create new architectural designs such as ceiling panel, contour lighting etc. The qualitative comparison of some of panel displays is summarized in Figure 1.5.



Performance	CRT	PDP	LCD	OLED
High resolution	○	●	☺	☺
Luminescence	☺	●	●	☺
Bright condition	☺	●	☺	○
Dark condition	○	☺	○	☺
Viewing angle	○	○	○	☺
Power consumption	●	○	○	○
Weight	●	○	☺	☺☺
Thickness	●	○	☺	☺☺

☺☺ Excellent    ☺ Very Good    ○ Acceptable    ● Poor

CRT= cathode ray tube; PDP= plasma display panel;  
 LCD= liquid crystal display; OLED= organic light emitting diode display

Figure 1.2. Qualitative comparison of displays  
 (Source: (Godlewski and Obarowska, 2007))

This qualitative comparison shows that the OLEDs will have a number of advantages over the other panel displays. That means the OLEDs may soon capture and dominate the lighting market. According to the latest studies, the full-colour flat panel displays based on OLEDs achieved better optical properties than the others (Godlewski and Obarowska, 2007).

### 1.3. Background

OLEDs are energy conversion devices (electricity-to-light), which are based on electroluminescence phenomenon, which has been an attractive subject since 1950's because of their potentially high quantum efficiency of luminescence and the ability to generate a wide variety of colors. The first organic electroluminescence (EL) cells were studied and observed by applying high-voltage alternating current (AC) field to crystalline thin films of acridine orange and quinacrine in 1953 by Bernanose et al. (Bernanose et al., 1953). In the early 1960's, researchers worked on single crystals of anthracene and discovered electroluminescence in a direct current (DC) mode with very high bias from an organic molecule (Pope et al., 1963). In 1967, AC EL was attained using an emissive polymer (Hartman and Armstrong, 1967). Subsequently, Heeger, MacDiarmid, and Shirakawa's research leads to development of the conductive organic

polymers for which they shared the 2000 Noble Prize in Chemistry (Shirakawa et al., 1977). In early attempts to develop organic EL devices, the achievements did not attract much attention because of the high operational voltages around 100 V, low light output and unstable materials. Vincett et al. observed bright blue EL an operating voltage below 30 V by using a thermally deposited thin organic film of anthracene (Vincett et al., 1982).

OLEDs with organic multilayer structures came out in 1980s. In 1986, a polythiophene thin film was inserted between indium-tin-oxide (ITO) anode and a perylene deposited film (Hayashi et al., 1986). The inserted films exhibited great enhancement on hole injection and device stability. In the late 1980's, there was a fundamental breakthrough when C. Tang and Van Slyke fabricated a novel electroluminescent device based on small molecules with promising characteristics such as a low operating voltage (<10V) with good brightness ( $1000\text{cd/m}^2$ ), respectable luminous efficiency ( $1.5\text{lm/W}$ ) and 1% external quantum efficiency at Eastman Kodak Company (VanSlyke and Tang, 1987). The double layer structure of this device consists of a hole transport layer amorphous diamine and an electron transport layer 8-hydroxyquinoline aluminum ( $\text{Alq}_3$ ) which also works as luminescent layer fabricated by vapor deposition.

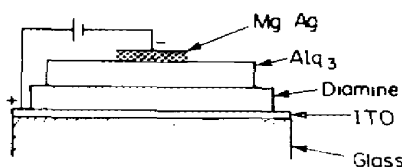


Figure 1.3. Prototype electroluminescent cell proposed by Tang and Van Slyke (Source: (VanSlyke and Tang, 1987))

In 1990, Burroughs et al. discovered OLED based on conjugated polymers which was the first of its kind where poly(p-phenylenevinylene) (PPV) was the polymer used (Burroughes et al., 1990). Moreover, the light emission was in the green-yellow spectrum and the quantum efficiency was only about 0.05%. Since then, there have been increasing interests and research activities in this field gained the momentum. Great progress has been made on the improvements of color, luminance efficiency, device stability and so on still continues. Figure 1.4 shows the developments on

efficiency of light emitting devices based on inorganic semiconductors and organic molecules since the early 1960s.

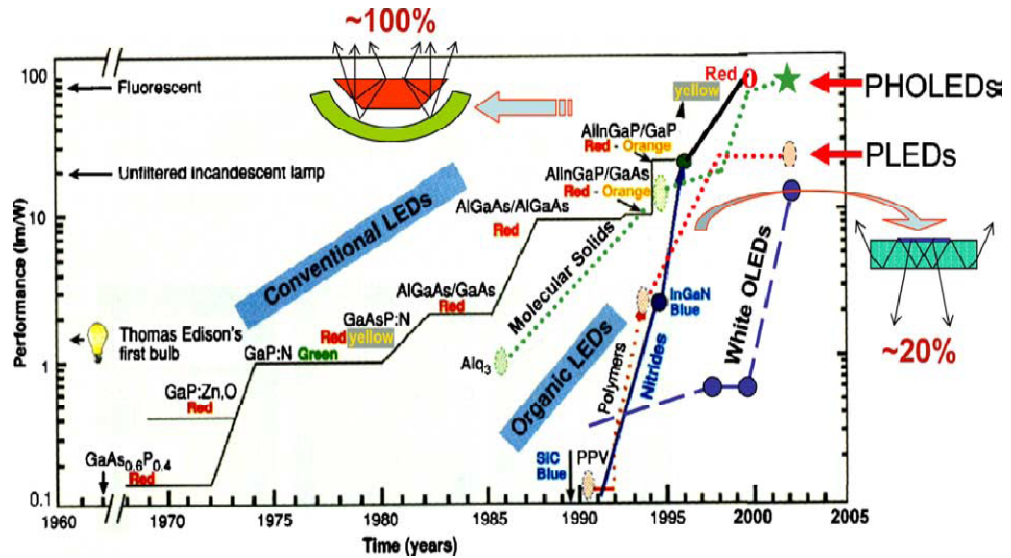


Figure 1.4. Evolution of inorganic and organic LED performance (Source: (Forrest et al., 2003))

## 1.4. Objectives of the Dissertation

The first aim of this work is to develop procedures to fabricate reproducible OLEDs. It involves tools/technology setup and development. It is necessary to understand the scientific fundamentals behind the operation. Therefore, the best beginning is fabrication of simple stable devices. Once we are able to reproduce stable light emission, we proceed to improve the performance by device optimization based on small molecules.

The second and major aim of this research is to investigate the performance of OLEDs based on ITO modified by self-assembled monolayer (SAM) technique. In recent years, OLEDs still have several problems need to be solved such as improving the brightness and luminous efficiency, lowering turn-on voltage and increasing the lifetime. However, these problems can be solved by synthesizing new materials to fabricate OLED devices with high brightness, elevated efficiency and desired color codes. Also, they can be solved by modifying the anode and the cathode of OLEDs from the standpoint of devices. Modifying the electrodes has many advantages. For

example, it does not need change any emitting material, therefore, does not change the emissive color but can improve the performance of the device remarkably (Xu et al., 2006). In this thesis, we have studied the progress in ITO anode modification of OLEDs to improve hole transport.

## **1.5. Dissertation Organization**

This thesis is organized in three main parts. Briefly, OLEDs and historical perspective of background theory and characterization methods for SAMs are discussed in Chapter 2 and Chapter 3, respectively. The experimental methods involving fabrication of OLEDs and measurement techniques are explained in Chapter 4. The main results on studied devices are presented in Chapter 5. And finally, the thesis is summarized in Chapter 6.

## CHAPTER 2

# ORGANIC SEMICONDUCTORS AND ORGANIC LIGHT-EMITTING DIODES

### 2.1. Organic Semiconductors

The organic semiconductors allows the modern field of organic electronics to grow into an almost billion dollar per year industry where conducting organic molecules are still used in variety of different applications such as organic light emitting diodes (OLEDs), organic field-effect transistors (OFETs) and photovoltaic cells. Organic electronics, in a sense plastic electronics is a branch of electronics that related to conductive organic semiconductor materials is an organic material with semiconductor properties.

Organic semiconductors were accepted as insulators with wide bandgaps and a rather low conductivity for a long time (Abkowitz et al., 1968; Shirakawa et al., 1977). Later on, mobility's of organic thin-film devices exceeding  $1 \text{ cm}^2/\text{Vs}$  have been reported, which is comparable to mobilities measured in amorphous silicon. (Haddock et al., 2005; Kelley et al., 2004). Even though organic semiconductors can be presented an amorphous structure, fewer intrinsic defects are found in a system of nonradical molecules compared to inorganic amorphous semiconductors where a large number of dangling bonds exists. Bandgaps of organic semiconductors are in the range of 1.5 to 3.5 eV. They emit light in the visible region. In addition, to exhibit any desired properties such as a specific ionization potential or a particular emission spectrum and an almost unlimited number of semiconductor materials, the organic molecules can be made suitable. Finally, we can say organic conductive materials are lighter and more tunable than inorganic materials.

The basic semiconducting properties of organic materials will be explained in the following sections.

### 2.1.1. Atomic Orbitals

To understand the charge transport mechanism in organic semiconductor, atomic orbitals and their tendency to form chemical bonds have to be reviewed.

Organic materials are composed of several atoms such as carbon, oxygen and sulfur with low atomic numbers. In an organic molecule, the bonds between the atoms are mainly covalent and are usually formed by a pair of shared electrons. If the Schrödinger equation is solved for hydrogen atom, wave functions can be identified to define the regions where one or two electrons can be found, namely the orbitals. In other words, the atomic orbitals are regions around the nucleus with a high probability of finding an electron. Electrons make contribution to atomic and molecular structure through orbitals. Moreover, each orbital is a probabilistic definition of the location of an electron appointed to that orbital. The Schrödinger equation mentioned above includes additional terms which cause slight deformations to the orbitals of the hydrogen atom for heavy atoms. Thus, orbitals in the organic compounds are often used to define chemical bonds between atoms, where the bond results from the overlap of orbitals from separate atoms. The electronic configuration of carbon atom consists of 2 electrons in core 1s level denoted as  $1s^2$  and other four electrons called valence electrons residing in 2s and 2p levels can be denoted as  $2s^2$  and  $2p^2$  which are the responsible for the formation of covalent bonds. It is clear that the carbon atom will form four bonds in an attempt to fill its shell and conserve a neutral charge on the atom (Oxtoby et al., 1998). In an effort to demonstrate electronic configuration in different compounds involving carbon, the concept of hybridized orbitals are used because the electronic configuration of the carbon atom. Hybridized orbitals are assumed to be mixtures of atomic orbital. In other words, the wave functions of the s and p atomic orbitals superpose to form a new set of equivalent hybrid orbitals. That is the reason why new set of orbitals is provided to minimize the total energy of the formed compound. Three kinds of hybrid orbitals are possible. The s and p orbitals of carbon can hybridize as  $sp^1$ ,  $sp^2$  and  $sp^3$  where the subscript denotes the number of p orbitals that are part of the superposition. The  $sp^1$ ,  $sp^2$  and  $sp^3$  hybrid orbitals for carbon atom are shown in Figure 2.1. Hybrid orbitals are shown in red below. Repulsion between pairs of electrons gives rise to these hybrid orbitals to have the maximum bond angles.

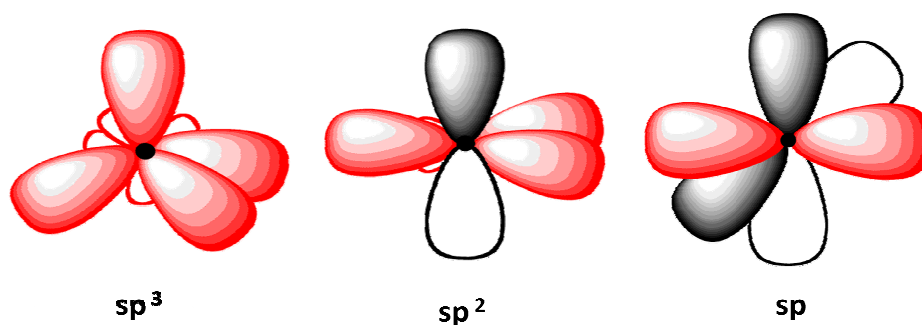


Figure 2.1. Illustration of the hybrid orbitals for carbon atom  
(Source: uvu 2011)

The larger lobe, namely the head has most of the electron density. Overlaps with an orbital of its bonding mate forms the bonds. The smaller lobe, namely tail is often omitted when depicting hybrid orbitals. On the other hand, the tail plays an important role in an organic reaction.

### 2.1.2. Chemical Bonds

When two atoms are bond through hybridized orbitals, two different types of bond exist, relying on their alignment with respect to the bonding direction as shown in Figure 2.2.

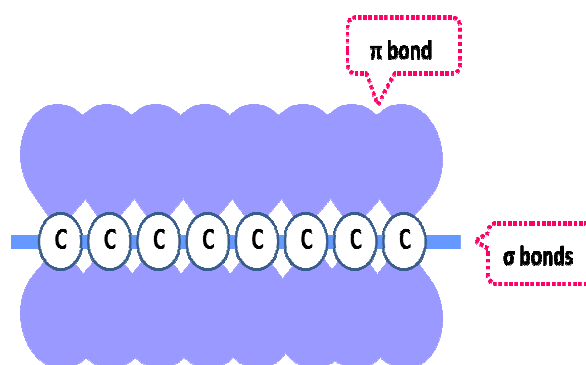


Figure 2.2. Schematic representation of  $\sigma$  and  $\pi$  bond in organic materials

For a conductive organic molecules in the film must have conjugated backbones which consists of a continuous line of alternating single and double bonded carbon atoms. This means that each carbon atom has three  $\sigma$  bonds and one  $\pi$  bond making them in  $sp^2$  configuration.

By overlapping the hybrid orbitals with  $sp^1$ ,  $sp^2$  and  $sp^3$  of two atoms, the covalent single bonds, namely sigma bonds are formed. Head to head overlap of atomic orbitals result in a sigma bonds, denoted as  $\sigma$ , are symmetrical about the axis joining the two nuclei which allows rotation of atoms along the bonding direction. Most often such rotation is hindered by existence of pi bonding, denoted as  $\pi$ . Two parallel p orbitals overlap side by side to form  $\pi$  bond. This bonding is constructed from electrons in unhybridized p orbitals and geometrically pure p orbitals are perpendicular to the axis joining two nuclei. As a consequence, when two carbon atoms are bonded through  $\sigma$  and  $\pi$  bonds, the later prevent rotation of these two atoms.

More important in organic semiconductors are the double and triple bonds, which consist of one  $\sigma$  bond and one or two  $\pi$  bonds, respectively, which occur in systems with  $sp^2$  or  $sp^1$  hybridization. It is significant to note that  $\pi$  bonds are remarkably weaker than  $\sigma$  bonds, which can be explained with a quantum mechanical perspective by the degree of overlap of the orbitals, meaning that their orbitals do not overlap to the same extent.

### **2.1.3. Molecular Energy Levels and Energy Bands**

Because of the weakness of  $\pi$  bond, the  $\pi$  electrons are effectively delocalized, they carry charges to flow through the molecule. Put in a different way, due to this formation, we have to identify wave functions that define the location of an electron on the whole molecule rather than just on an atom. This is owing to the fact that the overlap of the unhybridized p orbitals in the double bond will create a lower energy bonding orbital for the  $\pi$  electrons as depicted in Figure 2.3, known as molecular  $\pi$  bonding and antibonding orbitals.



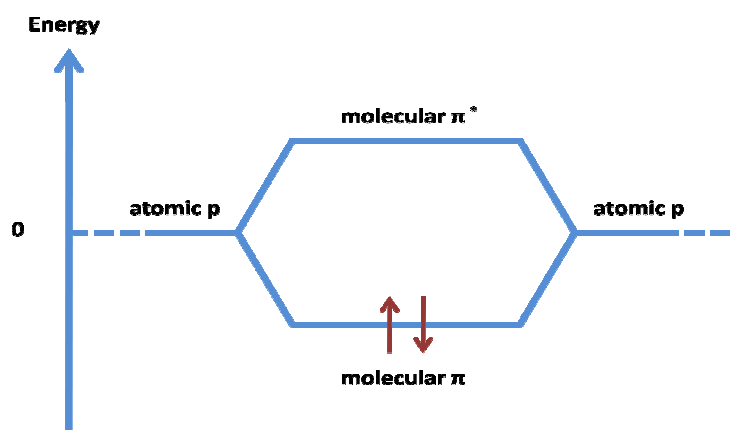


Figure 2.3. Illustration of bond energy diagram and creation of lower energy  $\pi$  bonding orbital

This backbone of molecular  $\pi$  bonding states forms a band like structure of overlapping  $\pi$  electrons. Most of these organic materials form amorphous or semi-crystalline films with lack of repeated crystalline structure found in inorganic crystals. Because of this, the  $\pi$  bonding states do not form a true band structure with allowed and forbidden states found in inorganic crystals; however, the idea of a  $\pi$  band structure can be useful approximation (Sutcu, 2010).

It should be noted that, because of several atoms and electrons, the Schrödinger equation becomes too complicated. That is why; eigenfunctions and eigenvalues of the Hamiltonian are generally approximated by neglecting certain terms in the Hamiltonian. Because of the  $\sigma$  bonds are stronger bonds than  $\pi$  bonds, removing electrons in  $\sigma$  bonds is harder than removing electrons in  $\pi$  bonds. Therefore, their contribution to the electrical current can be neglected. The wavefunction  $\Psi_{\pi}$  of a  $\pi$  molecular orbital can be identified in first approximation as linear combinations of the atomic p orbitals with wave function,  $\Phi_i$ , expressed as follows,

$$\Psi_{\pi} = \sum_{i=1}^N a_i \Phi_i \quad (2.1)$$

where  $N$  is the number of carbon atoms in the molecule and  $a_i$  are linear coefficients. The sum goes over all carbon atoms (Pope and Swenberg, 1999). Moreover,  $N$  molecular orbitals are orthogonal given the hermiticity of the Hamiltonian for  $N$  carbon

atoms. In the ground state of the molecule, when two electrons are placed in the same orbital, their spins must be paired which is also known as Pauli's exclusion principle (Pauli, 1947). The filled level actually occupied by the  $\pi$  electrons is analogous to the valence band and is called as the Highest Occupied Molecular Orbital (HOMO) level where the antibonding  $\pi^*$  band is equivalent to the conduction band. The next higher energy contains no electron is called as the Lowest Unoccupied Molecular Orbital (LUMO). The energy level difference between HOMO and LUMO called as band gap of organic semiconductor.

#### 2.1.4. Charge Transport Mechanism in Organic Semiconductor

Unlike inorganic semiconductors, the actual mechanism for this charge transfer mechanism in organic semiconductor is known as the disorder formalism and takes place through localized hopping of charges between excited and ground state of molecules. The charge is presented as a radical ion, which is associated with a local geometry relaxation due to large energetic and positional disorder. The charges then hop from molecule to molecule at a given rate with each hopping totally independent of their previous ones. This is the key mechanism that governs electron transport in these materials by reason of the charge transfer taking place through a series of completely random hops. Therefore, mobility values in organic semiconductors are far lower than in inorganic crystals (Dimitrakopoulos and Malenfant, 2002; Kippelen and Brédas, 2009; Sutcu, 2010)

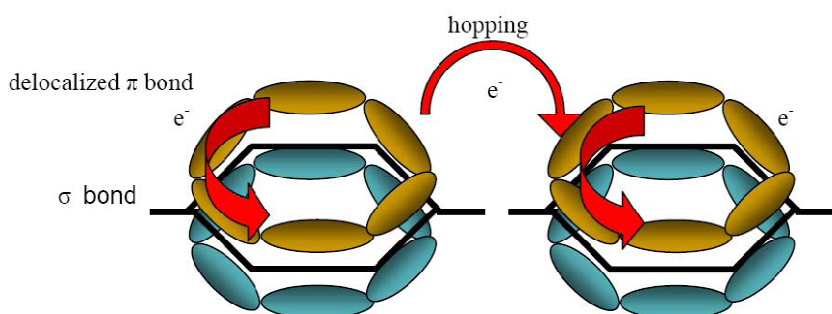


Figure 2.4. Schematic of charge transport by hopping  
(Source: (Vyavahare, 2009))

## 2.2. Organic Light-Emitting Diodes: Structure and Operation

In this part of this chapter, all of the structure and operation procedure of OLEDs including materials and mechanism will be described in details.

### 2.2.1. Basic Cell Configuration

The simplest manifestation of an OLED is extremely thin, practically two-dimensional multi-layer devices of large square area forms sandwich structure consisting of an emissive layer (EML) between two electrodes. At least one of them should be transparent to the light as given in Figure 2.5.

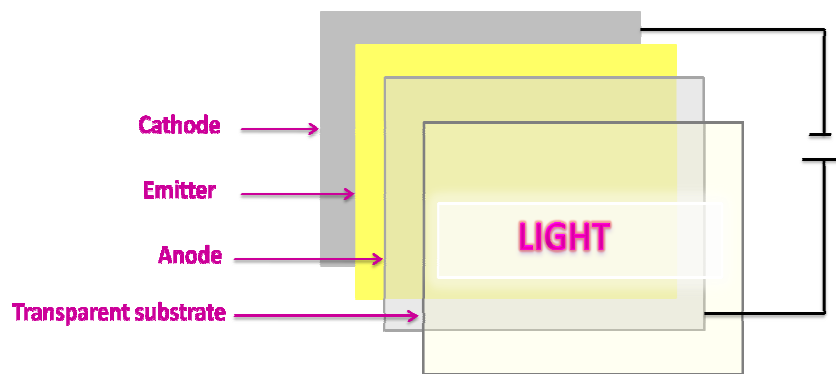


Figure 2.5. The simplest OLED device construction

The simplest device architecture for an OLED is so-called single-layer device where only one organic material is placed between the two electrodes, e.g. anode and cathode. More typical, with increased complexity, OLED structure consists of an anode, an anode buffer or hole injection layer (HIL), a hole transport layer (HTL), emissive layer (EML), an electron transport layer (ETL), electron injection layer (EIL) and a cathode. Furthermore, in some devices, hole blocking layer (HBL), electron blocking layer (EBL), and stabilizer layer can be used to reach the desired performance with increasing charge transfer from metallic anode to organic buffers. They are used to balance the injections of holes and electrons from the electrodes. For instance, for very high efficiencies, more complex multilayer structures up to six different layers have been used (He et al., 2004).

## 2.2.2. Materials

In OLED, interface between two layers supplies an efficient site to increase charge transfer for the recombination of the injected hole-electron pair and resultant electroluminescence. Put it in a different way, the most important phenomenon of the probability for the recombination of electrons and holes is affected by the amount of carriers, the balance between the numbers of two carriers and the mobility's of carriers. As a matter of fact, it relies upon the all criteria cited above for the material used in OLED structure. For this reason, the intrinsic properties of material should be taken care for a cell design.

For high luminescence efficiency (photoluminescence (PL), EL), adequate conductivity, good oxidative stability (water, oxygen), good radical cation/anion stability, good temperature stability ( $T_g$ ), coatability (thin, uniform films with no pinhole defects or impurities), not degrade during sublimation, no catastrophic film crystallization, color saturation/purity, narrow spectra and correct CIE coordinates are the general requirements for OLED materials.

OLED devices should contain substrate materials, electrodes and functional organic substances with environmentally safe. This part covers common OLED materials for all of these layers.

### 2.2.2.1. Anode Material

Anode material must be highly conductive in an attempt to reduce contact resistance and have high work function (WF) ( $\phi > 4.1$  eV) to promote efficient hole injection. In addition, it should have good stability for both thermal, chemical and high transparency to visible light, or else highly reflective if it is used as top emitting OLEDs. Moreover, it has to be good film forming and wetting properties of applied organic materials in order to ensure good contact with these adjacent organic layers. Indium tin oxide ( $\text{In}_2\text{O}_3\text{-SnO}_2$ : ITO) is composed of indium oxide ( $\text{In}_2\text{O}_3$ ) and a small amount of tin oxide ( $\text{SnO}_2$ ) (~10 wt%) (Sberveglieri et al., 1990; Wu et al., 1997). It has been the most widely and typically employed as the anode contact because of their high transparency over the visible region (80-90% integrated transmission), electrical conductivity ( $<80 \Omega^{-1}$ ) and relatively high work function (4-5 eV) (Ishii et al., 1999).

Also, it should have excellent adhesion to the substrates and easy patterning ability. The surface of the ITO electrode has an important effect on the efficiency of charge injection and the LED lifetime (Kim et al., 1998). There are several methods to grow ITO thin film on various substrates such as direct current magnetron sputtering, radio frequency magnetron sputtering, thermal evaporation, chemical vapor deposition and ion beam sputtering etc. (Selamet and Tuna, 2009).

#### **2.2.2.2. Cathode Material**

Cathode material must have high conductivity, low WF to promote electron injection, good film-forming and wetting properties to ensure good contact with adjacent organic layers. Also, good stability, highly reflective or transparent if used in top-emitting OLEDs are the requirements for cathode materials. Generally, cathode materials are pure metals or metal alloys with low WF such as Al ( $\phi=4.2$  eV), LiF/Al ( $\phi=3.6-3.8$  eV), Ca/Al, Mg/Ag ( $\phi=2.90$  eV), and Ba/Al (2.60 eV). Typically, calcium or an alloy magnesium and silver are the factors affecting the durability. A low work function material is used to enhance electron injection in OLEDs, also it means metal is easily oxidized. This problem can be solved by the replacement of calcium or magnesium/silver with aluminum (Al) (Aratani et al., 1993; Kido et al., 1990). However, then the threshold voltage increases because of high work function of aluminum. Consequently, injection of electrons is not as good as calcium or magnesium/silver. It would assist with durability of EL devices if an aluminum electrode could be used in such a way that the threshold voltage is unaltered.

#### **2.2.2.3. Organic Layers (Small Molecules)**

According as to the function of a materials in an OLEDs device, organic layers consisting of small molecular material can be classified into five groups, that they are electron transport emitters, dopant emitters, electron transport and hole blocking materials, hole transport materials, and electron and hole transport emitters (Mitschke and Bäuerle, 2000). In addition, they are chiefly relying upon their ionization potentials and electron affinities.

The HTL materials are very common in small molecule based OLEDs. They serve to supply a hole-conductive (via charge hopping) pathway for positive charge carriers to migrate from the anode into the EML. Most of these materials is built from aromatic amino groups or contain these groups which are known for their high mobility as compared to other organic molecules. Aromatic amines generally have low ionization potential (IP) giving rise to the readily formable cation radicals (holes) and a small electron affinity associated with a large band gap. Among these, N,N'-(3-methylphenyl)-1,1'-biphenyl-4,4'-diamine (TPD) (Chen et al., 1997; Stolka et al., 1984) and another TPD analogue, N,N'-bis(1-naphthyl)-N,N'-diphenyl-4,4'-diamine (NPB) (Deng et al., 1999) have been widely used and studied as effective organic materials for HTL in OLED applications. Moreover, they have modestly high hole drift mobility and are initially improved as charge transport layers in xerography. However, both of these materials are not thermally stable, the Tg's are below 100<sup>0</sup>C. In addition, TPD is not morphologically stable either, tending to crystallize easily.

Materials with electron accepting properties serve in OLEDs by ETL perhaps which is the most widely investigated layer in OLED. Analogous to HTL, ETL plays an important role of facilitating electron injection from the cathode, accepting electrons and transporting injected electrons to the emitting layer. That is, ideally transporting the electrons via a hopping mechanism involving transitory production of anion radicals of the molecules involved. The best-known and the most prevalent electron transport emitter, Tris-(8-hydroxyquinoline) aluminum (Alq<sub>3</sub>) synthesized for the first time in 1955 by Freeman and White (Freeman Jr and White, 1956), which effectively transports electrons and emits in the green is most often used small molecule in organic devices (Chen et al., 1997). Alq<sub>3</sub> was the first emission and electron transport material investigated by the Kodak group in their pioneering papers, and, so far, it is still one of the best electron transport materials, emission materials and host materials. Because of the hole mobility in HTL is much higher compared to the electron mobility in ETL, which make the ETL, Alq<sub>3</sub>, also acting as the emitter layer.

The common structures of small molecules that used in OLEDs applications are depicted in Figure 2.6.

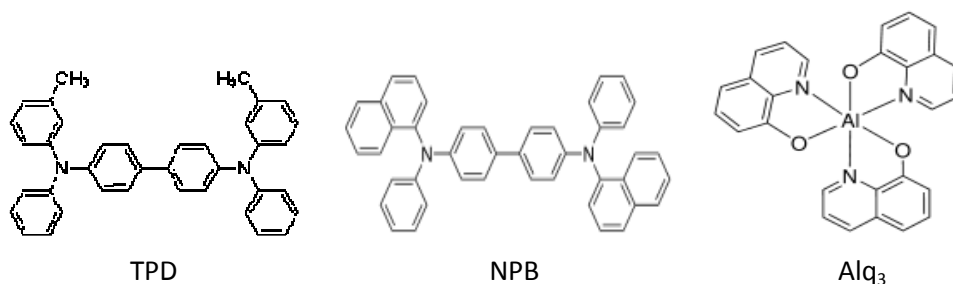


Figure 2.6. The chemical structures of TPD, NPB and Alq<sub>3</sub>

### 2.2.3. OLED Fabrication Procedure

There are two major fabrication techniques for OLEDs. They can be classified as wet and dry techniques. Dry coating techniques such as vacuum thermal evaporation and organic vapor phase deposition have been generally used for organic layers in small molecular OLEDs. However, wet coating techniques such as spin-coating, ink jet printing and contact stamping have been used for the polymer layers in polymer light-emitting diodes (PLEDs).

The following section describes the spin coating system and the vacuum thermal evaporation system which are the most commonly used in fabricating OLEDs in detail:

#### 2.2.3.1. Vacuum Thermal Evaporation System

Vacuum thermal evaporation system is the simplest deposition technique to evaporate a solid material (pure metal, eutectic or compound) by heating it to sufficiently high temperatures and recondensing it onto a cooler substrate to form a thin film. This process is usually performed in a vacuum of  $10^{-6}$  torr or better (Bröms et al., 1995), thus, the evaporated material undergoes any collisions along its path towards the substrate and also keeps the deposited materials as pure as possible. The second obvious advantage is the fabrication of multilayer devices in which the thickness of each layer can be controlled easily rather than the spin-coating technique. Because of this advantage, the thermal evaporation system greatly intensifies the efficiency of schematic device fabrication that aims at optimizing the various parameters. The other most important advantage is shadow mask usage. It provides us to coat the area which is desired. Figure 2.7 depicts

the schematic of vacuum thermal evaporation system for small molecules. In addition to depositing small molecules, it can be also used to deposit cathode materials such as aluminum with changing the filament container with boat made out of a resistive metal.

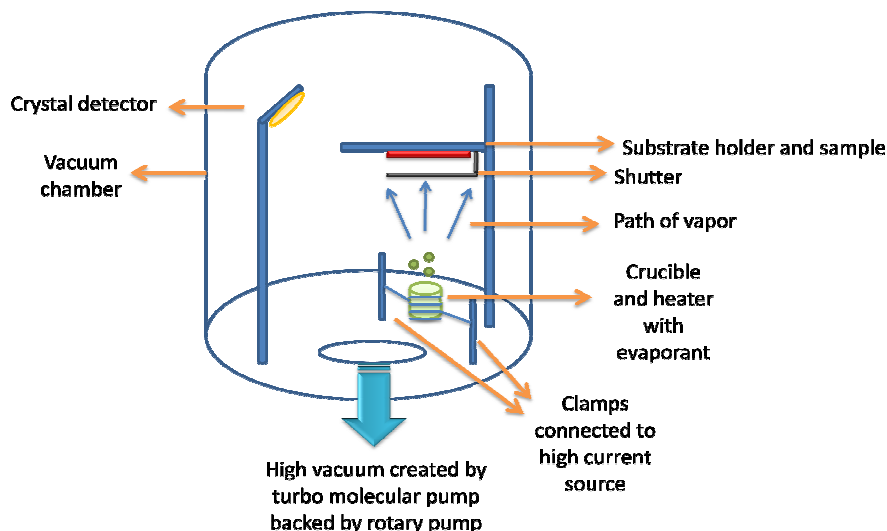


Figure 2.7. Schematic of Vacuum Thermal Evaporator for Small Molecules

### 2.2.3.2. Spin- Coating System

Studies have been carried out that there have been various coating techniques for polymer films including dip-coating, flow-coating, spray-coating, thermal spray-coating, plasma polymerization and spin-coating, etc. Among these deposition methods, the controllability of spin-coating technique is attractive and excellent when we want to create a well-defined film with a homogeneous lateral and vertical polymer distribution (Weill, 1986). It has been accepted method for many applications such as flat screen display coatings, dielectric/insulating layers for microcircuit fabrication. It does not require vacuum conditions and remarkably reduces the processing costs. Before using, the material to be made into the coating must be dissolved or dispersed into some kind of solvent. An excess amount of the solution is placed on the substrate and then rotated at high speed in order to spread the fluid by centrifugal force. Equally important, the higher the angular speed of spinning, the thinner the film. Besides, the residual thickness of the thin film depends not only on the spinning velocity but also on



concentration of the solvent and molecular weight. Figure 2.8 shows the schematic illustration of spin-coating system.

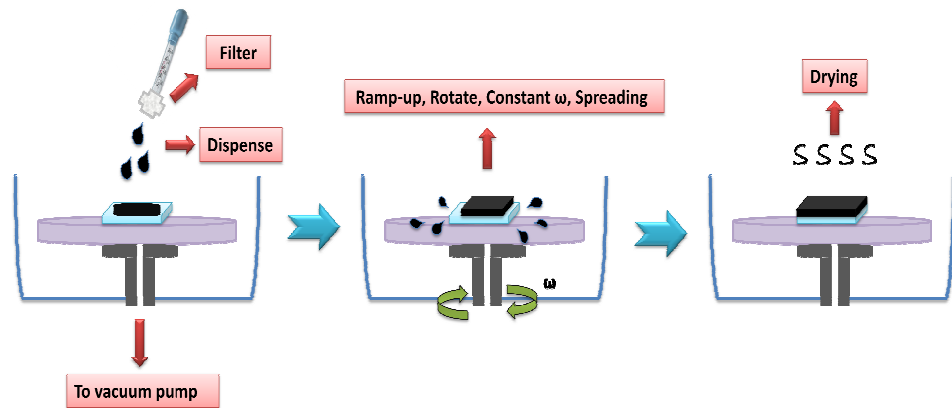


Figure 2.8. Schematic illustration of spin-coating system

## 2.2.4. Principle of Operation of OLEDs

An OLED emits light when electrical potential different is applied across the electrodes, as shown in Figure 2.9 (a) (Poulsen, 2011). In addition, although the voltages are low, from 2.5 to ~20 V, the active layers are so thin ( $\sim 10\text{Å}$  to 100nm) that the electric fields in the active layers are very high around  $10^5 - 10^7$  V/cm.

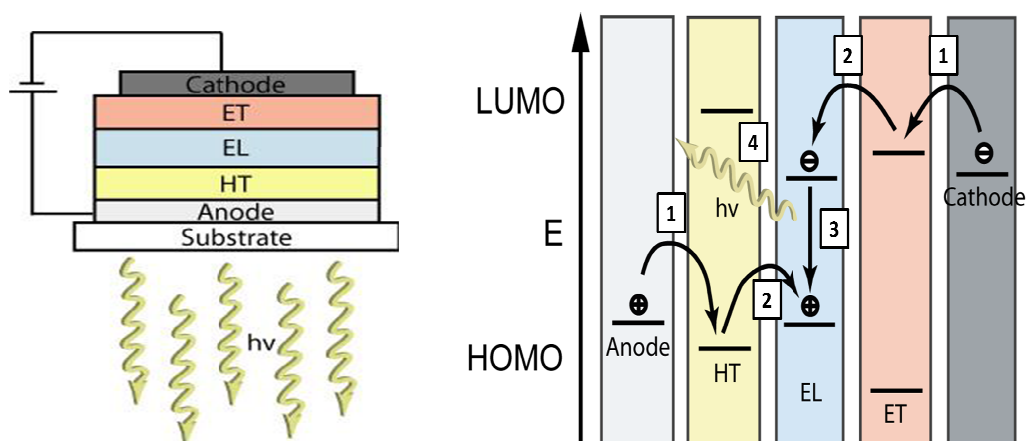


Figure 2.9. a) OLED device structure under applied bias. (b) Simplified energy band diagram representing the basic steps of EL; (1) charge carrier injection (2) charge carrier transport (3) exciton formation and (4) radiative decay

The generation of light from matter using electricity is called electroluminescence (EL) and it is the core of OLED operation. In an attempt to better understand the EL process, a simple energy band model to describe OLED behavior is presented in Figure 2.9 (b) (Poulsen, 2011). From the energy band model, it becomes easier to relate I-V characteristics with the basic processes required for EL in organic solids: charge carrier injection, charge carrier transport, exciton formation, emission of a photon and transport of the photon out of the device.

Electroluminescence can be generated by different factors resulting from external electric field applied to the sample. Among them the most important one is the recombination of charge carriers with opposite sign (Kalinowski and Godlewski, 1975; Kalinowski et al., 1983). In order to obtain electroluminescence process in the sample, the carriers of opposite sign should be injected and recombination should take place in the bulk (Kao and Hwang, 1981). Under driving voltage, electrons are injected from a metal cathode with low work function into the electronic state corresponding to the LUMO of the adjacent electron transporting layer. In this layer, the electrons hop via the LUMOs of neighboring molecules towards the anode. The transparent semiconducting ITO anode layer exhibits a low work function for hole injection into the HOMO of the adjacent hole transporting layer. Electrons and holes migrate to the recombination layer driven by the electric field, where they create an electron-hole pair, namely, excitons. Moreover, recombination may occur near to the heterointerface of adjacent layers, which results in the population of excited states of the emitter material and the excitation energy is released as photons. In addition, the level of excitation, namely, the emitted color is controlled by the chemical nature of the emitter (the HOMO-LUMO gap). Each of these steps is explained in more details in the following subsections.

## 2.2.5. Charge Transport Phenomenon in OLEDs

To understand the operation of OLED in detail, we could broadly define the operation in the following four stages:

- Charge injection
- Carrier transport
- Hole-electron recombination and exciton formation
- Light emission

### 2.2.5.1. Charge Injection

Generally, the relative positions of energy levels in the organic films and the metal electrodes create energy barriers for injection. Carrier injection is determined by the interfacial electronic properties. The understanding of the formation of energy barriers at cathode and anode interfaces is very challenging. Under the influence of applied electric field, holes from the positively biased electrode overcome the energy barrier and are injected into the HTL. In the same way as, the electrons are injected from the cathode into the ETL by overcoming the barrier at the organic-electrode interface. The injection can be improved by decreasing the energy barriers between electrodes and organic layers at the electrode-organic interface. The energy barrier is determined by the difference between the work function of cathode (anode) and the LUMO (HOMO) of the organic materials. For this reason, it is important to choose low work function electrode materials to be cathode (eg: Al) and high work function electrode materials to ease hole injection into the HTL (e.g. Indium tin oxide: ITO) as mentioned about section 2.2.2 materials part. Sometimes, introducing HIL and EIL at the electrode-organic interface can also enhance the carrier injection.

There are two types of charge injection mechanisms. They are Fowler-Nordheim tunneling or Richardson- Schottky (RS) thermionic emission (Sze, 1981). Both concepts are appropriate in inorganic semiconductors with extended band states and large mean free paths, which are not the case in organic semiconductors.

At typical organic /electrode interface the energy barrier is too high to generate any high current density. One of the possible injection mechanism is Schottky thermal injection which is through the localized levels induced by structural defects and unexpected impurities. The image force potential is generated because of Coulomb attraction between the injected electrons and the holes left behind in the metal after the electron injection, when a contact between the electrode and the organic layer is established. This image force potential reduces the energy of the interface state. In addition, it makes them energetically available for the electrons hopping from the metal Fermi surface. Conversely, the image force potential increases with decreasing distance, that is, decreases with increasing distance from the interface and therefore the bulk states deep in the organic layer remain energetically unavailable for charge hopping. Application of an external field reduces the energy of the available states in the bulk of organic layers. In shortly, hopping into bulk states away from the interface becomes more probable. The Schottky injection mechanism is described by the following current density equation (Sze, 1981);

$$J = \frac{4\pi q m k T^2}{h^3} \exp\left(-\frac{q\Phi}{kT}\right) \exp\left(\frac{qV}{kT} - 1\right) \quad (2.2)$$

where  $m$  is the effective mass of the electron/hole,  $k$  is Boltzmann's constant,  $h$  is the Planck's constant,  $V$  is the applied voltage between the anode and the cathode,  $\Phi$  is the injection barrier height and  $q$  is the magnitude of the charge of the electron. Figure 2.10 (a) gives a representation of Schottky thermal injection of the carriers from the metal electrodes.

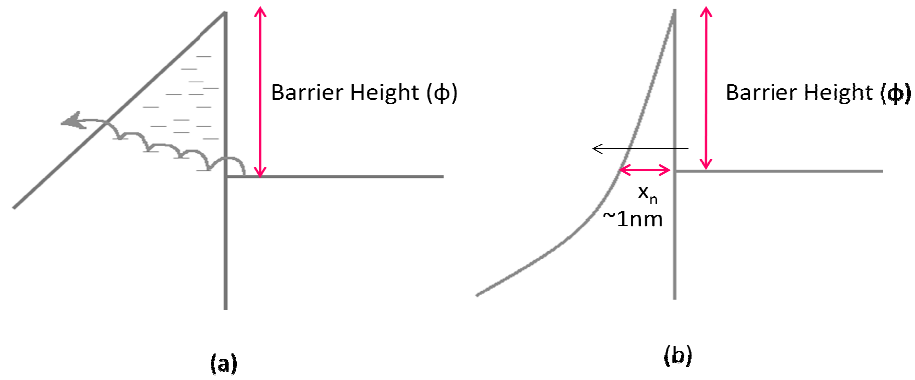


Figure 2.10. a) Schottky type carrier injection at metal-organic interface. The charge injection and transport takes place via impurity or structural disorder levels with thermal assistance. b) Fowler-Nordheim tunneling carrier injection under the influence of a local high electric field.

Fowler-Nordheim tunneling injection is another possibility of describing carrier injection. Electrons on the metal Fermi state can penetrate through the thin triangular energy barrier and hop into the energetically available state in the bulk. The charge injection due to this mechanism is characterized by the following expression (Sze, 1981);

$$J = \frac{q^3 V^2 m_0}{8\pi h \Phi m^*} \exp\left(-4 \frac{(2m^*)^{0.5} \Phi^{1.5}}{3hqV}\right) \quad (2.3)$$

where  $m^*$  is the effective mass of the electron and  $m_0$  is free electron mass. Figure 2.10 (b) shows the Fowler-Nordheim tunneling carrier injection under the influence of a high electric field. The Fowler-Nordheim mechanism is possible only when the electric field between the organic molecule and the metal electrode is in the order of  $10^7$  V/cm. Moreover, it is seen that the current injected is roughly exponential with T and applied field.

### 2.2.5.2. Charge Transport

In OLEDs, carrier transport phenomenon strongly depends on the electric field distribution. There is no universal transport mechanism in a wide temperature range. Phonon assisted thermionic emission might be a dominant mechanism at room temperature (RT). At low temperatures, tunneling can be dominant for carrier transport between molecules. Carrier transport in OLEDs has been described by space charge limited current (SCLC) theories at RT if charge injection is not a limiting factor. SCLC obeys the Mott-Gurney equation (Burrows et al., 1996);

$$J_{\text{SCLC}} = \frac{9}{8} \mu \epsilon \epsilon_0 \frac{V^2}{d^3} \quad (2.4)$$

where  $\mu$  and  $\epsilon$  are mobility and dielectric constant of the material,  $\epsilon_0$  is the permittivity of vacuum,  $d$  is the distance between contacts and  $V$  is the applied voltage. The SCLC type mechanisms are invariably found to dominate the conduction in device where strong injection is achieved from both electrodes. When an external electric field is applied, the holes are injected from the anode into the HTL and drift or hop across it. However, they decelerate at the internal interface due to the lower hole mobility in the ETL. The same mechanism is true for electrons as they cross the organic/organic interface. This process leads to substantial charge accumulation at the interface (Mu, 2007).

Hence, carrier mobility is field dependent, it can be described by a Poole-Frenkel (Murgatroyd, 1970);

$$\mu = \mu_0 \exp(\beta \sqrt{E}) \quad (2.5)$$

where  $\mu_0$  is the zero field mobility,  $\beta$  is an empirically determined coefficient and  $E$  is the external electric field.

The space charges can be either free carriers or trapped charges. The early observation of the temperature-dependent power law relation of current-voltage suggested a trapped charge limited current (TCLC) model (Mott and Gurney, 1940), which employed band models with a distribution of trapping levels below the conduction band. It was developed for bandlike transport rather than hopping transport. Furthermore, constant charge carrier mobility is required, which is contrary to the field-dependence of mobilities (Kepler et al., 1995). The nature of trapping needs to be clarified for proper device modeling. Thermally stimulated currents (TSC) and thermally stimulated luminescence (TSL) have been used to investigate the trap properties of Alq<sub>3</sub> (Forsythe et al., 1998; Werner et al., 2001). The trap energy can be defined as exponentially distributed on the band gap by the equation;

$$N_t(E) = \frac{N_t}{kT_t} \exp\left(\frac{E-E_{LUMO}}{kT_t}\right) \quad (2.6)$$

where  $N_t$  is the total trap density,  $k$  is Boltzmann's constant and finally  $T_t$  is the characteristic temperature of the exponential trap distribution ( $T_t = E_t/k$ , where  $E_t$  is the characteristic trap energy). Hence, the resulting TCLC model predicts a general high exponent power law. In the presence of traps, typically at organic layer interfaces or at defects within the film, as the forward bias is increased, the electron quasi-Fermi level rise towards the LUMO with increasing injected electron density. If traps are distributed in energy, they will be gradually filled with increasing field and the current will increase faster than quadratic in SCLC regime until all traps are filled. Briefly, observation of high power law dependence of current on voltage is called trapped charge limited current, TCLC.

### **2.2.5.3. Hole-Electron Recombination and Exciton Formation**

Following the transport mechanism, the recombination process will be located near the interface with low mobility carrier injection. The distance between the carriers decreases as they move towards electrodes with opposite polarity. When the distance between them is a few tens of nm, their mutual Coulomb interaction becomes important.

The electron and hole can then be looked upon as a single unit called exciton. Excitons are formed while holes and electron migrate from each side of the interface towards the recombination region. These excitons are also called ‘‘neutral excited species’’.

The excitons are generated in the emitter molecules if a single emitter material is used as an active layer. In that case, the emitting light is controlled by the energy bandgap between the HOMO and LUMO level of the emitter, namely, the color is determined by the nature of the emitter material.

For the further processes, we have to take into account the spins of both electrons and holes. Electron hole pairs that recombine tend to generate both singlet and triplet excitons. Spin  $\frac{1}{2}$  electron and spin  $\frac{1}{2}$  hole can generate four spin combinations, 3 triplets and 1 singlet as shown in Figure 2.11. Parallel spin pairs would recombine to form triplet excitons ( $S=1$ ) and anti-parallel spins recombine to form singlet excitons ( $S=0$ ). The spin of the holes is given by the spin of the residual electron at the emitter molecule. In a statistical limit, all four exciton substates will be formed with an equal probability.

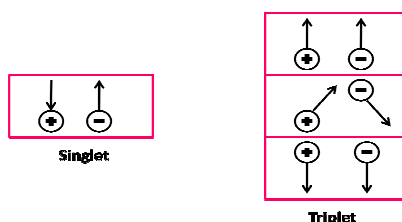


Figure 2.11. Diagram for possible singlet and triplet exciton formation

If singlet and triplet capture cross-sections are equal, it can produce only 25% efficiency for generation of singlet excitons. This factor is assumed to be insensitive to both devices and materials. Since the ground state of fluorescent molecules is typically singlet, and the transition from triplet to singlet is usually forbidden by spin conservation. For this reason, the maximum internal quantum efficiency is expected to be 25% for fluorescent in OLEDs.

The exciton might immediately emit light or exist for a few nanoseconds or microseconds before it emits. Various techniques are employed to enhance the probability of recombination and improve the device performance (Lian et al., 2007). Usually two materials with different LUMO and HOMO are chosen such that they can



create an effective energy barrier for blocking the carriers at their interface. Carrier density is then increased around the interface of ETL/HTL. Using dopant molecules in HTL/ETL is another technique used in improving the recombination probability as well as lifetime (Pfeiffer et al., 2003).

#### **2.2.5.4. Light emission**

Finally, after the recombination of carriers and formation of excitons, the excitons can either be in singlet or triplet state. The singlet or triplet exciton will recombine via photon emission (radiative decay) or non-radiative decay such as quenching and intersystem crossing transition. Transition of a singlet exciton from a single state to the ground state is very fast and efficient and results in the emission of light. This is fast and efficient in radiative decay because it does not involve in spin. Transition from the triplet state to the ground state of the triplet excitons involves spin flip. Therefore, the transition time is long. Moreover, decay is non-radiative where energy of the excitons is lost in the form of phonons. By incorporating certain dopants to give a triplet-to-singlet relaxation path, this fundamental limitation can be overcome and their inherent efficiency can be up to 100%.

#### **2.2.6. Device Efficiency**

Efficiency is a key issue for both energy consumption and durability of the device. A low I-V product for a given luminance indicates that the power consumption is less, which in turn implies a lower ohmic heating and therefore better lifetime.

The efficiency of OLEDs can be characterized by its;

- Quantum efficiency,
- Power efficiency (lm/W),
- Luminous efficiency (cd/A), sometimes called luminous yield (Forrest et al., 2003).

### 2.2.6.1. Quantum Efficiency

The device quantum efficiency  $\eta_q$  has two parts, namely, internal and external quantum efficiency. The internal quantum efficiency (IQE), defined as the ratio of the number of photons  $\phi$  generated within the device to the number of electrons flowing in the external circuit,  $j/e$ , is given as,

$$\eta = \frac{\phi}{j/e} \quad (2.7)$$

A large fraction of generated photons stays trapped and absorbed inside the device. In spite of this, the external quantum efficiency (EQE) refers to the number of photons emitted from the front face of the device per injected electron (Shinar, 2004). Simply, it is the 'p/e' ratio (photons/electrons). Since the mobility of holes is higher than that of electrons in organics, the efficiency is limited by the number of electrons in the device. The basic equation for external quantum efficiency can be denoted as;

$$\eta_{EL} = \varepsilon \gamma r_{ST} p_L \quad (2.8)$$

Where  $\eta_{EL}$  is the external quantum efficiency,  $\varepsilon$  is the out-coupling efficiency,  $\gamma$  is the charge balance factor,  $r_{ST}$  is the ratio of singlet excitons to triplet excitons and  $p_L$  is the photoluminescence quantum yield (Shinar, 2004). For maximized efficiency, each term in the equation 2.8 should be optimized. It should be noted that the quantum efficiency relies on the device structure and its operating conditions.

### **2.2.6.2. Power Efficiency**

Power efficiency  $\eta_p$  of an OLED is the ratio of the light output in lumens to the electrical power input in watts. The derived unit is hence lm/W. Power efficiency is widely used for OLED solid state lighting applications. A typical incandescent bulb has a power efficiency of 15 lm/W while a fluorescent bulb has nearly 60 lm/W. The latest experimental OLEDs have already reached power efficiency of about 100 lm/W. With ongoing research on novel ways of synthesizing and processing chemicals, one can expect higher efficiencies to be reached in the lighting industry. Though we have given an overview of the different efficiencies involved in evaluating the performance of an OLED, the actual measurement technique is slightly more complex. An important factor that needs to be accounted is that the emission from an OLED is Lambertian. That means the light emission from a luminescent film is omnidirectional (Bulovic and Yu, 2008). Therefore, the large viewing angle of these displays comes inherently with the technology. A more rigorous model has to be constructed that takes into account the device geometry, reflection of light from the cathode, finite thickness of glass and total internal reflection at the glass-air interface etc. (Greenham et al., 1994).

### **2.2.6.3. Luminous Efficiency**

Luminous efficiency, namely current efficiency of an OLED is identified as the ratio of the luminance ( $\text{cd/m}^2$ ) to the current density ( $\text{A/m}^2$ ). As a consequence, the derived unit for luminous efficiency is cd/A. The cd/A value is widely used in the OLED display industry for characterization and determination the OLED performance. It should be noted here that cd/A is a photometric unit and not a radiometric unit. While radiometry is the measure of optical radiation, photometry is the measurement of light in the visible spectrum. Put it in a different way, photometry is weighted by the spectral response of the eye. It is worthwhile to refer here that typical display applications such as TV monitor, laptop screens have a luminance of around  $100 \text{ cd/m}^2$  to  $200 \text{ cd/m}^2$ . Accordingly it is very important to improve the cd/A efficiency at these luminance values where the OLED is generally driven for display applications. It can be found that luminance of OLEDs is around  $10^6 \text{ cd/m}^2$  (Schaffel et al., 2001).

## CHAPTER 3

### SELF-ASSEMBLED MONOLAYER

Recently, a considerable number of studies have been interested in regarding the work function increase of an ITO electrode using ultraviolet (UV) and oxygen plasma methods. Conversely, the work function increases obtained using these methods are not high and the process has expensive. A surface modification is the technique to convert or enhance the physical and/or chemical characteristics of a surface. In electrical, mechanical and biological applications, because of change in the resistance caused by friction and abrasion, corrosion and the other detrimental physical properties are induced on the material surface. Due to these reasons, surface modifications to introduce more functional properties have been researched and developed (Maboudian and Howe, 1997). There are several surface modification techniques such as drying methods with vacuum process and wet methods using hydrogen passivation and application of hydrogen-bonded fluorinated monolayers and a covalently-bonded hydrocarbon self-assembled monolayer (SAM).

SAMs are one of the useful techniques to improve macroscopic bulk properties and microscopic molecular properties of functional materials. SAMs are being examined extensively due to their ease of formation and their wide applicability (Ulman, 1996). As it is well known that surface hydroxy groups on the ITO can support a SAM with various kinds of functionalities, such as carboxylic acids (Berlin et al., 1998), phosphonic acids (Appleyard et al., 1999), and silanes (Koide et al., 2000). Some previous researches report application of a SAM as either a current blocking layer (Koide et al., 2000) or a moisture penetration blocking layer (Choi et al., 2001). Enhanced charge injection as a result of the surface dipolar layer of a SAM has also been reported. Bruner et al. reported a similar phenomenon, that variation of the molecular dipole adsorbed on the ITO surface can change the work function of the ITO (Bruner et al., 2002).

For OLED applications, SAM is generally used at the anode/organic interface to enhance the carrier injection and to improve the stability in an organic light emitting device. The reduction of pinhole formation at the anode/organic interface and the

increment of anode work function modifies hole injection barrier height and hence it enhances the electroluminescence characteristics of OLED devices (Hatton et al., 2001; Zhu et al., 2002).

### **3.1. Introduction to Self-assembled Monolayer**

Modern approaching to modify solid surfaces can be classified into two broad categories: physical treatment and chemical treatment. Physical treatment, as the name indicates, does not involve a chemical reaction, and includes paint coating, sublimation, sputtering, or evaporating. In contrast, chemical treatment generates new species on the surface via chemical reactions, and includes chemical vapor deposition (CVD), atomic layer deposition (ALD), or SAM formation.

SAMs are the most elementary form of a nanometer-scale organic thin film material. Nuzzo and Allara are considered as pioneers of SAM research since 1983, due to their published work “Adsorption of Bifunctional Organic Disulfides on Gold Surfaces” (Nuzzo and Allara, 1983). They reported a new technique to form well-ordered monolayers in contrast to the well-known Langmuir-Blodgett deposition. This new technique involves spontaneous organization of organic disulfides absorbed on freshly evaporated gold substrates. Since then, the preparation, formation, structure and applications of SAMs have gained much attention in the surface engineering field. The most extensively studied system is derived from the adsorption of alkanethiols on gold surfaces. Thus, a considerably amount of literature is available on this issue, especially, the book published by A. Ulman (Ulman, 1998) or the most recent reviews published by Schreiber (Schreiber, 2000) and Love (Love et al., 2005) for a general overview.

Self-organization (self-assembly) of atoms and molecules form a geometric repeated of symmetry at the molecular level. SAMs are ordered molecular structures formed by the adsorption of an active surfactant on a solid surface by self-organization processes (Ulman, 1996). In contrast to ultra-thin film made by such as MBE and CVD, SAMs are highly ordered, oriented and can incorporate a wide range of groups both in alkyl chain and at the chain terminal. Therefore, a variety of surfaces with specific interactions can be produced with fine chemical control (Ulman, 1991).

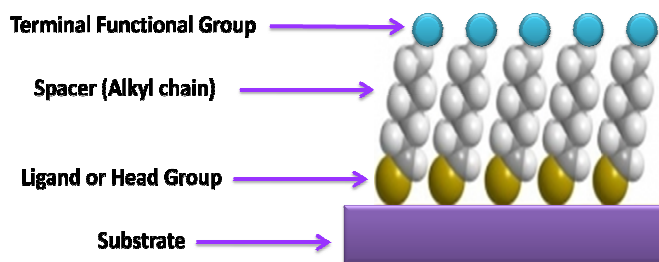


Figure 3.1. An array of molecules self-assembled on a flat substrate surface

The general structure of SAMs can be depicted as Fig. 3.1. Self-assembled molecules usually divided into three parts;

- (I) head group
- (II) alkyl groups
- (III) interfacial (terminal)

First part is head group that is surface active and causes exothermic process of chemisorption on the surface of the substrate. Moreover, it has specific affinity for the substrate and forms the chemical bond with surface atoms of the substrate. In other words, organization of SAM starts with the interaction between the head and the substrate by means of chemisorption and last to the thermodynamic equilibrium. The second part is alkyl or alkyl derived chains play an important role in the packing density of the molecules. Alkyl groups assist in formation of ordered molecular structure by short-range dispersive inter-chain Van der Waals interactions when the distance between adjacent molecules is very small. In that case, the molecules tend to reorganize because of these interactions between alkyl chains. However, if the alkyl chain is substituted with any other polar bulky function, then long-range interactions are predominant. The third part is interfacial group that is usually used as a functional part which opens up the possibility of successive anchoring or chemical reactions. The SAM's structure can be designed by the factors such as competing interactions among substrate, alkyl groups, head groups, interfacial groups and the sizes of each group. Thus, SAM can modify the functionality of an interface by its structure as well as by self-assembled molecules.

### 3.2. Formation and Utilization of SAMs

SAMs have strong affinities for the substrate. That is why, they formed by the exposure of surfactant molecules on a solid surface. The process to prepare self-assembled monolayers is simple and only minimum amounts of organic molecules are needed. They are formed by immersing an appropriate substrate into a solution of organic compound (surface-active material), possessing the ability to spontaneously form an ordered molecular layer on the substrate. Put it in a different way, the substrate surface is simply immersed into a dilute ( $\mu\text{M}$ - $\text{mM}$ ) solution of appropriate molecules whereby strong specific interactions between the molecules' reactive head groups and the surface of the substrate, resulting in chemisorptions. Once pinned to the surface, the molecules start organizing themselves into an ordered, densely packed layer (Ulman, 1991). Organization is driven by Van der Waals interactions between the chains, as the system aims to optimize lateral interactions and reach potential energy minimum. In addition, this organization process, which takes one day is enough to complete, is illustrated in Figure 3.2 below.

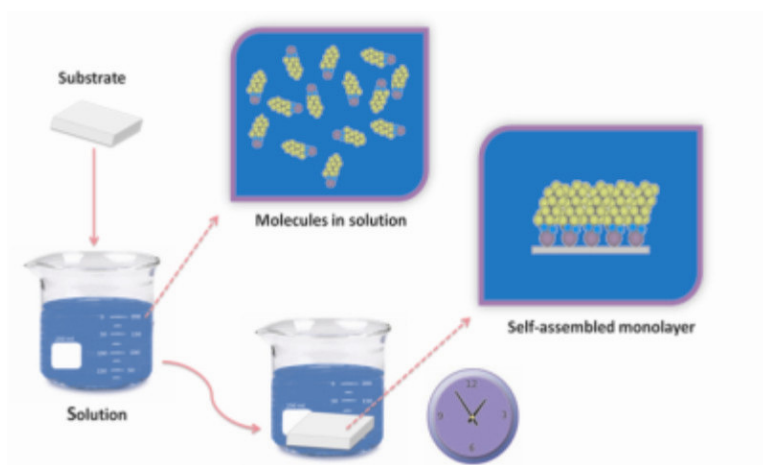


Figure 3.2. Formation of SAM by immersing a substrate in appropriate solution

Depending on the structure of the molecules, these films can be disordered or well-packed as shown in Figure 3.3. The degree of order in monolayers is a product of

many factors, including geometric aspects, electrostatic and dipole-dipole interactions within the monolayers.

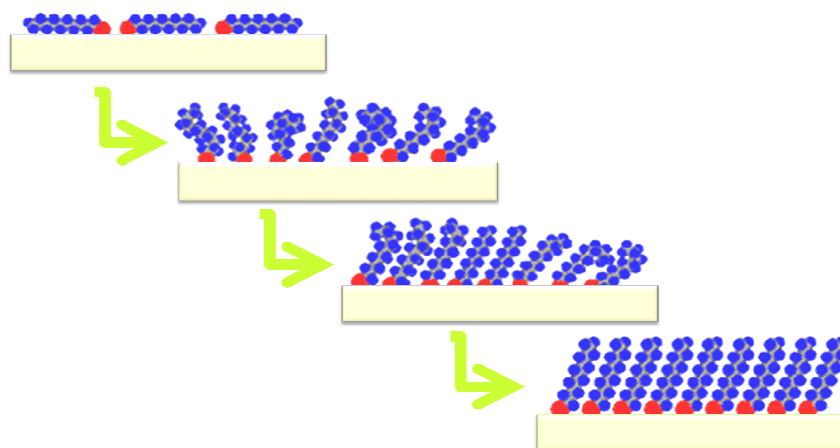


Figure 3.3. Schematic illustration of the formation of SAMs of surfactant molecules on a solid surface

SAMs are prime technological interest. Due to the large number of properties that can be designed into SAM films, they propose almost unlimited possibilities for studies to correlate many surface and film parameters with friction and adhesion. For instance, the binding to the substrate can be changed by using molecules with different head groups that they are  $-SH$  (thiols),  $-SiR_3$  (silanes),  $-COOH$  (acids), etc.

The softness or elastic compliance can also be changed by modifying the chain length and/or the type of chemical bonds inside the chains (single, double, and triple C-C bonds), by fluorination, and by inclusion of several heteroatoms, like O (in ethers), etc. All of these affects also modify the rigidity of the chains. The end groups that are exposed to the vacuum or liquid interface can also be conveniently modified to affect the friction and adhesion forces (Carpick and Salmeron, 1997; Ivanisevic and Mirkin, 2001).

### 3.3. Parameters Affecting on SAM Formation

To be able to prepare good quality SAM films, some parameters must take into account can be summarized as follows:



First of all, the interactions between the functional groups including the tails of SAM molecules strongly affect the structural properties of the SAMs. For example, molecule-substrate interactions and lateral chain-chain interactions are quite significant for formation of SAMs. The tail groups are found to have major influence on the structure of SAMs. This formation will prove useful in controlling the surface densities and lattice structures of SAMs in technological applications that employ these species. More and more, the lateral interactions are important in the molecular rearrangement at the physisorption stage and they may be responsible for the formation of metastable structures as well. Because of formation of metastable structures, these SAMs are expected to comprise locally at samples surfaces. This also results different molecular packing (Tamada et al., 1998).

Due to the specific interactions between molecules and substrates, SAMs are formed with various solvents and diversely designed molecules ending up with controlled and modified surface properties. Several different solvents are usable at low concentrations typically between 0,1 and 2 mM that are used in preparation of SAM solutions. Generally, low concentration is preferred because of giving opportunity to the molecules to find a place on substrate and it reduces the steric affect. However, more concentration leads to defect on SAM formation besides steric affects. In order to form this process, solubility properties are gained quite importance. So as to decrease molecular density, SAM molecules need to be solved in their prefer solvents. Furthermore, ethanol and water solvents are the most common solvents which use in SAM solution.

The length of the alkyl tail and the nature of the end group also affect on the properties such as the angle of tilt with the surface and the extent of motion within the monolayer itself. Using long chain has advantages and disadvantages. Long chain increases value of Van der Waals as additional molecules that mean increasing order of SAM. However, it causes rising in molecular weight and this is ended up with deviation from the tilt angle. Beside this affect, due to the molecules motion, increasing length chain results formation time rising. That is, formation time increases with increasing length of chain.

Time has an effective role, so as to form structure of SAM. Inefficient time leads to incomplete composition. On the other hand, enough time is needed for obtaining the complete structure. In other words, in order to obtain well-ordered SAMs, proper

formation time which changes from molecule to molecule is required. Besides, extra time may not cause serious problems but it can give rising to collapse of molecules. From literature, suitable time for maximize the SAM grafting on substrate is more than 24 hours. The limited point here, SAMs formation lasts from the initial adsorption to the final thermodynamic equilibrium as seen in the Figure 3.4.

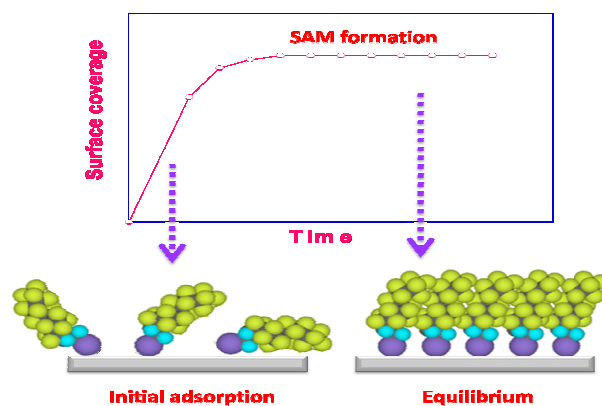


Figure 3.4. Schematic illustration of the formation of SAMs of surfactant molecules on a solid surface with its principle components of time

Figure 3.4 shows the time effect on SAM formation. There is no multilayer forming and adsorption times of two to three days are optimal in forming highest-quality monolayers. In addition, it is observed that, it is possible to decrease defects by means of increasing time. After forming SAMs, if there are more free molecules in solution, they mostly stay in solutions because there is no any place for them on substrate surface.

The other most important parameter that plays important role on SAM formation is contact shape of molecules to surface. When the SAM molecules are tied to substrates, they can also make an angle with the surface which relies on individual properties of molecules. From the literature, the highest contact angle was recorded on monolayer where the diacetylene group is connected to carboxylic head group.

Substrates and film defects observed after formation can be counted as another effective parameter effecting SAM formation. Naturally forming defects within SAMs, such as domain boundaries, substrate vacancies and lattice vacancies can be utilized as “placeholders” for insertion of individual molecules. In addition to this, we can say the

condition of the defects keeps changing with increasing adsorption time (Diao et al., 2001).

Smoothness, contamination, drying, temperature and size of SAMs molecule are of course highly important parameter for preparing SAMs. Except for effects of temperature and size of molecules, the other parameters lead to defects on the films. The influence of temperature and molecule size has not been clear yet. They have just ability to change reaction kinetics. For instance, temperature has highly interesting impact on SAM formation. High or low temperature cause spoilt on organics and this can prohibit SAMs formation on substrates (Diao et al., 2001). We know that low temperature decreases the reaction kinetic from thermodynamics. Moreover, high temperature also damages the bond formation as well as increasing reaction kinetics. Furthermore, the usage of big molecules leads to better bonding with the surface and higher kinetics of reaction.

In conclusion, we can say working with optimum SAM conditions cause low defects formation. The reaction conditions and their effects are the most significant for SAM formation (Gül and Okur, 2006).

### **3.4. SAM-HTL**

SAMs are used as hole injection materials (HIMs) in OLEDs. The use of a HIL material to enhance charge injection into the OLED device has spawned a number of materials, which have been shown to provide benefits, particularly in terms of lower operating voltages and extended lifetimes of OLED devices. The HIL behaves as an interface connection layer between the anode and the HTL in an attempt to improve the film forming property of the subsequent organic layer and to facilitate efficient hole injection. HIMs should have good adhesion to the anode substrate and should perform to smooth the anode surface.

SAM is a surface modification by chemically attaching a monolayer (or thicker layers) of organic species is an efficient way to control the chemical and electronic properties of ITO electrodes in OLED applications at the molecular level. This approach has the potential for practicing excellent control over the dipoles on the ITO surface and, thus, the charge injection properties. Such an approach, utilizing attachment of organotin, phosphorus, and phenolic species, has been presented to be effective in

controlling the anode WF (Schwartz et al., 2003). Moreover silane monolayer species are used for a similar purpose too (Lee et al., 2002). Comprehensively, this approach may offer a chemical solution to many of the issues raised by the device performance of ITO and has become a very active area of researches. Marks' group introduced two new HIMs, 4,4'-bis[(p-trichlorosilylpropyl-phenyl) phenylamino] biphenyl (TPD-Si<sub>2</sub>Cl) and 4,4'-bis[(p-methoxylysilylpropylphenyl) phenylamino]biphenyl (TPD-Si<sub>2</sub>OMe), which combine the hole-transporting efficiency of TPD and the strong cross-linking and densification tendencies of organosilanol groups (Huang et al., 2002). Covalent chemical bonding of TPD-Si<sub>2</sub> to the anode such as ITO and its self-cross-linking as a hole injection and adhesion interlayer can increase OLED hole injection and device stability. High-efficiency and high-luminance small-molecule OLEDs are fabricated by introduction of the TPD-Si<sub>2</sub> interlayer, which significantly enhances OLED current and light output by a factor of ~50–80 as well as improving the external quantum efficiencies (EQEs) (Huang et al., 2003). Furthermore, the HTLs enhance PLEDs anode hole injection and exhibit significantly greater electron-blocking capacity than PEDOT–PSS (Yan et al., 2005). The organosiloxane HIM approach proposes convenience of fabrication, flexibility in choosing HTL components, and reduced HTL-induced luminescence quenching, and can be applied as a general strategy to improve PLED performance. Moreover, the similar molecular structures of SAM and HTL are supposed to give a better interfacial compatibility that is enhancement of the hole injection and reduce the turn-on voltage (Cui et al., 2002; Meng, 2007).

### **3.5. Applications of SAMs**

Self-assembly monolayer, forming by self-assembly of surfactant molecules at the surface has been studied extensively due to the potential properties such as wettability, modification, biocompatibility, and corrosion resistance of substrate surface. Corrosion protection, lubrication, biosensors and arrays, biomolecule immobilization, bio materials, diffusion barrier, drug delivery and molecular electronics are some of SAM applications. Lately, grafting SAM on ITO or metal surface is widely used in photo-electronic and electronic fabrications. SAMs have been utilized as bridging layers to assemble nano-particles onto the ITO surface for the purpose of improving the incident photon to current conversion efficiency (IPCE) of a solar cell

(Shipway et al., 2000; Subramanian et al., 2001). Furthermore, SAM modified ITO substrates were also found to enhance the adhesion between inorganic ITO and organic HTL, and reduce the pinholes in OLED device (Carrard et al., 1999; Lee et al., 2002).

### **3.6. Characterization Techniques of SAMs**

Monolayers formed through self-assembly can be characterized in an attempt to determine their composition and structure (including defects) since they are important in the study due to specific electronic properties of the material. Characterization of self-assembled monolayers helps to provide the presence of particular molecules on the substrate surface which could be used for building further molecular-scale devices.

SAMs have been studied by many different and complementary surface science techniques such as UHV techniques (X-ray photoelectron spectroscopy (XPS), Auger electron spectroscopy (AES), low energy atom diffraction (LEAD), temperature programmed desorption (TPD), grazing incidence X-ray diffraction (GIXD), etc.), spectroscopic methods (infra-red (IR), Raman, etc.), scanning probe microscopic methods (Scanning tunneling microscopy (STM), atomic force microscopy (AFM), etc.) and electrochemical methods (EC methods). Moreover, ellipsometry are also used to measure thicknesses of the SAMs.

# CHAPTER 4

## EXPERIMENTAL DETAILS

This chapter consists of the experimental procedure which has been performed in the process of fabricating and characterizing OLED devices. First section covers the general features of the fabrication process and the stages of the device fabrication in detail. The second section describes the measurement setup and the last section details with the techniques used for the characterization of the devices.

### 4.1. Device Fabrication

This part explains the different experimental procedures involved in the fabrication of OLEDs. Our basic device fabrication method can be explained as follows:

- A proper etching,
- Cleaning of the ITO substrate,
- Plasma treatment,
- Sam formation,
- Thermal evaporation of the hole, emissive and transport layers,
- Thermal evaporation of the electrodes (Aluminum Deposition).

In this part, all experimental processes will be described step by step.

#### 4.1.1. Etching of ITO Substrates

For device fabrication, etching process is attributed to a process where material is removed from the substrate. There are two types of etching process namely, dry etching and wet etching. Wet etching is process that uses liquid chemicals and etchants to remove materials from the substrate. In other words, a simple wet etching process may just consist of dissolution of the material to be removed in a liquid solvent, without

changing the chemical nature of the dissolved material. In our process, in order to create desired pattern of ITO coated glass, a wet chemical etching method was used to etch ITO on glass as shown in Figure 4.1. This procedure prevents electrical short circuit in the final device. Zinc powder and hydrochloric acid (HCl) aqueous solution ( $H_2O:HCl=4:1$  by volume) have been used. First of all, ITO-coated glass samples were cut into  $15\text{mm}\times 15\text{mm}$  pieces. Approximately  $10\text{mm}\times 15\text{mm}$  strip of ITO was stacked with electrical sticky tape. Then, Zinc powder was put onto the open part of ITO substrate. 20% diluted HCl aqueous solution was distilled on to the Zinc powder. After the etching process, the substrate was rinsed with de-ionized water and the tape was removed from the ITO substrate. The final pattern of ITO coated glass substrate with one side etched can be seen from Figure 4.2.

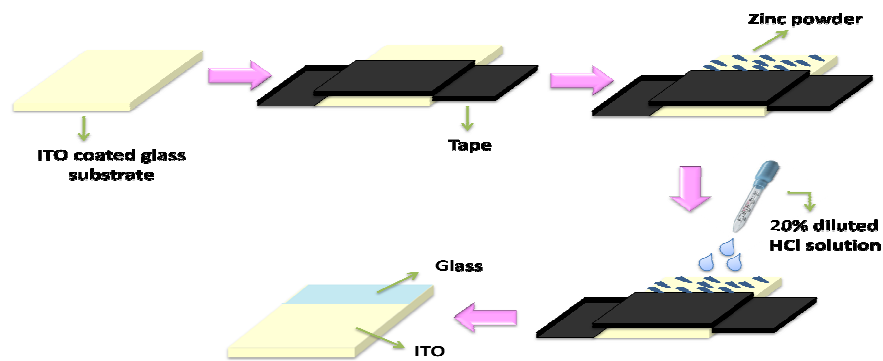


Figure 4.1. The etching process on ITO coated glasses

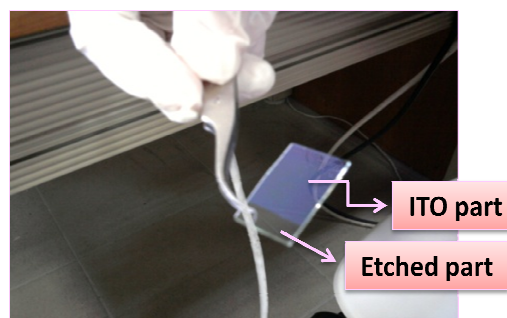


Figure 4.2. Picture of etched ITO

### 4.1.2. Cleaning Procedure of ITO Substrates

Cleaning process is a very significant step on the fabrication device. If the organic film is directly deposited on the ITO surface, its surface properties are anticipated to affect the performance of the device. Even a small dust particle on the substrate can generate a discontinuous structure, resulting in abnormal device behavior such as shorting and unstable I-V characteristics. ITO substrates must be as clean as possible before the deposition of the thin film. In an attempt to clean substrates, each slide was swabbed by rubbing with acetone, followed by a sequence of 30 min. ultrasonic baths in detergent in de-ionized water, de-ionized water, acetone, ethanol, iso-propanol, and finally, de-ionized water again. The cleaning procedure is summarized as given in Figure 4.3.

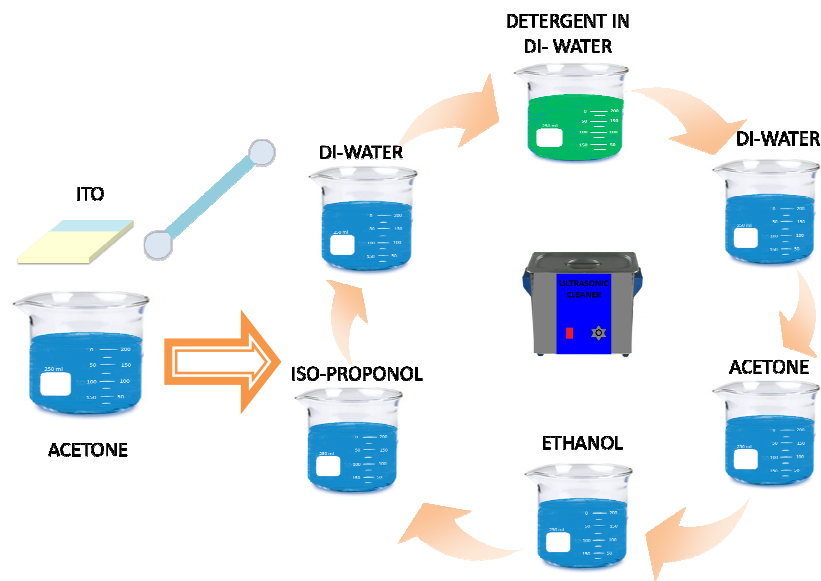


Figure 4.3. Cleaning procedure of etched ITO

Finally before the use, the substrates were dried in a nitrogen gas flow. In addition, after the completion of the chemical cleaning procedure, oxygen plasma method is applied on the ITO surface.



### 4.1.3. Oxygen Plasma Treatment

The effect of plasma treatment on the OLED performance is not clearly known. However, it is suspected that the influence of the plasma treatment on ITO surface, ITO work function has a significant effect on OLED performance (Lu and Yokoyama, 2004). Other factors such as the removal of organic residue from the ITO surface and the reduction in surface roughness may also influence OLED performance.

By means of oxygen radicals and ions, organic bonds like those in oils and greases (hydrocarbons) are split and removed as small molecules or atoms depicted in Figure 4.4. These chemical reactions mainly produce carbon dioxide and carbon monoxide as decomposed products. In other words, plasma cleaning is convenient for removing very thin films, especially hydro-carbonates and oxides, which remain after conventional chemical cleaning procedure.

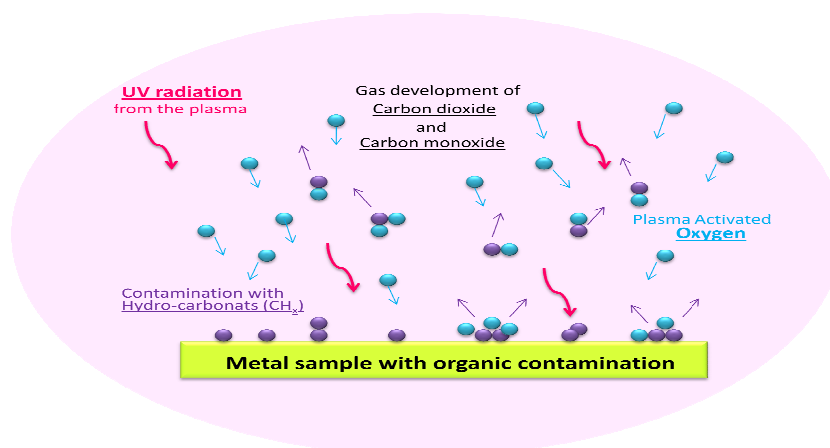


Figure 4.4. Schematic of oxygen plasma treatment mechanism (Source: (Deiries et al., 2005))

Moreover, the main purpose of this study is to bind chemically the SAM molecules on to the ITO surface with ester linkage by oxygen plasma method. For this purpose, ITO surfaces were subjected to oxygen plasma for approximately 15 minutes to enrich the hydroxyl groups and oxygen bridges on the ITO surface as shown in Figure 4.5. Figure 4.6 shows the picture of our system for plasma cleaning. After the plasma cleaning, the ITO surface becomes ready to coat SAM materials for possible chemical bond.

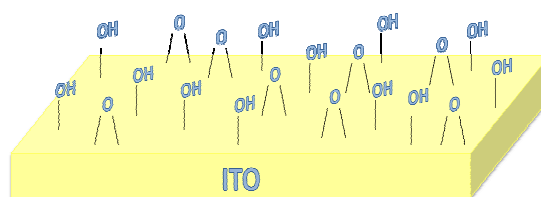


Figure 4.5. The schematic representation of ITO surface after oxygen plasma

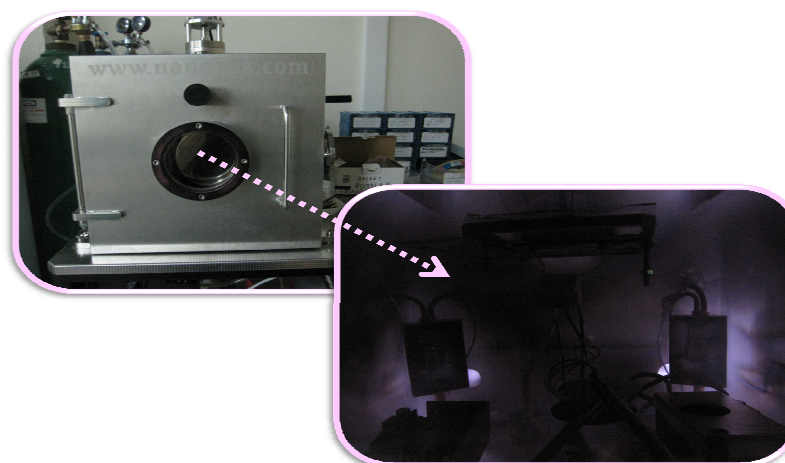
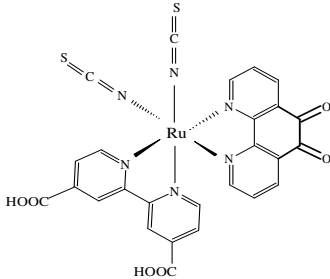
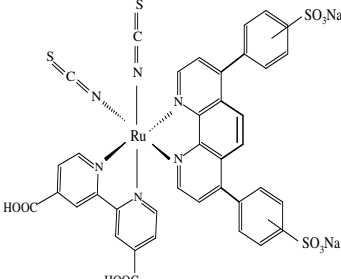
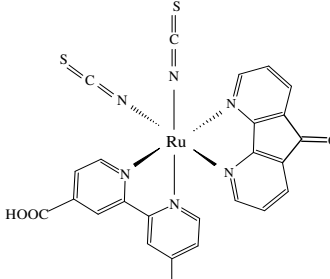


Figure 4.6. The picture of oxygen plasma cleaning in our thermal evaporation system

#### 4.1.4. SAM Formation

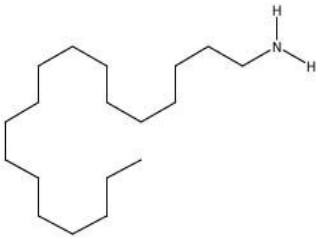
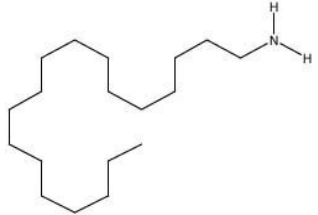
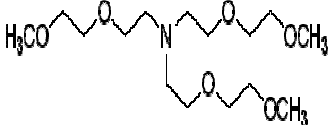



As schematically illustrated in Figure 4.7, when ITO substrate is immersed in a solution of precursor molecules with chemically reactive to the substrates surface, the molecules are chemisorbed on the surface with their reactive sites being faced to the surface. In this study, eleven different SAM molecules were utilized. They are K-27, K-28, K-30 with Ruthenium(II) bipyridyl complexes (Ocakoglu et al., 2007), Diaminododecane, Tridecylamine, Mercaptoundecanoic acid, Mercaptohexdecanoic acid, Octadecylamine-HCl, Octadecyltrichlorosilane and Tris[2-(2-methoxyethoxy)ethyl]amine. SAM solvent concentrations are kept fixed as 1mM for all SAMs. Organics with their solvent and their chemical structures are given at the Table 4.1. It should be noted that silanes, acids and amines can bind ITO surface chemically. For this reason, these SAM molecules were examined in this study.

Table 4.1. Organics of SAM used in the experiments with chemical structures and the preparation conditions

ORGANICS	MOLARITY	SOLVENT	CHEMICAL STRUCTURE
<p><math>\text{Ru}^{\text{II}}</math>(1,10-phenanthroline-5,6-dione)(4,4'-dicarboxy-2,2'-bipyridyl)-di(thiocyanate)</p> <p>(K-27)</p>	1mM	Ethanol	 <p><b>K27</b></p>
<p><math>\text{Ru}^{\text{II}}</math>(bathophenanthroline sulfonate)(4,4'-dicarboxy-2,2'-bipyridyl)-di(thiocyanate)</p> <p>(K-28)</p>	1mM	Ethanol	 <p><b>K28</b></p>
<p><math>\text{Ru}^{\text{II}}</math>(4,5-diazafluoren-9-one)(4,4'-dicarboxy-2,2'-bipyridyl)-di(thiocyanate)</p> <p>(K-30)</p>	1mM	Ethanol	 <p><b>K30</b></p>

(cont. on next page)

Table 4.1 (cont.)

Octadecylamine-HCl (ODA-HCl)	1mM	Ethanol	
Octadecylamine-HCl (ODA-HCl)	1mM	Methanol	
Tris[2-(2-methoxyethoxy)ethyl]amine (TDA-1)	1mM	Methanol	
Octadecyltrichlorosilane (ODT-Cl-Si)	1mM	Chloroform	
Mercaptoundecanoic acid (MDA)	1mM	Ethanol	
Mercaptohexadecanoic acid (MHDA)	1mM	Ethanol	

(cont. on next page)

Table 4.1 (cont.)

1,12-Diaminododecane (DDA)	1mM	DI-Water	<chem>NCCCCCCCCCCCCN</chem>
Tridecylamine (TDA)	1mM	Toluene	<chem>CCCCCCCCCCCCCN</chem>

To obtain well formed SAMs, formation time must be taken into consideration. Therefore, ITO substrates were left into the organic solutions for 48 hours as shown in Figure 4.8, after applying oxygen plasma procedure. Then, to avoid any possible readsorbption of desorbed SAM, prepared modified ITO substrates were rinsed with their pure solvent. Then, they were dried with a stream of dry nitrogen to coat organic thin film.

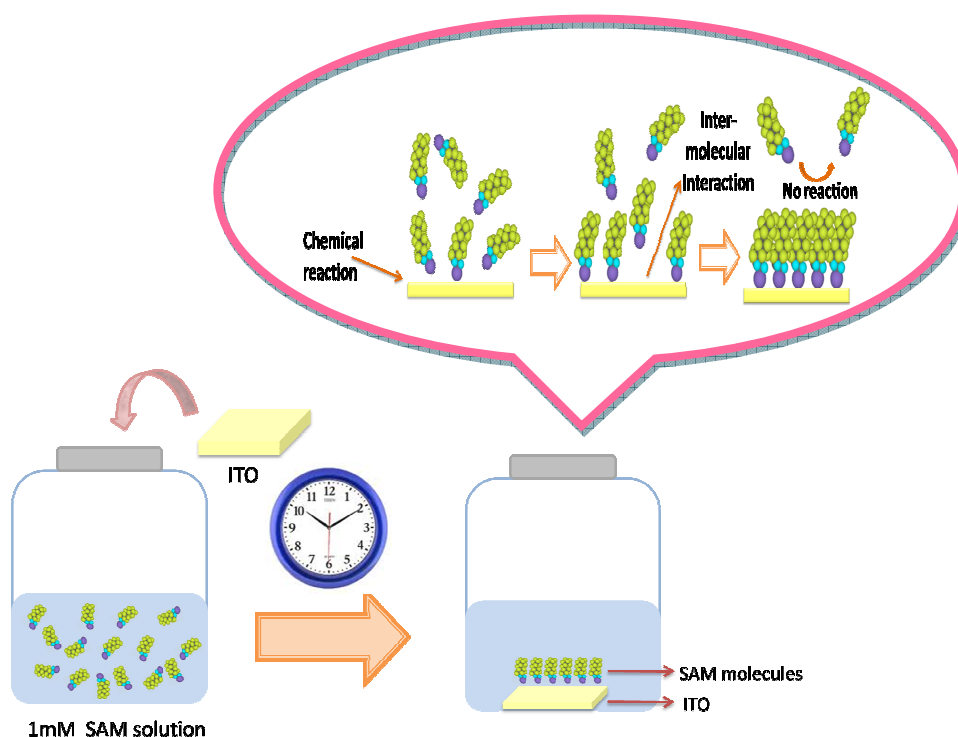


Figure 4.7. Preparation procedure for self-assembled monolayer

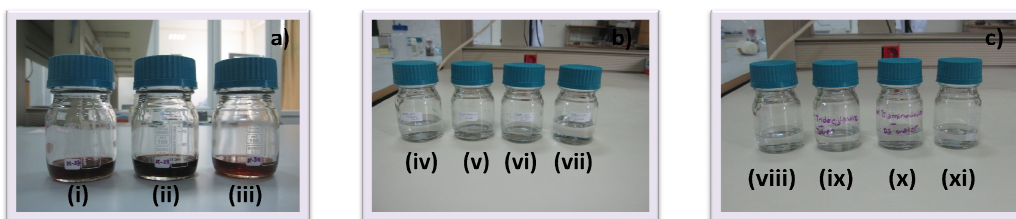


Figure 4.8. The picture of organic solvents (SAM solvents): a) (i) K-27, (ii) K-28, (iii) K-30, b) (iv) ODA-HCl (MEOH), (v) TDA-1, (vi) ODA-HCl (ETOH), (vii) ODT-Cl-Si, c) (viii) MDA, (ix) TDA, (x) DDA, (xi) MHDA

#### 4.1.5. Organic Layer and Cathode Deposition

The picture of our thermal evaporation system for organic molecules and metal electrodes are shown in Figure 4.9 and Figure 4.10, respectively. Thermal evaporation technique is fast and comparatively simple; it registers a low-energy impact on the ITO surface without surface damage.

For high quality film evaporation could be achieved in vacuum around  $10^{-6}$  Torr. High vacuum is not only necessary to avoid reaction between the vapor and atmosphere but also to increase the mean free path of vapor atoms. By this way, they do not undergo collisions with the surrounding gas molecules inside the evaporation chamber. In an attempt to reach high vacuum, turbo molecular pump with back pumping was used in the system. Deposition rate and thickness of the film on the substrate were controlled by a shutter to provide high quality thin films without contamination coming from other materials in the boat at the beginning. Thickness of the deposited films was measured by thickness monitor and the shutter was closed when required thickness was reached.

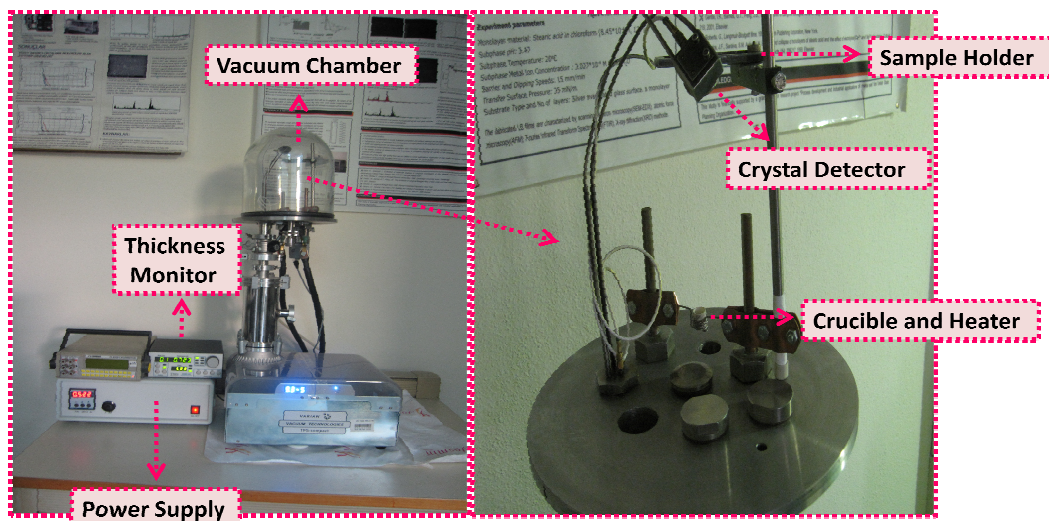


Figure 4.9. The picture of our thermal evaporation system for organic molecules

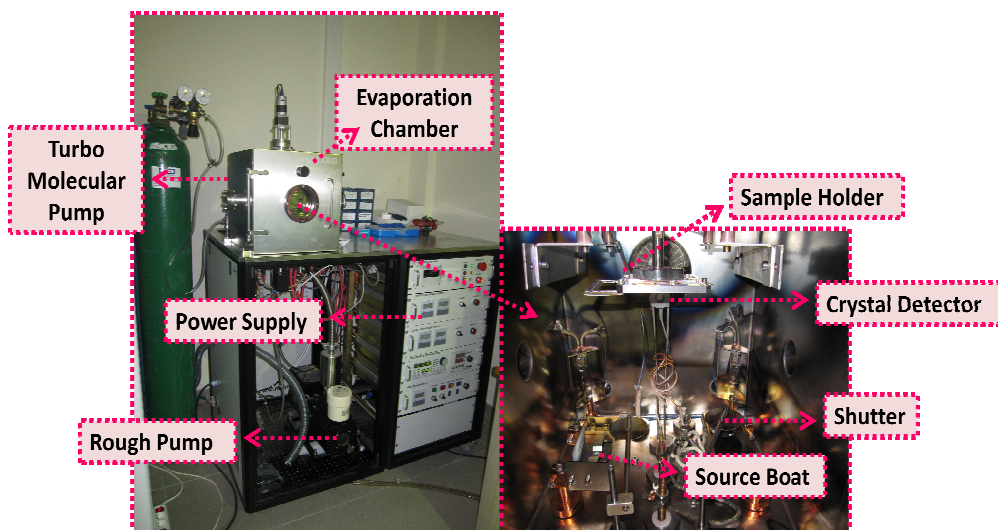


Figure 4.10. The picture of our thermal evaporation system for metals

This technique includes evaporation of the organic material in a ceramic crucible with heating coil as shown in Figure 4.11 (a) and material of metal in filament boat as shown in Figure 4.11 (b) heated by high current source and re-condensation of the heated material from vapor state onto cooler substrate in a vacuum.

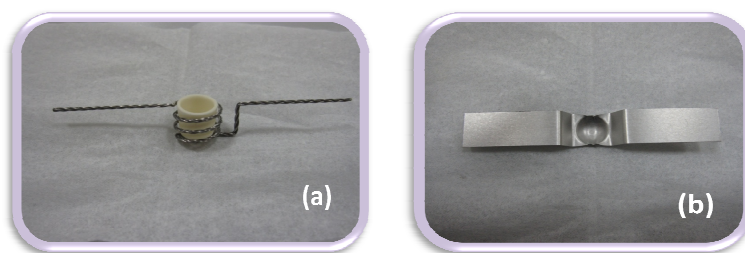


Figure 4.11. Thermal evaporation of material by joule heating from applying bias to (a) heating coil or (b) source boat

After the surface modification, the substrates were loaded onto a sample holder in the thermal evaporator for coating organic layer as shown in Figure 4.9. An NPB (99%, Aldrich Co.) was used as HTL in this work. 50 nm thick of NBP layer was deposited at a rate of  $2-3 \text{ \AA}^0\text{s}^{-1}$  followed by 40 nm thick of  $\text{Alq}_3$  (99.995% trace metals basis Aldrich) that used as EML deposited at a rate of  $1-2 \text{ \AA}^0\text{s}^{-1}$ . Finally, 200 nm thick of Al (99% trace metals basis) was deposited at a rate of  $5-10 \text{ \AA}^0\text{s}^{-1}$  in thermal evaporation coater from NANOVAK Co., Turkey as shown in Figure 4.10. For Al evaporation, a suitable mask was used pattern for the OLEDs as given in Figure 3.4.

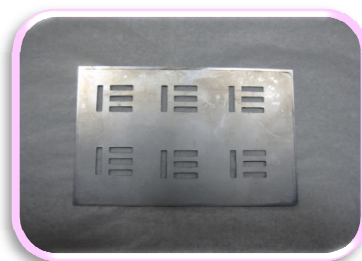


Figure 4.12. Mask pattern used for aluminum evaporation

The active area for the emission of each device was  $0.04 \text{ cm}^2$ . The final device can be seen in Figure 4.13.



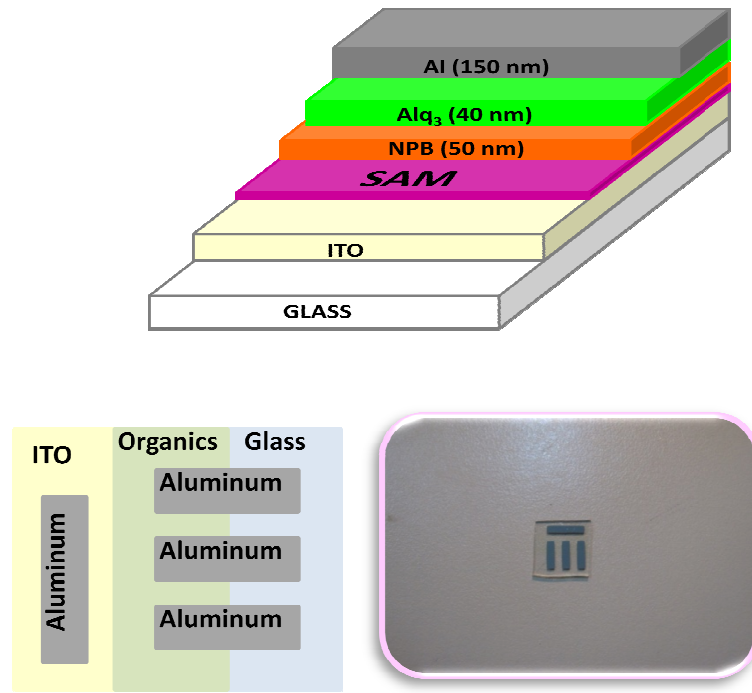


Figure 4.13. The final measurement configurations of OLED

## 4.2. Device Characterization Techniques

This part includes the characterization of OLEDs used in this study. The characterization methods were divided into three parts as electrical characterizations, optical characterizations and surface characterizations. In addition, all measurements were done in ambient air at room temperature without any encapsulation.

### 4.2.1. Electrical Characterization

In order to obtain the current-voltage (I-V) characteristics of the devices, two 0.1 mm copper (Cu) lead wires were connected to electrodes by silver paint using 2-point technique.

The I-V measurement system consisting of a specially designed probe, a Keithley 236 Precision Source-Measure Unit and a Keithley 6517A Electrometer/High resistance Meter, was also computer controlled using a program written in LabView™ as seen in Figure 4.14 and Figure 4.15.

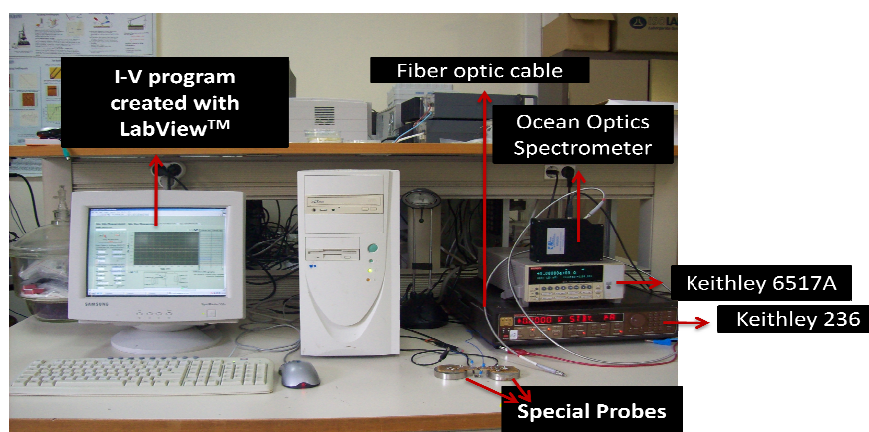


Figure 4.14. The experimental setup of I-V characterization and spectrometer

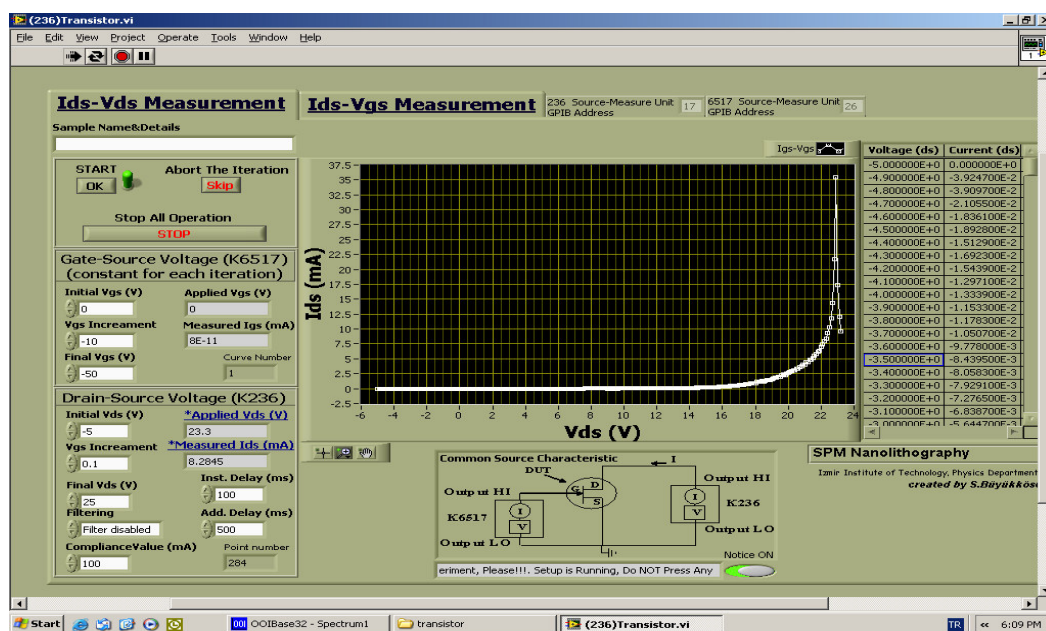


Figure 4.15. I-V program created with LabView™

In addition, the charge transfer between inorganic conductive surface ITO and organic HTL is one of the most important parameters to improve efficiency in the OLEDs. To observe how SAM materials affect the charge transfer between the two surface and to investigate tunneling of charge carriers to the organic semiconductor material between ITO and Al, the current-voltage relationship were examined using Schottky diode characteristics. The device performance of the Schottky diode relies on

electrical and electronic characteristics of the metal/organic semiconductor junction. As a result, the understanding of electronic properties of the interface between metal and organic semiconductor is important for the device application. Furthermore, Space-charge-limited current (SCLC) measurements have been applied to evaluate carrier mobility under steady state of current in an organic layer.

#### 4.2.2. Optical Characterization

Perkin Elmer Lambda 950 model UV-visible spectrometer, shown in Figure 4.16 was used to measure transmittances of the ITOs and SAM-modified ITO substrates.

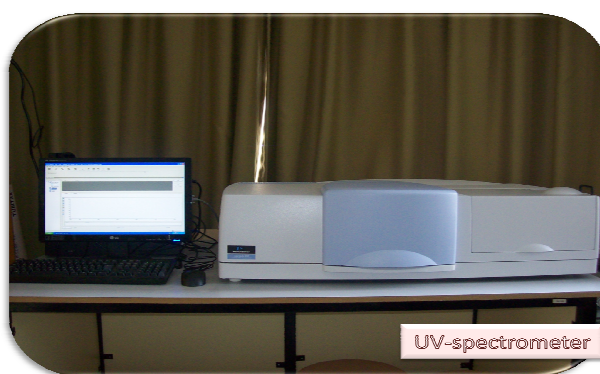


Figure 4.16. UV/VIS/NIR Spectrometer (Perkin Elmer, Lambda 950)

Moreover, electroluminescence spectra's of all OLED devices were recorded with Ocean Optics HR2000 High-Resolution Spectrometer shown in Figure 4.16. The interface program can be shown in Figure 4.17.

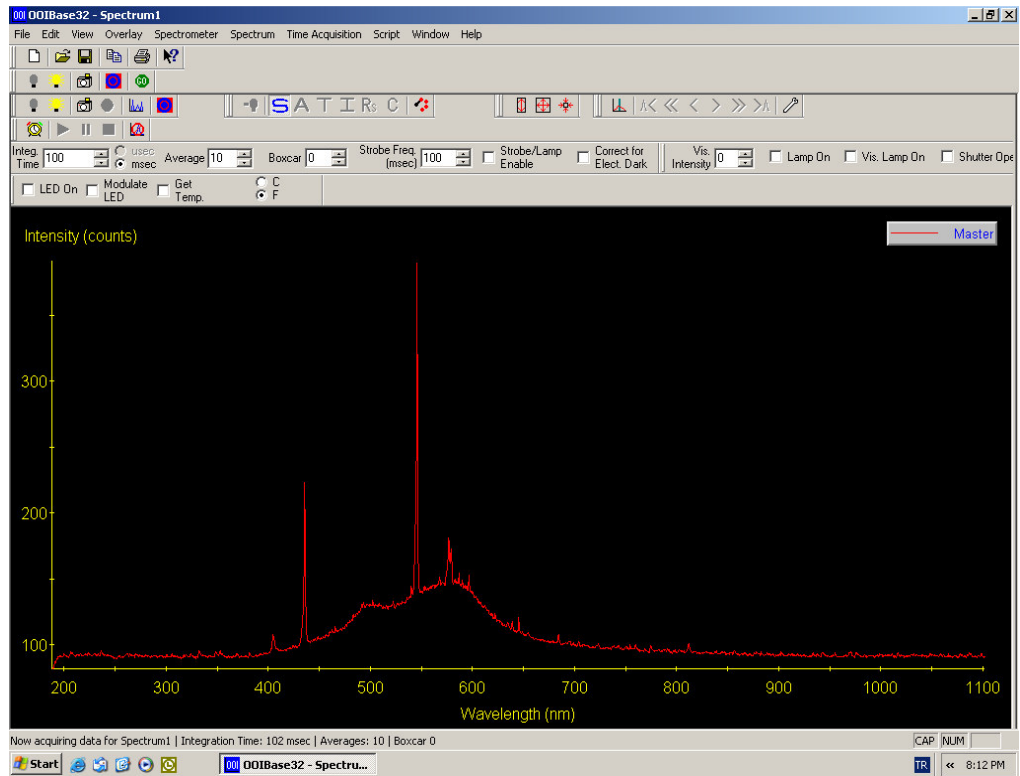


Figure 4.17. The program of EL spectrum (Ocean Optics)

### 4.2.3. Surface Characterization

The Atomic Force Microscopy (AFM) is the foremost tools for imaging, measuring and manipulating films at the nanoscale. The underlying main idea of the AFM working principle is to trace the movement of tip under interactive forces with sample. Schematic representation of AFM system can be seen in Figure 4.18.

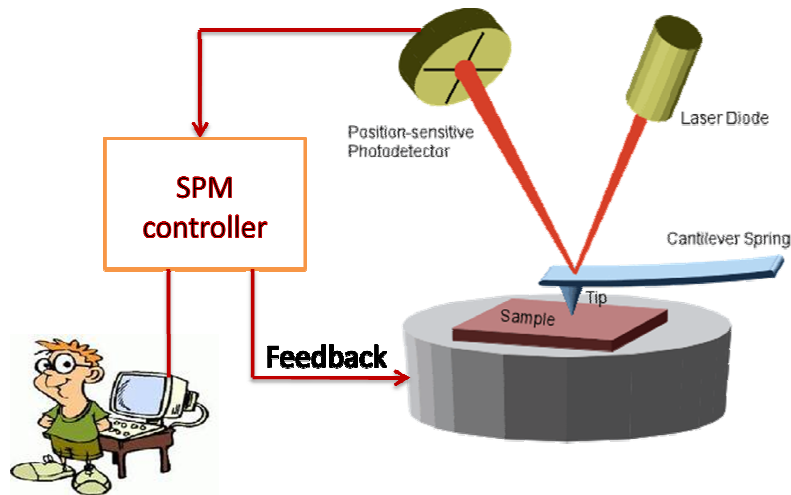


Figure 4.18. Representation of the basic principle of AFM

The morphology of modified ITO surfaces was examined in semi-contact (tapping) mode operation with using commercial Scanning Probe Microscopy instrument (Solver Pro 7 from MNT-MDT, Russia) as shown in Figure 4.19. In semi-contact mode, the cantilever is driven to oscillate up and down at its resonance frequency by a small piezoelectric element mounted in the AFM tip holder. During all scans, a conductive diamond like carbon coated tip (DLC tip from the same company) with a curvature of 75 nm was employed with a closed loop feedback system kept active.  $2 \mu\text{m} \times 2 \mu\text{m}$  areas were chosen for AFM topography analysis of the SAM-modified ITO substrates.

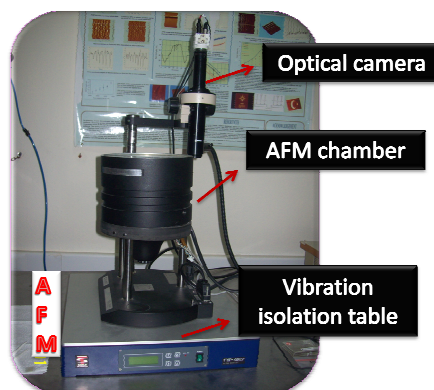


Figure 4.19. The picture of our AFM system

Moreover, in order to observe whether the ITO was modified with SAM, Kelvin Probe Force Microscopy (KPFM) was used to measure work functions of ITO and SAM-modified ITOs. From the difference between the value of the contact potentials of modified and a bare electrode (ITO), the potential shift due to the adsorbed self-assembled monolayer can be determined. Kelvin mode of Scanning Probe Microscopy was used to measure contact potential difference between the probe and the sample (Nonnenmacher et al., 1991). Kelvin mode is based on the two-pass technique. In the first pass the topography is reached using standard semi-contact mode (mechanical excitation of the cantilever). In the second pass this topography is retraced at a set lift height from the sample surface to detect the electric surface potential  $\Phi(x)$  ([www.ntmdt.com](http://www.ntmdt.com)). During this second pass the cantilever is no longer excited mechanically but electrically by applying to the tip the voltage containing dc and ac components.

## CHAPTER 5

### RESULTS AND DISCUSSION

The basic idea of this study is to enhance hole injection at the interface of ITO/NPB by self-assembly monolayer technique. For this purpose, eleven different SAM molecules are used. In this chapter, experimental results for OLEDs are given and the characterization features are explained briefly using theoretical predictions of the device properties.

#### 5.1. Optical Characterization Results

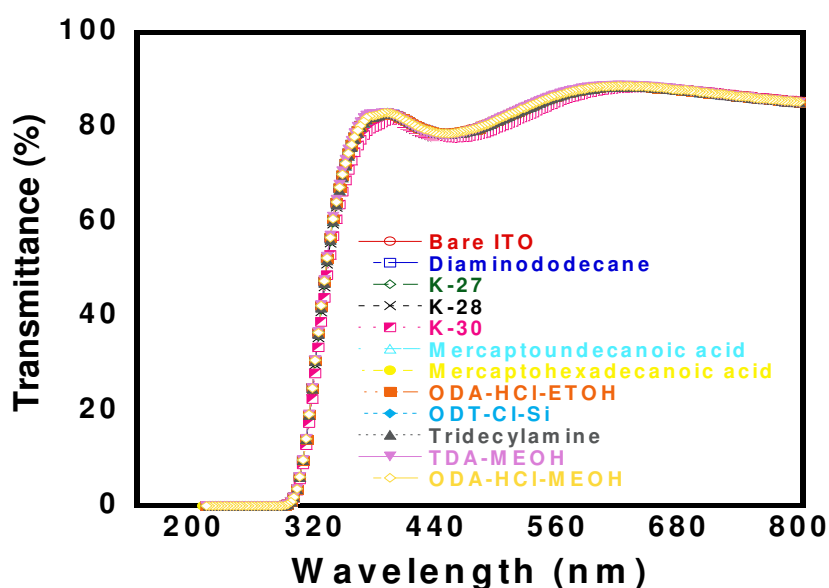


Figure 5.1. UV-VIS spectra result of bare ITO and modified ITO with various SAMs

Figure 5.1 shows UV-VIS spectrum results of bare ITO and SAM-modified ITOs. The transmittance of an ITO with SAM was not changed by the presence of a SAM, because SAM molecules create very thin monolayer with one molecule in length. These results depict that the SAM process does not induce any structural and/or

chemical changes at the surface that can influence the optical properties (Jee et al., 2006).

## **5.2. Surface Characterization Results**

We classified eleven SAM molecules used in this study into four different groups to analyze them easily. Ru complexes, K-27, K-28 and K-30, are the first group. MDA and MHDA are the second group. DDA and TDA are the third group and finally ODA (ETOH), ODA (MEOH), TDA-1 and ODT-Cl-Si are taken as fourth group. AFM and KPFM are used for surface characterization.

### **5.2.1. Atomic Force Microscopy Results**

The surface morphology of bare ITO and SAMs on ITO was observed by AFM in tapping mode, sampling  $2\mu\text{m}\times 2\mu\text{m}$  scan areas. Two-dimensional topographic images of bare ITO and modified ITO with various SAMs are given in below. Moreover, the effect of NPB thin film on the substrate was studied for the two groups of SAMs to observe changes of surface structure. Figure 5.2 shows AFM images of bare ITO, ITO/K-27, ITO/K-28, ITO/K-30, ITO/NPB, ITO/K-27/NPB, ITO/K-28/NPB and ITO/K-30/NPB. Figure 5.3 shows AFM images of bare ITO, ITO/MHDA and ITO/MDA. Figure 5.4 shows AFM images of bare ITO, ITO/DDA and ITO/TDA. Figure 5.5 shows AFM images of bare ITO, ITO/ODA-HCl-ETOH, ITO/ODA-HCl-MEOH, ITO/TDA-1, ITO/ODT-Cl-Si, ITO/NPB, ITO/ODA-HCl-ETOH/NPB, ITO/ODA-HCl-MEOH/NPB, ITO/TDA-1/NPB and ITO/ODT-Cl-Si/NPB. As it is seen from the topography images, no significant change of surface morphology was observed on ITO after the SAM formation. SAM-modified ITO substrates and bare ITO have similar surface features since SAM molecules create very thin monolayer with a thickness of 2nm.



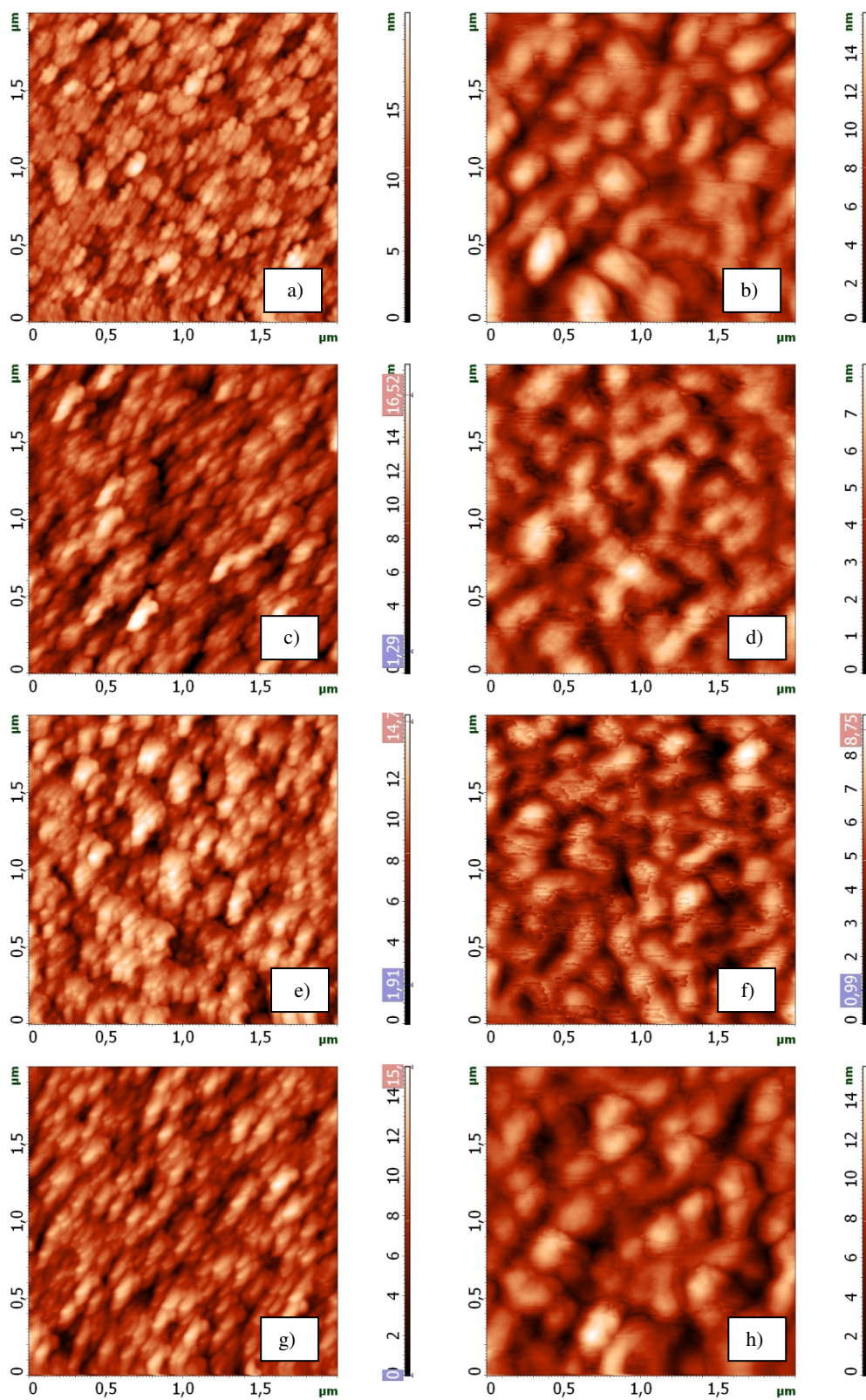


Figure 5.2. Surface topography image of a) bare ITO, b) ITO/NPB, c) ITO/K-27, d) ITO/K-27/NPB, e) ITO/K-28, f) ITO/K-28/NPB, g) ITO/K-30 and h) ITO/K-30/NPB surface with  $2\mu\text{m}\times 2\mu\text{m}$  scan area

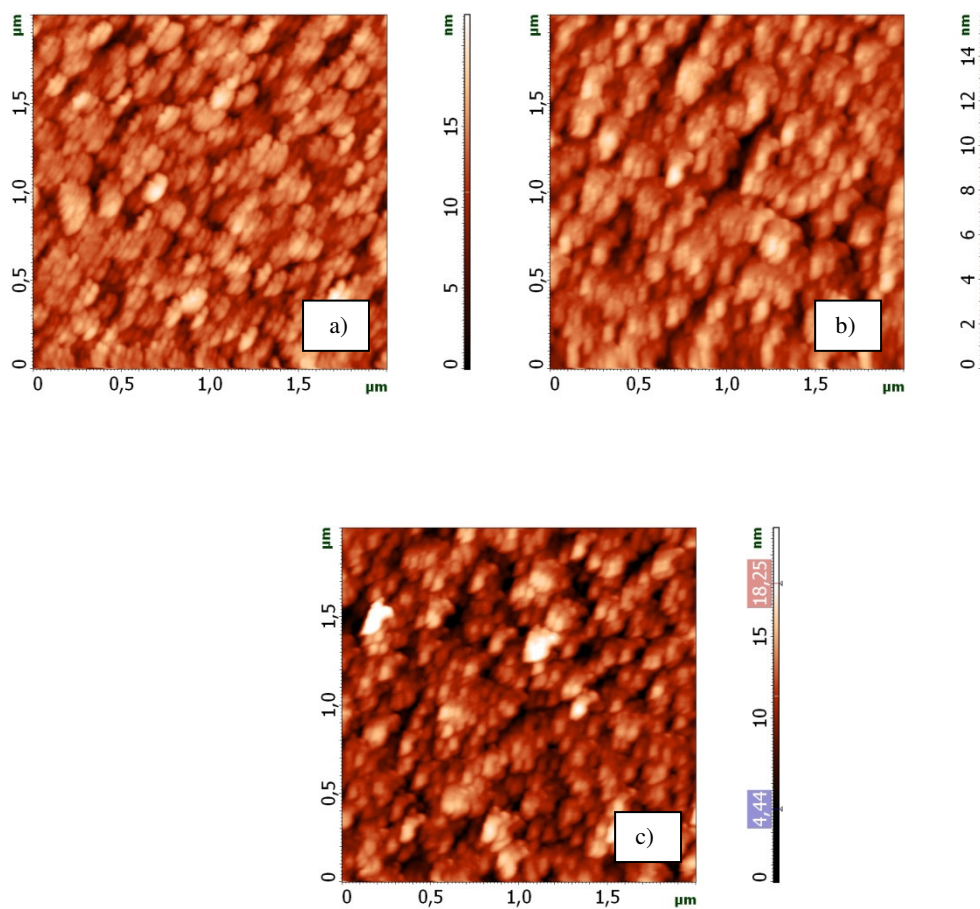


Figure 5.3. Surface topography image of a) bare ITO, b) ITO/MHDA and c) ITO/MDA surface with  $2\mu\text{m}\times 2\mu\text{m}$  scan area

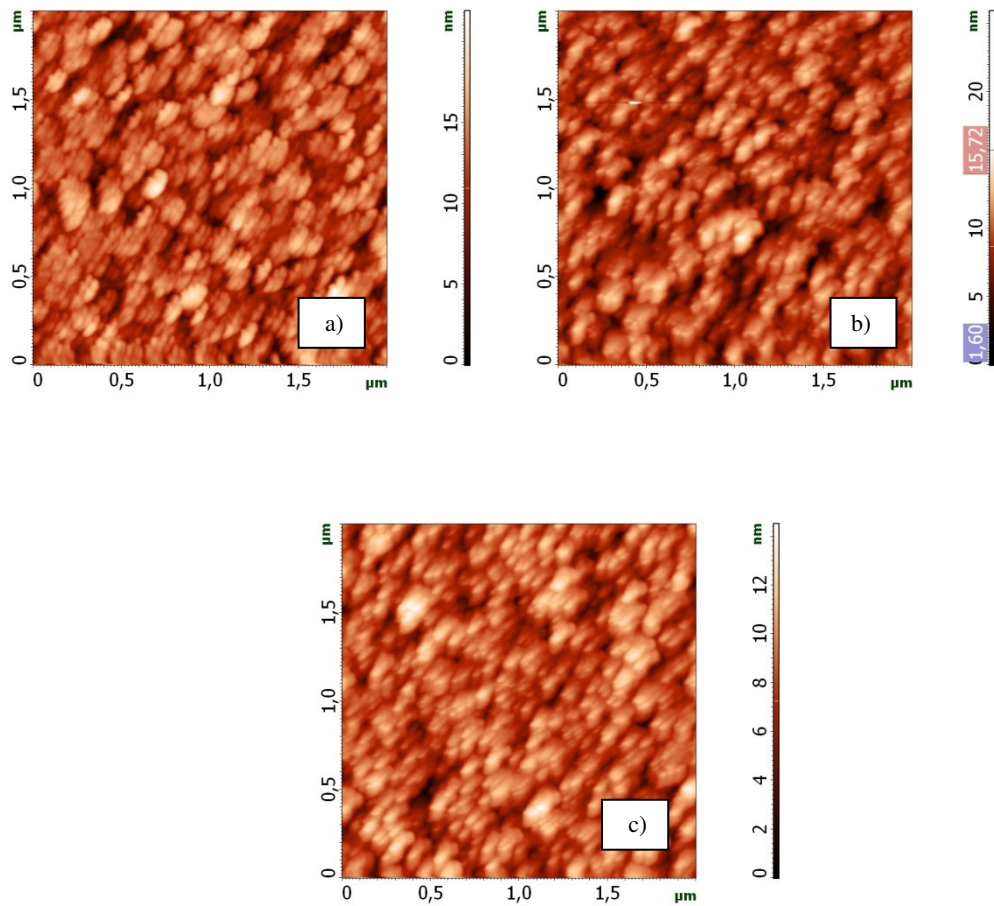


Figure 5.4. Surface topography image of a) bare ITO b) ITO/DDA and c) ITO/TDA surface with  $2\mu\text{m}\times 2\mu\text{m}$  scan area

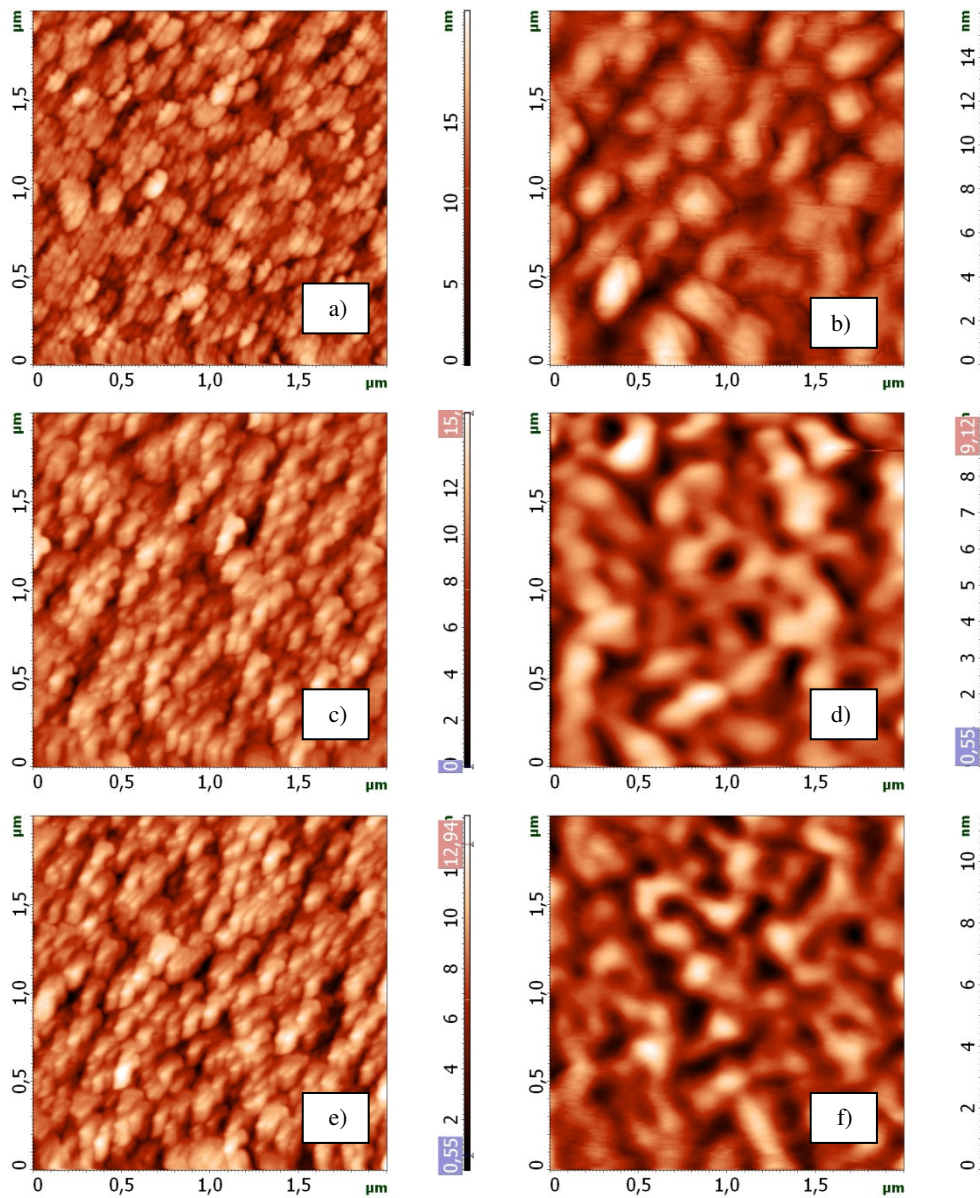


Figure 5.5. Surface topography image of a) bare ITO, b) ITO/NPB, c) ITO/ODA-HCl-ETOH, d) ITO/ODA-HCl-ETOH/NPB, e) ITO/ODA-HCl-MEOH, f) ITO/ODA-HCl-MEOH/NPB, g) ITO/TDA-1, h) ITO/TDA-1/NPB, i) ITO/ODT-Cl-Si and j) ITO/ODT-Cl-Si/NPB surface with  $2\mu\text{m}\times 2\mu\text{m}$  scan area

(cont. on next page)

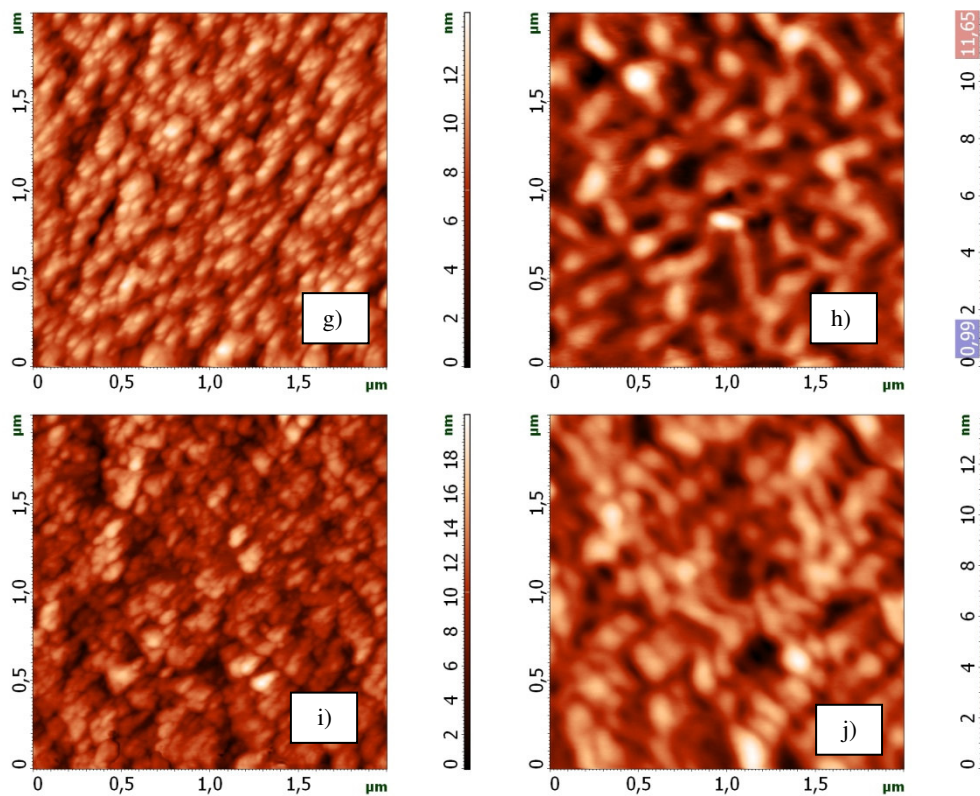


Figure 5.5. (cont.)

In addition, the surface roughness estimated from the AFM images show the differences of the bare ITO and the SAM modified-ITO morphologies. Root mean square (RMS) gives roughness information about the surface of the substrate. Therefore, to distinguish the surface morphology differences caused by SAM formation and NPB material deposition, roughness analysis were taken for topography images indicated above. RMS roughness of SAMs modified ITOs and bare ITO is given in Table 5.1, Table 5.2, Table 5.3 and Table 5.4 for the four groups of SAMs, respectively.

Table 5.1. Roughness values of bare ITO, ITO/K-27, ITO/K-28, ITO/K-30, ITO/NPB, ITO/K-27/NPB, ITO/K-28/NPB and ITO/K-30/NPB

Thin Films	Roughness (rms)
Bare ITO	2.81335 nm
ITO/K-27	2.32295 nm
ITO/K-28	2.05235 nm
ITO/K-30	2.07858 nm
ITO/NPB	2.29328 nm
ITO/K-27/NPB	1.23428 nm
ITO/K-28/NPB	1.22401 nm
ITO/K-30/NPB	2. 30771 nm

Table 5.2. Roughness values of bare ITO, ITO/MHDA and ITO/MDA

Thin Films	Roughness (rms)
Bare ITO	2.81335 nm
ITO/MHDA	2.23186 nm
ITO/MDA	2.43863 nm

Table 5.3. Roughness values of bare ITO, ITO/DDA and ITO/TDA

Thin Films	Roughness (rms)
Bare ITO	2.81335 nm
ITO/DDA	1.91059 nm
ITO/TDA	1.83069 nm

Table 5.4. Roughness values bare ITO, ITO/ODA-HCl-ETOH, ITO/ODA-HCl-MEOH, ITO/TDA-1, ITO/ODT-CI-Si, ITO/NPB, ITO/ODA-HCl-ETOH/NPB, ITO/ODA-HCl-MEOH/NPB, ITO/TDA-1/NPB and ITO/ODT-CI-Si/NPB

Thin Films	Roughness (rms)
Bare ITO	2.81335 nm
ITO/ODA-HCl-ETOH	1.93015 nm
ITO/ODA-HCl-MEOH	1.87838 nm
ITO/TDA-1	1.90614 nm
ITO/ODT-CI-Si	2.58813 nm
ITO/NPB	2.29328 nm
ITO/ODA-HCl-ETOH/NPB	1.49190 nm
ITO/ODA-HCl-MEOH/NPB	1.84773 nm
ITO/TDA-1/NPB	1.69804 nm
ITO/ODT-CI-Si/NPB	2.06678 nm

The results show that ITO has a rough surface. The RMS roughness of bare ITO was obtained as 2.81335 nm, which is expected to severely limit adsorbate mobility and disrupt the circulation of solution over the surface (Hatton et al., 2001). As it is seen from the tables, all SAM molecules improve the surface roughness. With the SAM

modification, the roughness of the ITO surface decreases. The most effective one is TDA measured as 1.83069 nm. Moreover, Table 5.1 and Table 5.4 shows that the film morphology becomes smoother with the NPB film coating due to the deposit filling into cavities (Chong et al., 2007). The thickness of NPB film is 50 nm used in constructing the OLED device. The RMS roughness decreases further to about 1 nm for substrates ITO and SAM-modified ITOs. The present results show that the interfacial morphology of NPB film is sensitively affected by the surface composition of substrate. On the other hand, the substrate effect on the surface morphology becomes less significant with increase of film thickness (Chong et al., 2007).

### **5.2.2. Kelvin Probe Force Microscopy Results**

Local contact potential difference (CPD) of self-assembled monolayer on ITO substrates and bare ITO were investigated with conductive TiN tip by KPFM. The Kelvin Probe Surface Potential Current versus Bias Voltage plots of bare ITO and SAM modified ITO surfaces with Ru complexes, MHDA, MDA, DDA, TDA, ODA-HCl, TDA-1 and ODT-Cl-Si are shown in Figure 5.6, Figure 5.7, Figure 5.8 and Figure 5.9, respectively. The surface potential values of bare ITO and SAM modified ITOs is given in Table 5.5, Table 5.6, Table 5.7 and Table 5.8.



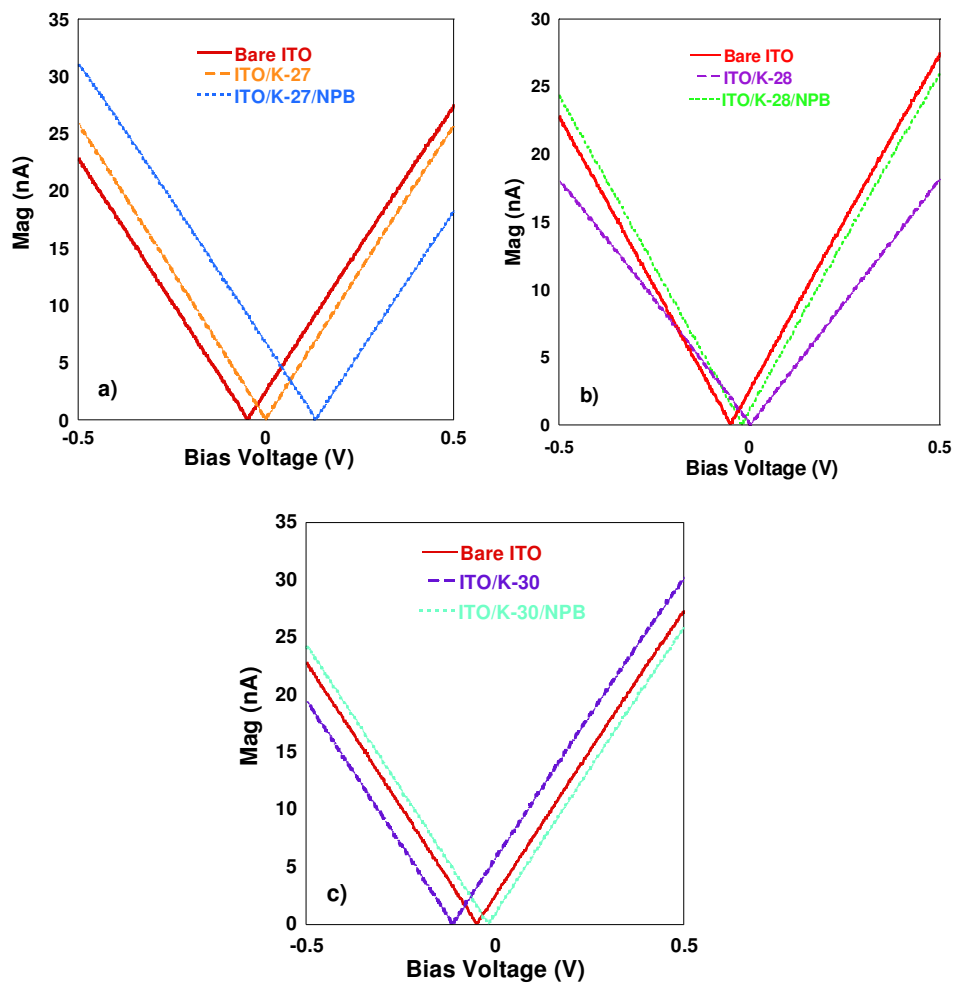


Figure 5.6. The local contact potential difference of bare ITO and SAM modified ITO a) K-27, b) K-28 and c) K-30

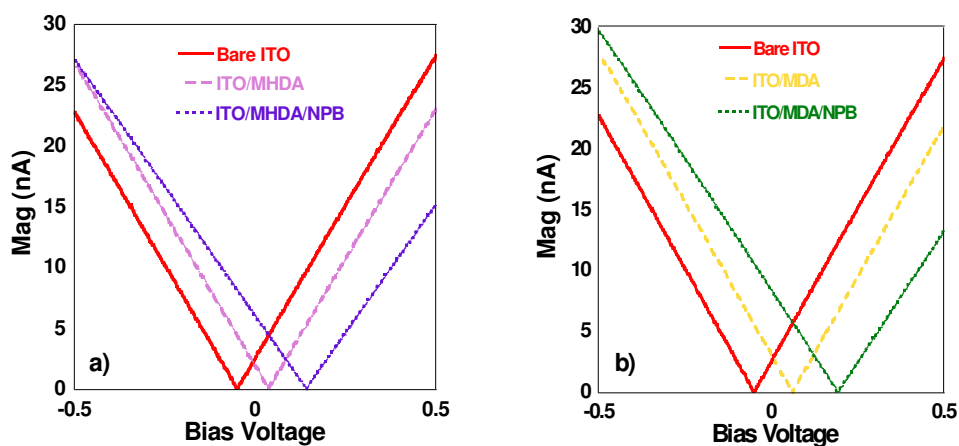


Figure 5.7. The local contact potential difference of bare ITO and SAM modified ITO a) MHDA and b) MDA

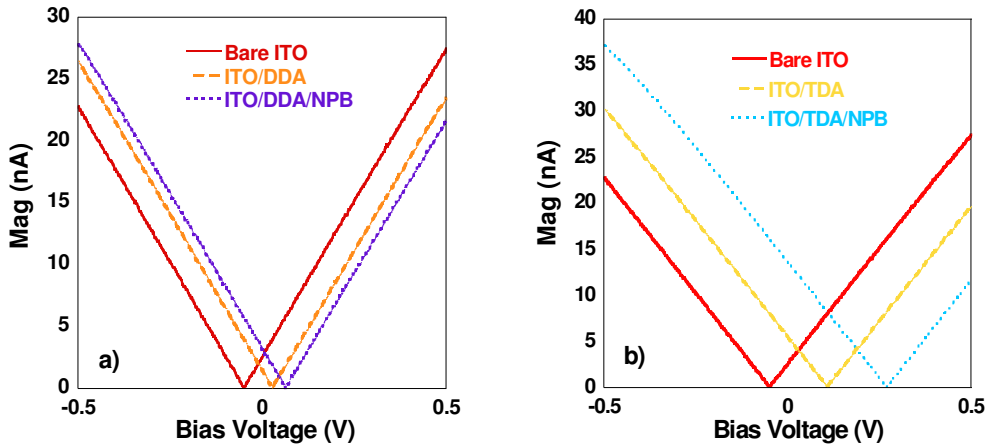


Figure 5.8. The local contact potential difference of bare ITO and SAM modified ITO a) DDA and b) TDA

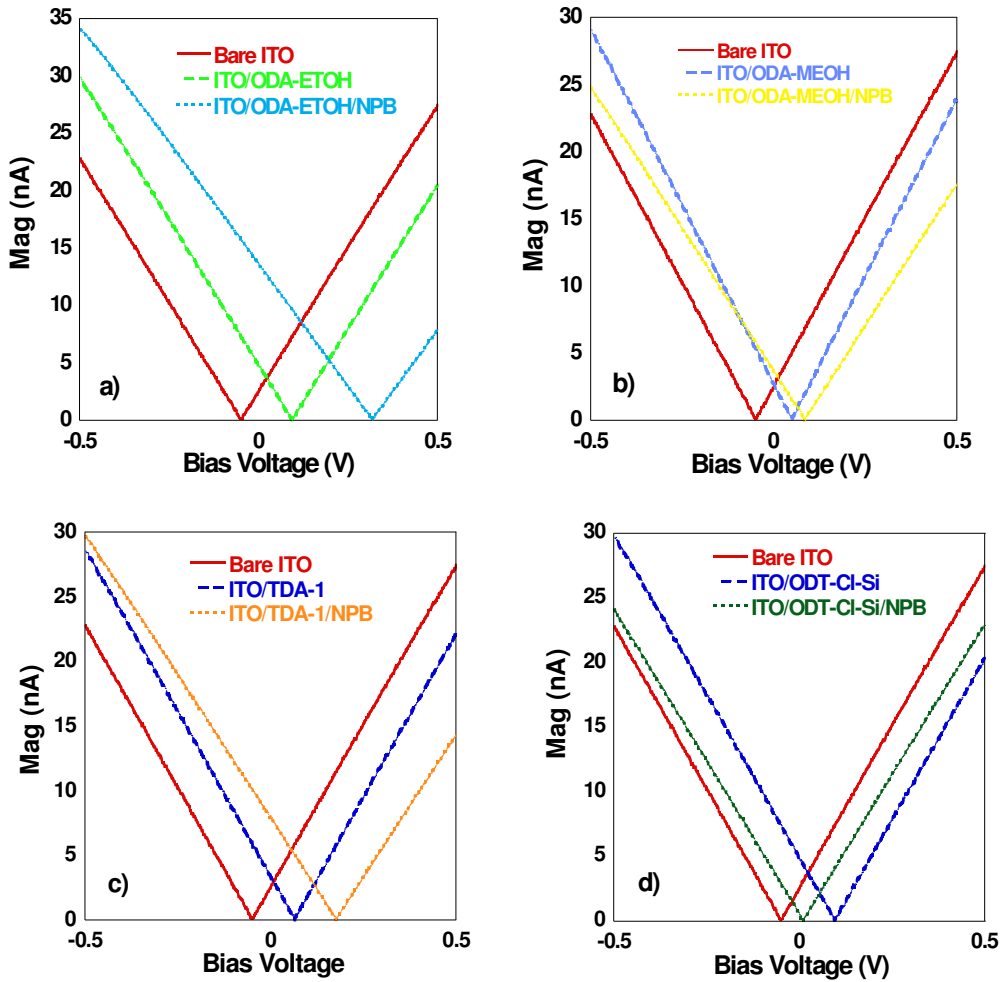


Figure 5.9. The local contact potential difference of bare ITO and SAM modified ITO a) ODA-HCl-ETOH, b) ODA-HCl-MEOH, c) TDA-1 and d) ODT-Cl-Si

Table 5.5. The measured surface potentials of bare ITO and K-27, K-28 and K-30 modified ITOs

Thin Films	Surface Potential (mV)
Bare ITO	-52.23 mV
ITO/K-27	2.48 mV
ITO/K-28	4.46 mV
ITO/K-30	-115.59 mV
ITO/K-27/NPB	131.84 mV
ITO/K-28/NPB	-20.00 mV
ITO/K-30/NPB	-18.81 mV

Table 5.6. The measured surface potentials of bare ITO and MHDA and MDA modified ITOs

Thin Films	Surface Potential (mV)
Bare ITO	-52.23 mV
ITO/MDA	36.58 mV
ITO/MDA/NPB	139.56 mV
ITO/MHDA	64.23 mV
ITO/MHDA/NPB	192.69 mV

Table 5.7. The measured surface potentials of bare ITO and DDA and TDA modified ITOs

Thin Films	Surface Potential (mV)
Bare ITO	-52.23 mV
ITO/DDA	26.73 mV
ITO/DDA/NPB	61.49 mV
ITO/TDA	105.59 mV
ITO/TDA/NPB	270.99 mV

Table 5.8. The measured surface potentials of bare ITO and ODA-HCl-ETOH, ODA-HCl-MEOH, TDA-1 and ODT-Cl-Si modified ITOs

Thin Films	Surface Potential (mV)
Bare ITO	-52.23 mV
ITO/ODA-ETOH	91.62 mV
ITO/ODA-MEOH	48.38 mV
ITO/TDA-1	64.98 mV
ITO/ODT-Cl-Si	95.85 mV
ITO/ODA-ETOH/NPB	316.75 mV
ITO/ODA-MEOH/NPB	83.33 mV
ITO/TDA-1/NPB	176.39 mV
ITO/ODT-Cl-Si/NPB	7.77 mV

These results show that the surface potentials of SAM modified ITOs are increased with respect to the bare ITO. According to Figure 5.6 and Table 5.5, K-27 and K-28 increase the surface potential about 55 mV. However, K-30 decreases the surface potential value about 63 mV. From Figure 5.7 and Table 5.6, it is clear that the surface potential values are changed by SAM formation with MHDA and MDA. In this group, MHDA increases the surface potential as the most up to 116 mV. For the third group, it can be said that TDA improves the surface potential as the most about 157 mV as shown in Table 5.7. Moreover, for the fourth group, the surface potential increased by the silane SAM as the most about 148 mV. Chlorosilanes spontaneously self-assemble onto a wide range of ITO surfaces (Malinsky et al., 1999) and they are known to bind to oxide surfaces via covalent bond. Accordingly, our KPFM results confirmed this.

Briefly, these results revealed that the surface potential values are increased by the presence of SAM molecules. These increments confirm the monolayer formation on ITO surface. That means the surface potential differences show the modification of ITO surface with SAM molecules. In addition, change in surface potential also shows the increments in the work function of the surface because contact surface potential proportional to the work function of the surface. As a result of this, Fermi level of the ITO surface approaches to the HOMO level of the organic layer with the SAM modification. Therefore, the carrier injection enhanced with the decreasing threshold voltage.

### **5.3. Electrical Characterization Results**

In this part, Space-charge-limited current model was used to calculate carrier mobility of our devices to find out the contribution of SAM molecule on devices. And then barrier height was obtained using Thermionic Schottky model. And finally, current-voltage and EL spectrum were measured to distinguish the effect of SAM on OLED devices.

#### **5.3.1. Space Charge Limited Current Results**

J-V characteristics show two distinct regions at low and high biases such as Schottky thermionic region and SCLC region respectively. At high voltages, J-V

characteristics switch to the SCLC. At high voltages, the carriers eventually fill up all the trap states in the organic film and the OLED operates in a space-charge-limited conduction regime (Chu and Song, 2007; Khan et al., 2008). In this regime, the injected charge eventually builds up an interfacial field opposite to the injecting electrodes which limits further injection of charge into the device. The SCLC can be expressed as;

$$J = \frac{9}{8} \varepsilon \varepsilon_0 \mu \frac{E^2}{L} \quad (5.1)$$

where  $E$  is the electric field,  $\varepsilon$  and  $\varepsilon_0$  are the relative dielectric constant and the permittivity of the free space, respectively, and  $L$  is the thickness of the organic layer. The carrier mobility  $\mu$  is affected by the energetic disorder because of the interaction of hopping charges with randomly oriented and randomly located dipoles in the organic thin film (Malliaras et al., 1998). Therefore, the mobility is dependent on the electric field and can be expressed by a Poole-Frenkel (PF) equation (Patel et al., 2002),

$$\mu(E) = \mu_0 \exp(\beta\sqrt{E}) \quad (5.2)$$

where  $\mu_0$  is the zero-field mobility and  $\beta$  is Poole-Frenkel factor. From the combination of Eqs. 5.1 and 5.2, the field dependent SCLC can be easily expressed as follows;

$$J = \frac{9}{8} \varepsilon \varepsilon_0 \frac{E^2}{L} \mu_0 \exp(\beta\sqrt{E}) \quad (5.3)$$

SCLC measurements have been used to evaluate carrier mobility under steady state current in an organic layer to evaluate the hole mobility of hole transport layer NPB with SAM molecules. Figure 5.10 shows the current density-voltage characteristics of Ru complex with device configurations: ITO/K-27/NPB/Al, ITO/K-28/NPB/Al, ITO/K-30/NPB/Al and ITO/NPB/Al. Figure 5.11 shows the current

density-voltage characteristics for the modified and bare diodes with device configurations of ITO/MDA/NPB/Al, ITO/MHDA/NPB/Al and ITO/NPB/Al. Figure 5.12 shows the current density-voltage characteristics of modified and bare diodes with the configuration of ITO/NPB/Al, ITO/DDA/NPB/Al and ITO/TDA/NPB/Al. Figure 5.13 depicts the current density-voltage characteristics of modified and bare devices with device configurations: ITO/NPB/Al, ITO/ODA-HCl-ETOH/NPB/Al, ITO/ODA-HCl-MEOH/NPB/Al, ITO/TDA-1/NPB/Al and ITO/ODT-Cl-Si/NPB/Al.

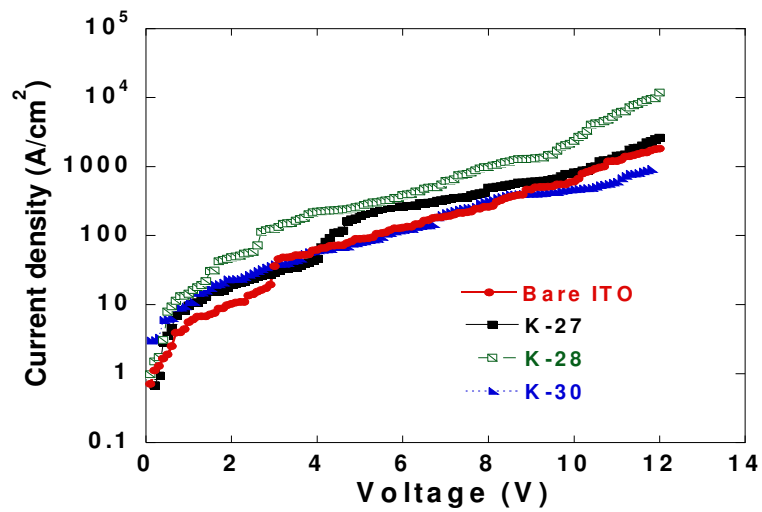


Figure 5.10. Current density vs voltage (J-V) characteristics for the devices: ITO/K-27/NPB/Al, ITO/K-28/NPB/Al, ITO/K-30/NPB/Al and ITO/NPB/Al. The thickness of NPB was kept constant for all diodes.

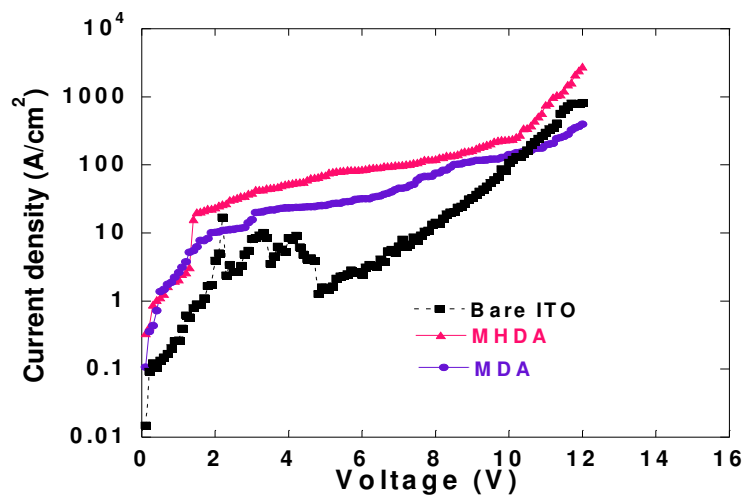


Figure 5.11. Current density vs voltage (J-V) characteristics for diodes with the configuration of: ITO/MDA/NPB/Al, ITO/MHDA/NPB/Al and ITO/NPB/Al. The thickness of NPB was kept constant for all diodes.

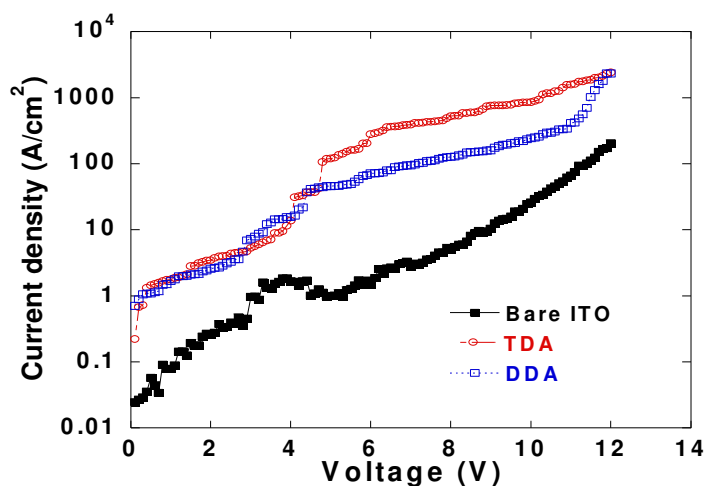


Figure 5.12. Current density vs voltage (J-V) characteristics for diodes with the configuration of: ITO/DDA/NPB/Al, ITO/TDA/NPB/Al and ITO/NPB/Al. The thickness of NPB was kept constant for all diodes.



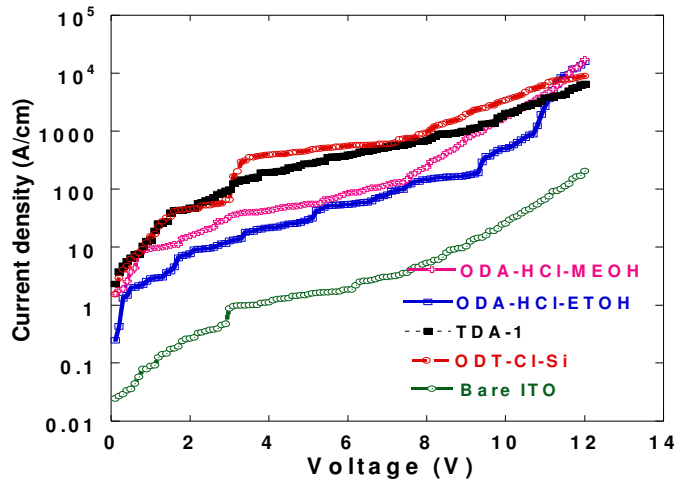


Figure 5.13. Current density vs voltage (J-V) characteristics for the devices: ITO/ODA-HCl-ETOH/NPB/Al, ITO/ODA-HCl-MEOH/NPB/Al, ITO/ODT-CI-Si/NPB/Al, ITO/TDA-1/NPB/Al and ITO/NPB/Al. The thickness of NPB was kept constant for all diodes.

Using current density-voltage characteristics, the logarithm of  $J/E^2$  versus the square root of the mean electric field was obtained as shown in Figure 5.14, Figure 5.15, Figure 5.16 and Figure 5.17, respectively.

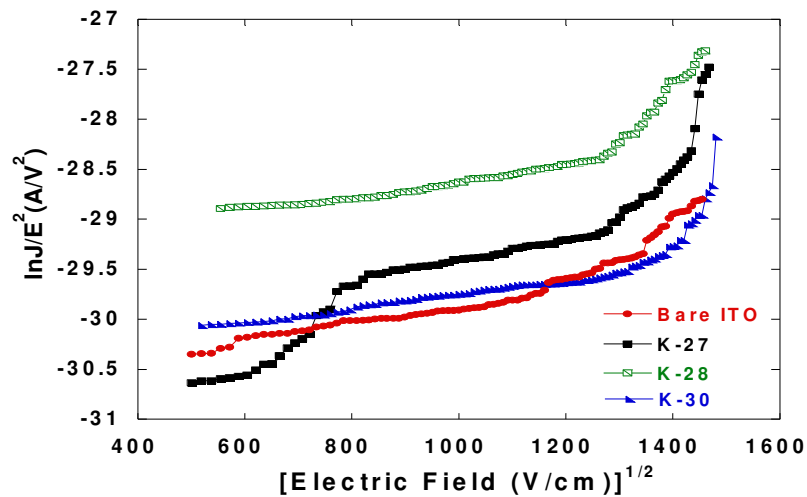


Figure 5.14. The logarithm of  $J/E^2$  versus the square root of the applied electric field for ITO/K-27/NPB/Al, ITO/K-28/NPB/Al, ITO/K-30/NPB/Al and ITO/NPB/Al diodes

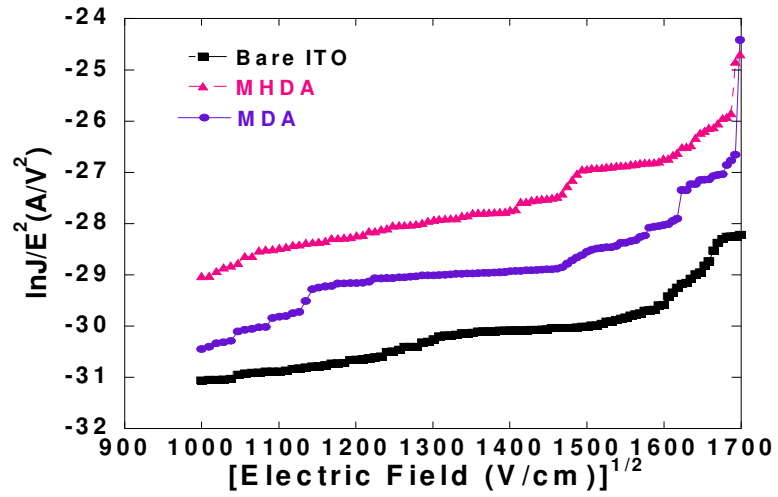


Figure 5.15. The logarithm of  $J/E^2$  versus the square root of the applied electric field for ITO/MDA/NPB/Al, ITO/MHDA/NPB/Al and ITO/NPB/Al diodes

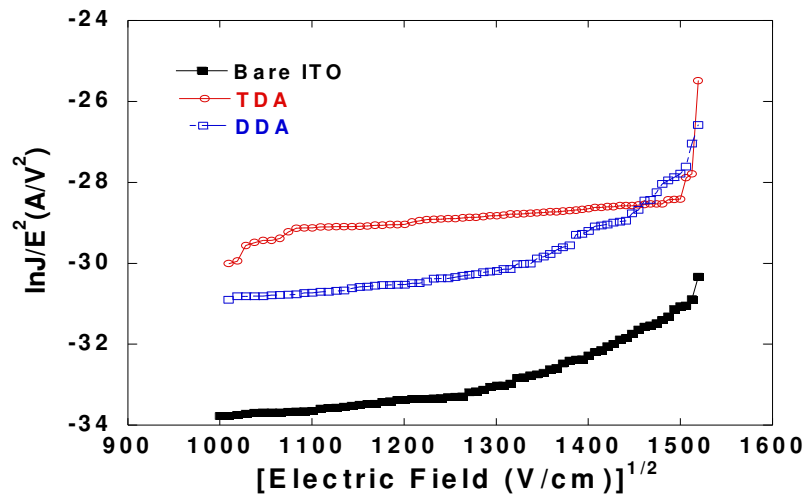


Figure 5.16. The logarithm of  $J/E^2$  versus the square root of the applied electric field for ITO/DDA/NPB/Al, ITO/TDA/NPB/Al and ITO/NPB/Al diodes

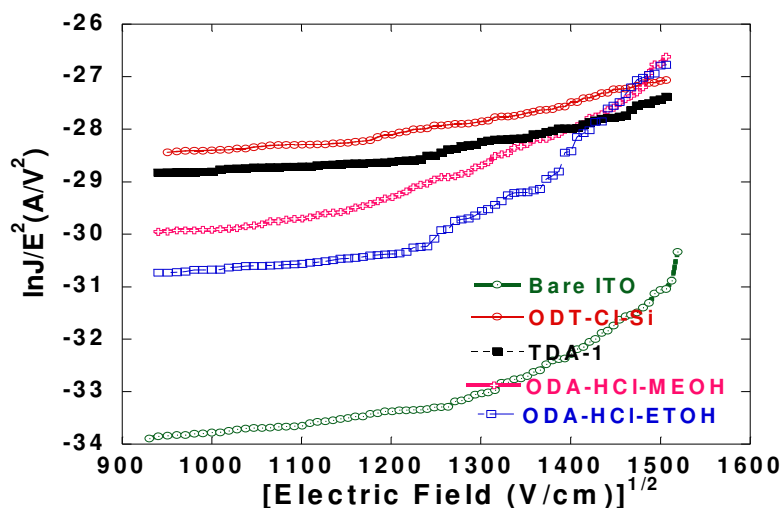


Figure 5.17. The logarithm of  $J/E^2$  versus the square root of the applied electric field for ITO/TDA-1/NPB/Al, ITO/ODA-HCl-ETOH/NPB/Al, ITO/ODA-HCl-MEOH/NPB/Al, ITO/ODT-Cl-Si/NPB/Al and ITO/NPB/Al diodes

The parameters  $\beta$  and zero-field mobility ( $\mu_0$ ) were obtained from the slope and the intercept of  $\log(J/E^2)$  versus  $\sqrt{E}$ , respectively. In all calculations, the relative dielectric constant  $\epsilon$  is assumed to be 3 (Chu and Song, 2007) and the permittivity of the free space  $\epsilon_0$  is taken as  $8.85 \times 10^{-12}$  F/m. For each group of SAM,  $\mu$  versus  $\sqrt{E}$  can be obtained from Figure 5.14, Figure 5.15, Figure 5.16 and Figure 5.17, respectively. Figure 5.18, Figure 5.19, Figure 5.20 and Figure 5.21 show the field dependence of hole mobility of NPB with SAM molecules.

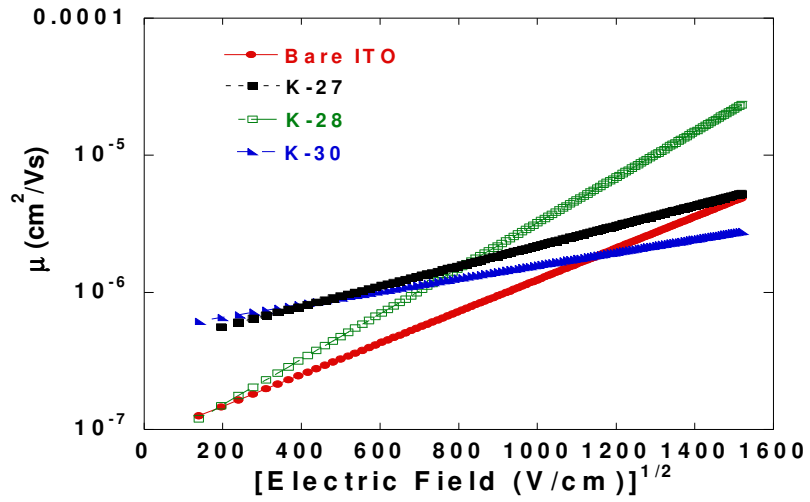


Figure 5.18. The carrier mobility  $\mu$  of ITO/K-27/NPB/Al, ITO/K-28/NPB/Al, ITO/K-30/NPB/Al and ITO/NPB/Al diodes with varying electric field

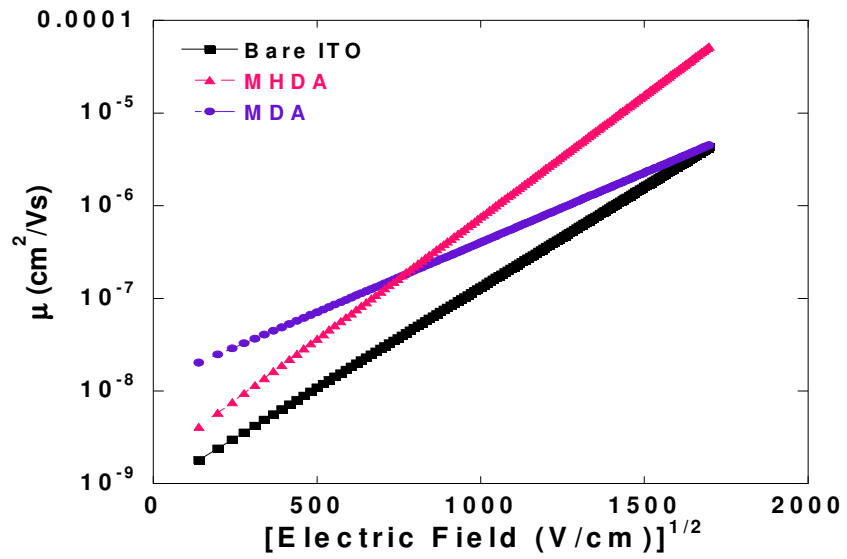


Figure 5.19. The carrier mobility  $\mu$  of ITO/MDA/NPB/Al, ITO/MHDA/NPB/Al and ITO/NPB/Al diodes with varying electric field

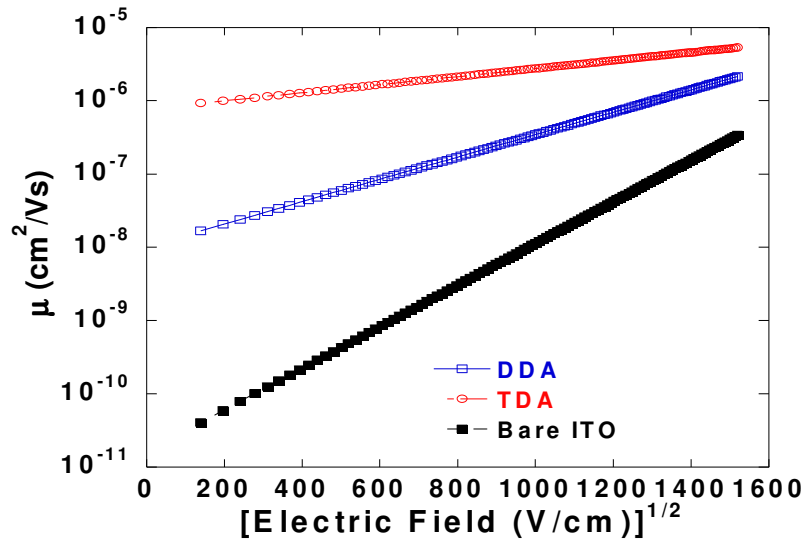


Figure 5.20. The carrier mobility  $\mu$  of ITO/DDA/NPB/Al, ITO/TDA/NPB/Al and ITO/NPB/Al diodes with varying electric field

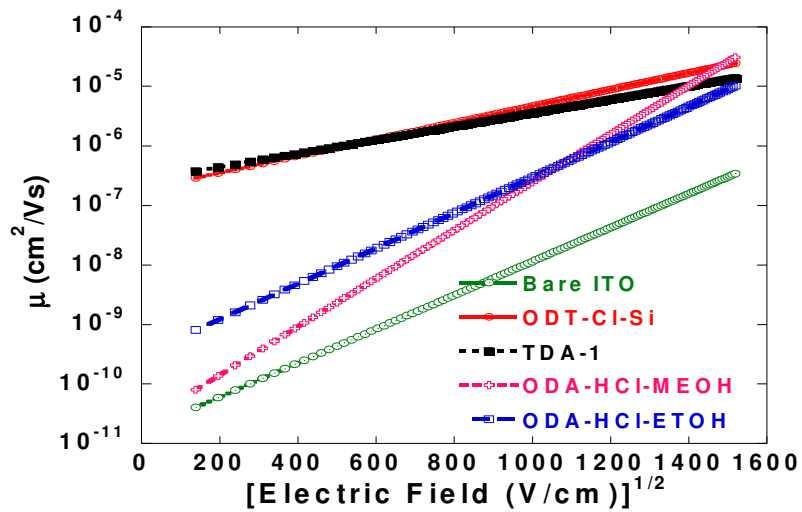


Figure 5.21. The carrier mobility  $\mu$  of ITO/ODA-HCl-ETOH/NPB/Al, ITO/ODA-HCl-MEOH/NPB/Al, ITO/TDA-1/NPB/Al, ITO/ODT-CI-Si/NPB/Al and ITO/NPB/Al diodes with varying electric field

The hole mobilities of bare ITO/NPB/Al, ITO/K-27/NPB/Al, ITO/K-28/NPB/Al and ITO/K-30/NPB/Al were obtained  $4.6 \times 10^{-6} \text{ cm}^2/\text{Vs}$ ,  $5.2 \times 10^{-6} \text{ cm}^2/\text{Vs}$ ,  $2.3 \times 10^{-5} \text{ cm}^2/\text{Vs}$  and  $2.7 \times 10^{-6} \text{ cm}^2/\text{Vs}$  at  $1500 \text{ (V/cm}^2)^{1/2}$  respectively as shown in Figure 5.18. The Space-Charge-Limited Current analysis results show that the charge mobility of NPB hole transport material on ITO increases by using K-28 compare to the others in

this group. In addition, K-27 is almost the same as bare one. As seen Figure 5.18, K-30 has been affecting the mobility of NPB very little in comparison.

The hole mobilities of ITO/NPB/Al, ITO/MDA/NPB/Al and ITO/MHDA/NPB/Al diodes were obtained as  $3.0 \times 10^{-6} \text{ cm}^2/\text{Vs}$ ,  $3.2 \times 10^{-5} \text{ cm}^2/\text{Vs}$  and  $2.3 \times 10^{-6} \text{ cm}^2/\text{Vs}$  at  $1600 \text{ (V/cm}^2)^{1/2}$  respectively as shown in Figure 5.19. The Space-Charge-Limited Current analysis results indicate that the charge mobility of NPB hole transport material on ITO increases by using MHDA compare to the others in this group. In addition, MDA gives almost the same result as bare one.

The hole mobility of bare ITO/NPB/Al, ITO/DDA/NPB/Al and ITO/TDA/NPB/Al were obtained  $2.9 \times 10^{-7} \text{ cm}^2/\text{Vs}$ ,  $2.1 \times 10^{-6} \text{ cm}^2/\text{Vs}$  and  $5.1 \times 10^{-6} \text{ cm}^2/\text{Vs}$  respectively at  $1500 \text{ (V/cm}^2)^{1/2}$  as shown in Figure 5.20. The Space-Charge-Limited Current analysis results show that the charge mobility of NPB hole transport material on ITO increases with using TDA molecule. It is the most effective one in this group.

The hole mobility of bare ITO/NPB/Al, ITO/ODA-HCl-ETOH/NPB/Al, ITO/ODA-HCl-MEOH/NPB/Al, ITO/TDA-1/NPB/Al and ITO/ODT-Cl-Si/NPB/Al were obtained  $3.1 \times 10^{-7} \text{ cm}^2/\text{Vs}$ ,  $9.3 \times 10^{-6} \text{ cm}^2/\text{Vs}$ ,  $2.8 \times 10^{-5} \text{ cm}^2/\text{Vs}$ ,  $1.4 \times 10^{-5} \text{ cm}^2/\text{Vs}$  and  $2.2 \times 10^{-5} \text{ cm}^2/\text{Vs}$  respectively at  $1500 \text{ (V/cm}^2)^{1/2}$  as shown in Figure 5.21. The Space-Charge-Limited Current analysis results indicate that the charge mobility of NPB hole transport material on ITO increases using these SAM molecules, ODA-HCl, TDA-1, ODT-Cl-Si, by far. From mobility results, it can be seen that SAM molecules modified the ITO surface and changed the surface characteristics.

### 5.3.2. Schottky Thermal Injection Results

Schottky contacts have an important role for electronic technology (Okutan et al., 2005). The device performance of Schottky diode depends on electrical and electronic characteristics of the metal/organic semiconductor junction. Therefore, electronic properties of the interface between metal and organic semiconductors are important for device application (Yakuphanoglu, 2007).

In OLEDs, electrons and holes are injected from metal contacts into an undoped organic material where they subsequently recombine to emit light. In order to achieve efficient injection, it is necessary that both the electron and hole injecting contacts have

small Schottky barriers. In this study, we demonstrate that the Schottky barrier between a metal and an organic material can be manipulated by the insertion of SAM molecules. Figure 5.22 shows the current-voltage characteristics of the ITO/Al, ITO/NPB/Al, ITO/K-27/NPB/Al, ITO/K-28/NPB/Al and ITO/K-30/NPB/Al diodes. Figure 5.23 shows the current-voltage characteristics of the ITO/MDA/NPB/Al, ITO/MHDA/NPB/Al, ITO/NPB/Al and ITO/Al diodes. Figure 5.24 shows the current-voltage characteristics of the ITO/NPB/Al, ITO/DDA/NPB/Al, ITO/TDA/NPB/Al and ITO/Al diodes. And finally, the current-voltage characteristics of the ITO/NPB/Al, ITO/ODA-HCl-ETOH/NPB/Al, ITO/ODA-HCl-MEOH/NPB/Al, ITO/TDA-1/NPB/Al, ITO/ODT-Cl-Si/NPB/Al and ITO/Al diodes are given in Figure 5.25.

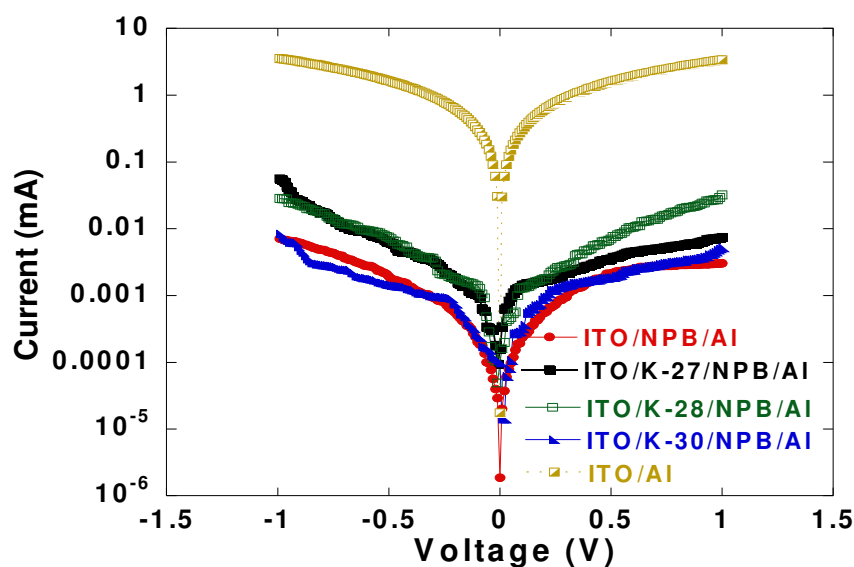


Figure 5.22. I-V characteristics of the ITO/K-27/NPB/Al, ITO/K-28/NPB/Al, ITO/K-30/NPB/Al, ITO/NPB/Al and ITO/Al Schottky diodes

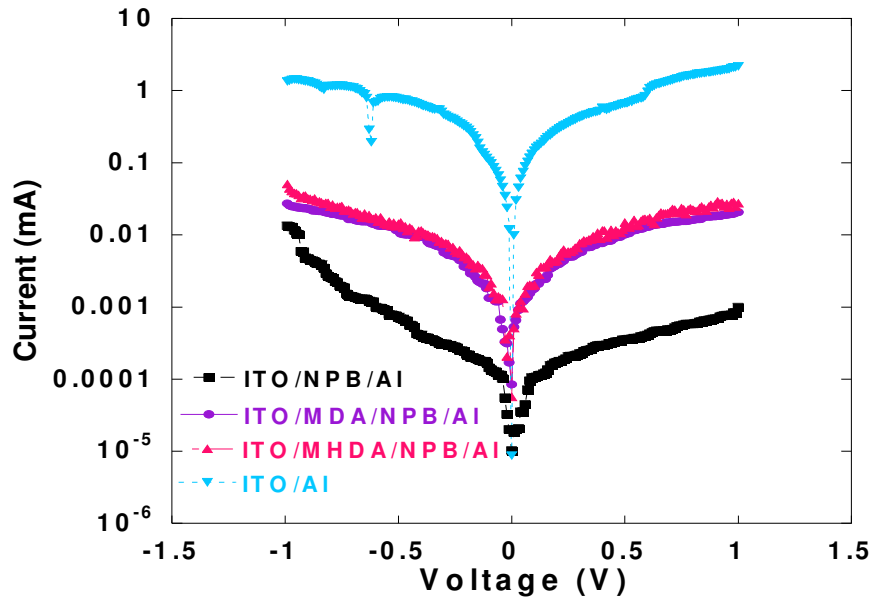


Figure 5.23. I-V characteristics of the ITO/MDA/NPB/Al, ITO/MHDA/NPB/Al, ITO/NPB/Al and ITO/Al Schottky diodes

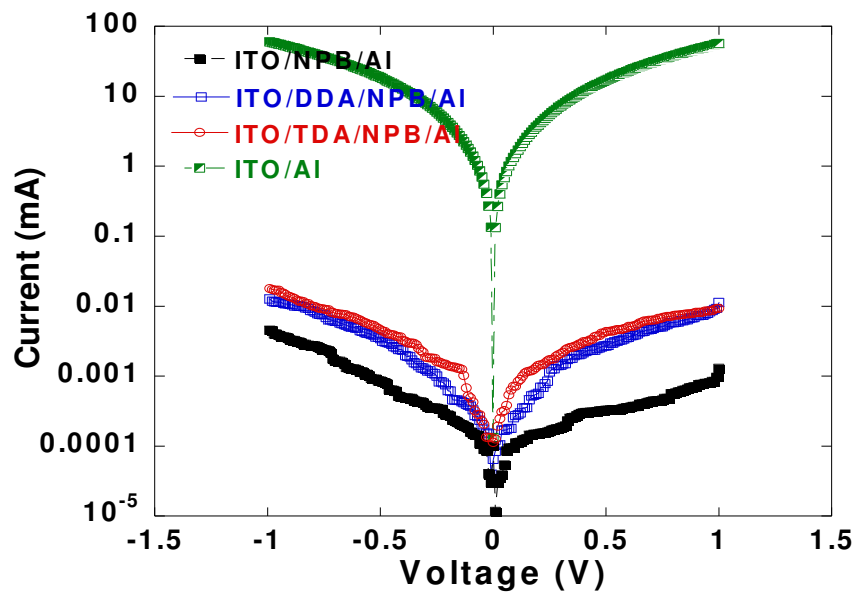


Figure 5.24. I-V characteristics of the ITO/DDA/NPB/Al, ITO/TDA/NPB/Al, ITO/NPB/Al and ITO/Al Schottky diodes



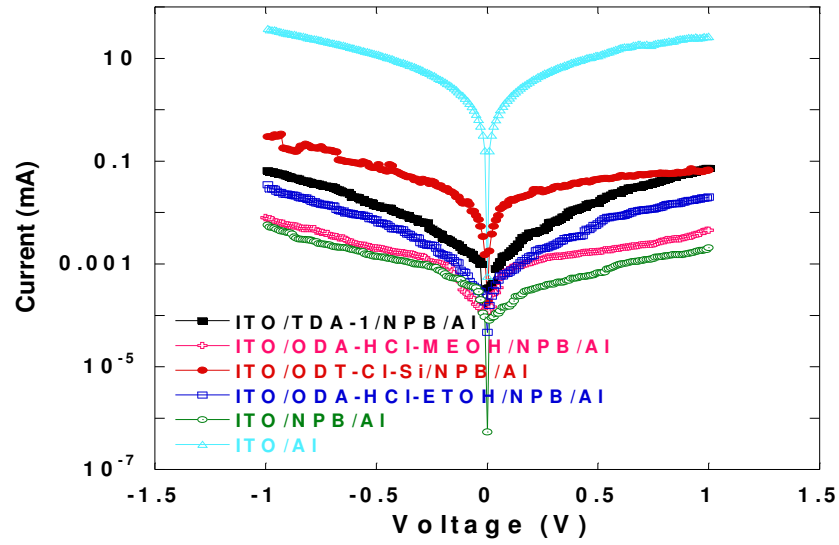


Figure 5.25. I-V characteristics of the ITO/ODA-HCl-ETOH/NPB/Al, ITO/ODA-HCl-MEOH/NPB/Al, ITO/TDA-1/NPB/Al, ITO/ODT-CI-Si/NPB/Al, ITO/NPB/Al and ITO/Al Schottky diodes

The current voltage characteristic of the diode is analyzed by the following relation (Rhoderick and Williams; Sze, 1981);

$$I = I_0 \exp\left(\frac{qV}{nkT}\right) \left[1 - \exp\left(-\frac{qV}{kT}\right)\right] \quad (5.4)$$

with

$$I_0 = AA^*T^2 \exp\left(-\frac{q\phi_B}{kT}\right) \quad (5.5)$$

where  $n$  is the ideality factor,  $k$  is the Boltzmann constant,  $q$  is the electronic charge,  $A$  is the contact area,  $A^*$  is the Richardson constant,  $T$  is the temperature and  $\phi_B$  is the barrier height. The saturation current was obtained from the intercept of the linear portion of  $\log I$  at  $V=0$ . The barrier height of these devices calculated using  $I_0$  are given in Table 5.9, Table 5.10, Table 5.11 and Table 5.12, respectively.

Table 5.9. Barrier height values of the ITO/K-27/NPB/Al, ITO/K-28/NPB/Al, ITO/K-30/NPB/Al and ITO/NPB/Al Schottky diodes

Diode	$\Phi_B$ (Barrier Height)
ITO/K-27/NPB/Al	0.465 eV
ITO/K-28/NPB/Al	0.448 eV
ITO/K-30/NPB/Al	0.458 eV
ITO/NPB/Al	0.491 eV

Table 5.10. Barrier height values of the ITO/MDA/NPB/Al, ITO/MHDA/NPB/Al and ITO/NPB/Al Schottky diodes

Diode	$\Phi_B$ (Barrier Height)
ITO/MDA/NPB/Al	0.420 eV
ITO/MHDA/NPB/Al	0.418 eV
ITO/NPB/Al	0.504 eV

Table 5.11. Barrier height values of the ITO/DDA/NPB/Al, ITO/TDA/NPB/Al and ITO/NPB/Al Schottky diodes

Diode	$\Phi_B$ (Barrier Height)
ITO/DDA/NPB/Al	0.471 eV
ITO/TDA/NPB/Al	0.443 eV
ITO/NPB/Al	0.521 eV

Table 5.12. Barrier height values of the ITO/ODA-HCl-ETOH/NPB/Al, ITO/ODA-HCl-MEOH/NPB/Al, ITO/TDA-1/NPB/Al, ITO/ODT-Cl-Si/NPB/Al and ITO/NPB/Al Schottky diodes

Diode	$\Phi_B$ (Barrier Height)
ITO/ODA-ETOH/NPB/Al	0.496 eV
ITO/ODA-MEOH/NPB/Al	0.469 eV
ITO/TDA-1/NPB/Al	0.461 eV
ITO/ODT-Cl-Si/NPB/Al	0.416 eV
ITO/NPB/Al	0.500 eV

Electronic properties of a Schottky diode depend on its barrier height. As seen in Table 5.9, it is clear that the barrier height difference between the anode ITO and the HTL material decreased using K-27, K-28 and K-30 SAM molecules. The SAM of K-28 is the most effective one to decrease barrier height in this group. For the second group of SAMs, the barrier height between the ITO/Al and ITO/NPB/Al is minimized with MHDA SAM modification the most as shown in Table 5.10. Moreover, MDA gives almost the same result as MHDA as shown in Figure 5.23. Their barrier height values are almost the same about 4.19 eV. As it can be seen from Figure 5.24, surface modification with DDA and TDA SAM molecules increases the conduction compared to ITO/NPB/Al diode. That means the barrier height decreased by SAM modification with DDA and TDA molecules as given in Table 5.11. Figure 5.23 shows the minimization of barrier height using ODA-HCl, TDA-1 and ODT-Cl-Si SAM molecules. ODT-Cl-Si is the most effective one to reduce barrier height in this group as given in Table 5.12. Based on all these results, the barrier height of ITO/Al diode is low and the barrier height of ITO/NPB/Al diode is high. The barrier heights of these devices get closer using SAM molecules, namely ITO modification. Hence, hole injection into organic NPB layer becomes easier. That means the improvement of the device performance.

### 5.3.3. Current-Voltage and Electroluminescence Characteristics

The current density vs. voltage (I-V) characteristics of the OLED devices, ITO/NPB/Alq<sub>3</sub>/Al, ITO/K-27/NPB/Alq<sub>3</sub>/Al, ITO/K-28/NPB/Alq<sub>3</sub>/Al and ITO/K-30/NPB/Alq<sub>3</sub>/Al are shown in Figure 5.26. Figure 5.27 shows the current density vs. voltage (I-V) characteristics of the OLEDs with the device configuration of ITO/NPB/Alq<sub>3</sub>/Al, ITO/MDA/NPB/Alq<sub>3</sub>/Al and ITO/MHDA/NPB/Alq<sub>3</sub>/Al. The current density vs. voltage (I-V) characteristics of the OLED devices, ITO/NPB/Alq<sub>3</sub>/Al, ITO/DDA/NPB/Alq<sub>3</sub>/Al and ITO/TDA/NPB/Alq<sub>3</sub>/Al are shown in Figure 5.28. And finally, the current density vs. voltage (I-V) characteristics of the OLEDs with the device configuration of ITO/ODA-HCl-ETOH/NPB/Alq<sub>3</sub>/Al, ITO/ODA-HCl-MEOH/NPB/Alq<sub>3</sub>/Al, ITO/TDA-1/NPB/Alq<sub>3</sub>/Al, ITO/ODT-Cl-Si/NPB/Alq<sub>3</sub>/Al and ITO/NPB/Alq<sub>3</sub>/Al are given in Figure 5.29.

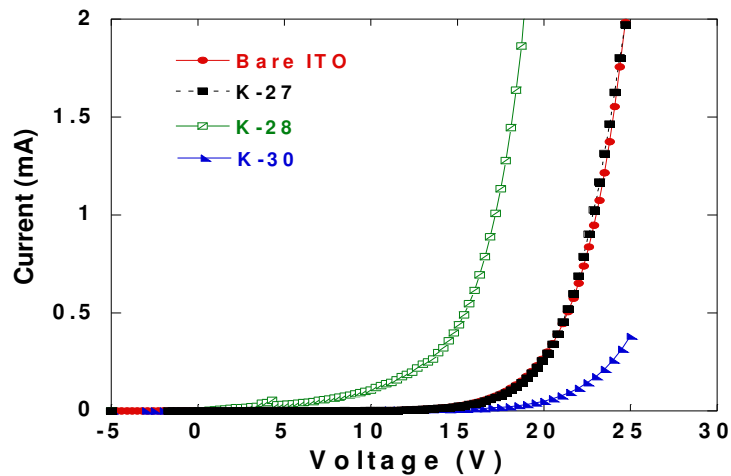


Figure 5.26. I-V characteristics for the OLED devices: ITO/K-27/NPB/Alq<sub>3</sub>/Al, ITO/K-28/NPB/Alq<sub>3</sub>/Al, ITO/K-30/NPB/Alq<sub>3</sub>/Al and ITO/NPB/Alq<sub>3</sub>/Al

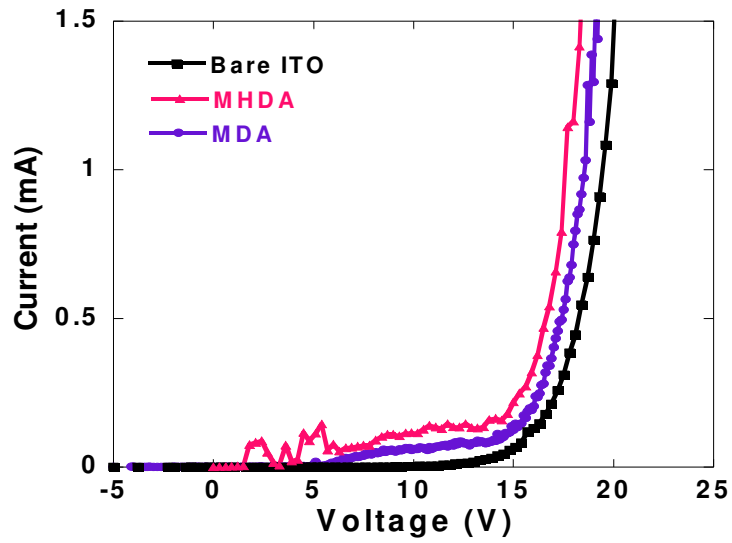


Figure 5.27. I-V characteristics for the OLED devices: ITO/MDA/NPB/Alq<sub>3</sub>/Al, ITO/MHDA/NPB/Alq<sub>3</sub>/Al and ITO/NPB/Alq<sub>3</sub>/Al

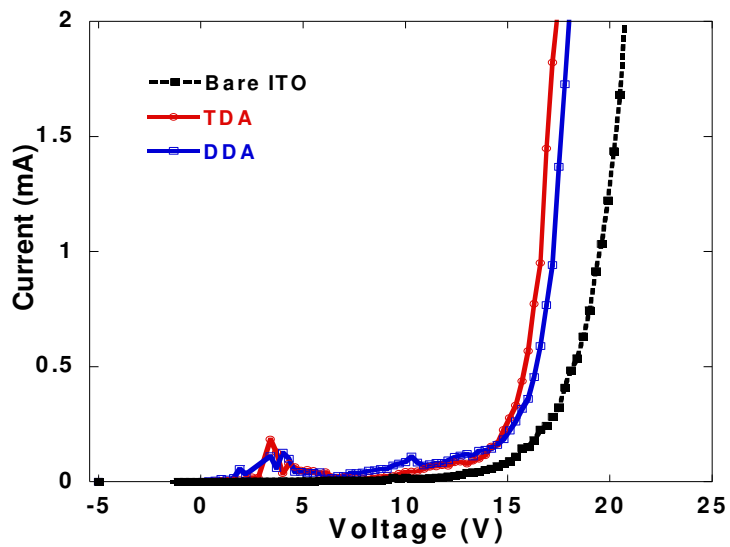


Figure 5.28. I-V characteristics for the OLED devices: ITO/DDA/NPB/Alq<sub>3</sub>/Al, ITO/TDA/NPB/Alq<sub>3</sub>/Al and ITO/NPB/Alq<sub>3</sub>/Al

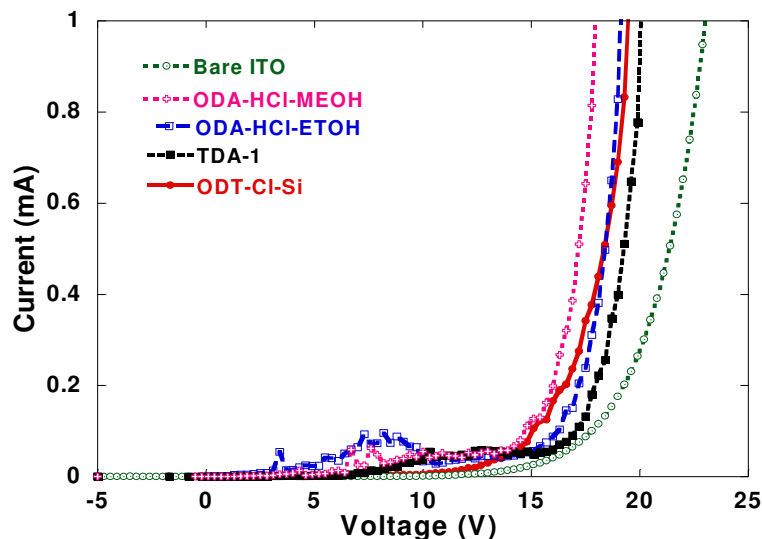


Figure 5.29. I-V characteristics for the OLED devices: ITO/ODA-HCl-ETOH/NPB/Alq<sub>3</sub>/Al, ITO/ODA-HCl-MEOH/NPB/Alq<sub>3</sub>/Al, ITO/TDA-1/NPB/Alq<sub>3</sub>/Al, ITO/ODT-CI-Si/NPB/Alq<sub>3</sub>/Al and ITO/NPB/Alq<sub>3</sub>/Al

The turn-on voltages of OLED devices are measured as 13 V (K-27), 8.2 V (K-28), 16 V (K-30) and 14.2 V (bare ITO) as shown in Figure 5.26. These results confirm the effects that hole injection is enhanced by K-27 and especially K-28 SAMs, but blocked by K-30. As seen, the turn-on voltage of K-28 modified device is significantly improved about 6 V compared to the bare device, which is may be caused due to the decrease of energy barrier for hole injection owing to the dipole moment of SO<sub>3</sub>Na. However, the turn-on voltage was increased for the K-30 modified device. The effect of K-30 SAM on the I-V characteristic is consistent with its effect on the other measurement techniques, such as SCLC and KPFM.

The turn-on voltages of OLED devices are measured as 7 V (MHDA), 9.1 V (MDA) and 13.6 V (bare ITO) as shown in Figure 5.27. The turn-on voltage for both SAMs are improved compare to the bare OLED. The effect of these two SAMs on the I-V characteristic is consistent with its effect on the other measurement techniques. Based on these results, we can say the length of SAM chain causes alteration in device operation. Logically, the short-chain SAM is expected to give better respond than the long-chain SAM because short-chain, namely short way means more hole crossing. However, our results show that the long-chain SAM, MHDA, responds better than the short-chain SAM (MDA) as shown in Figure 5.27. MHDA reduce the-turn-on voltage

about 6.6 V compare to the bare OLED and reduce 2.1 V compare to the MDA. As it is known, long-chain increases value of Van der Waals as additional molecules that mean increasing order of SAM. Therefore, these results may be associated with this situation.

The turn-on voltages of OLED devices are measured as 8.5 V (TDA), 9.1 V (DDA) and 13 V (bare ITO) as shown in Figure 5.28. The turn-on voltage for both SAMs are improved compared with the bare OLED device. The turn-on voltages of SAM modified devices with TDA and DDA are improved approximately 4 V compared to the bare device. The effect of these two SAMs on the I-V characteristic is consistent with its effect on the other measurement techniques such as SCLC model and Schottky model. The effects of these SAMs are almost same on OLED device. Especially, TDA modified device has lower turn-on voltage than bare OLED device and DDA modified device, which may be attributed to the good adhesion property, for the interface between ITO anode and NPB layer, because of the high hydrophobic property.

The turn-on voltages of OLED devices are measured as 7 V (ODA-HCl-MEOH), 9.4 V (ODA-HCl-ETOH), 9.1V (TDA-1), 8.2 V (ODT-Cl-Si) and 13 V (bare ITO) as shown in 5.29. The turn-on voltages for the both modified OLED devices with ODA-HCl, TDA-1 and ODT-Cl-Si are significantly improved approximately 5 V compared with the bare OLED device. In addition, it can be said the solvent type is important parameter for device operation based on these result (ODA-HCl). ODA-HCl solved in methanol responds better than ODA-HCl solved in ethanol.

These improvements can be explained with inelastic tunneling mechanism over extra energy levels between HOMO and LUMO of SAM molecules with  $\pi$ -conjugated structure used as tunnel barrier at the interface.

Figure 5.30 shows EL spectrum of the OLED devices with the configuration of ITO/NPB/Alq<sub>3</sub>/Al ITO/K-27/NPB/Alq<sub>3</sub>/Al, ITO/K-28/NPB/Alq<sub>3</sub>/Al and ITO/K-30/NPB/Alq<sub>3</sub>/Al. Figure 5.31 shows EL spectrum of the OLED devices with the configuration of ITO/NPB/Alq<sub>3</sub>/Al, ITO/MDA/NPB/Alq<sub>3</sub>/Al and ITO/MHDA/NPB/Alq<sub>3</sub>/Al. The EL spectrum of the OLED devices with the configuration of ITO/DDA/NPB/Alq<sub>3</sub>/Al, ITO/TDA/NPB/Alq<sub>3</sub>/Al and ITO/NPB/Alq<sub>3</sub>/Al are shown in Figure 5.32. And finally, The EL spectrum of the OLED devices with the configuration of ITO/ODA-HCl-ETOH/NPB/Alq<sub>3</sub>/Al, ITO/ODA-HCl-MEOH/NPB/Alq<sub>3</sub>/Al, ITO/TDA-1/NPB/Alq<sub>3</sub>/Al, ITO/ODT-Cl-Si/NPB/Alq<sub>3</sub>/Al and ITO/NPB/Alq<sub>3</sub>/Al are shown in Figure 5.33.

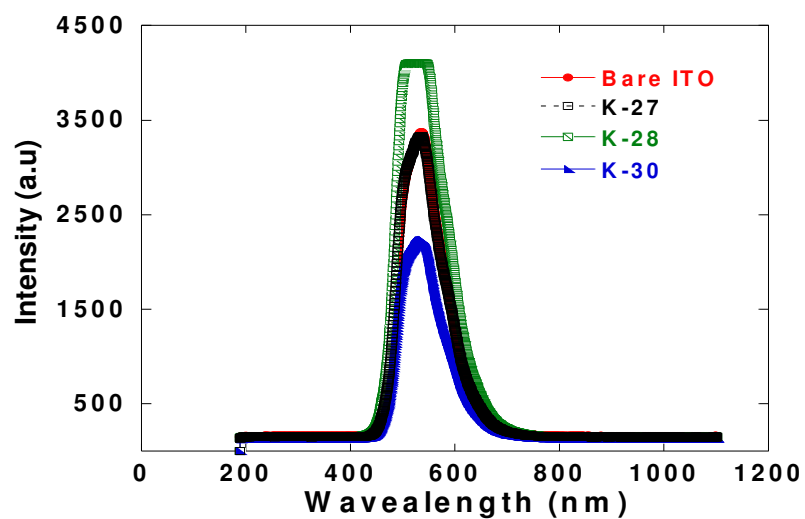


Figure 5.30. EL spectrum of the ITO/SAM (K-27, K-28 and K-30) modified or unmodified/NPB/Alq<sub>3</sub>/Al OLED devices

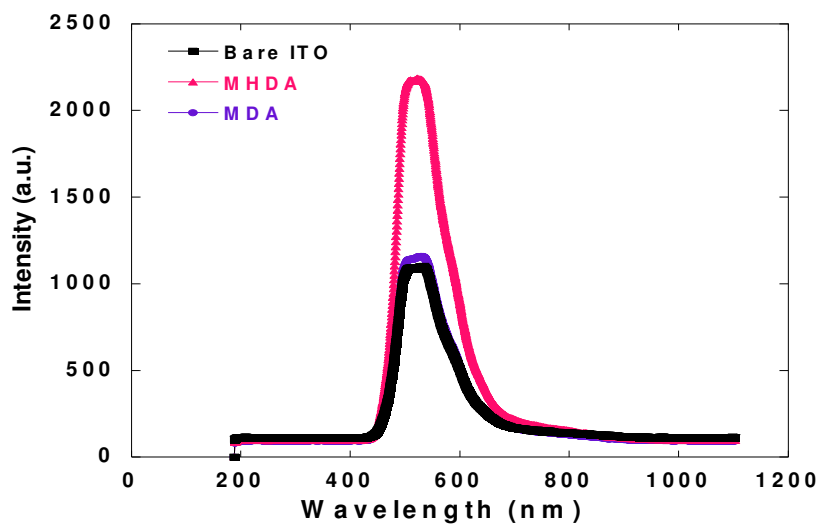


Figure 5.31. EL spectrum of the ITO/SAM (MDA and MHDA) modified or unmodified/NPB/Alq<sub>3</sub>/Al OLED devices



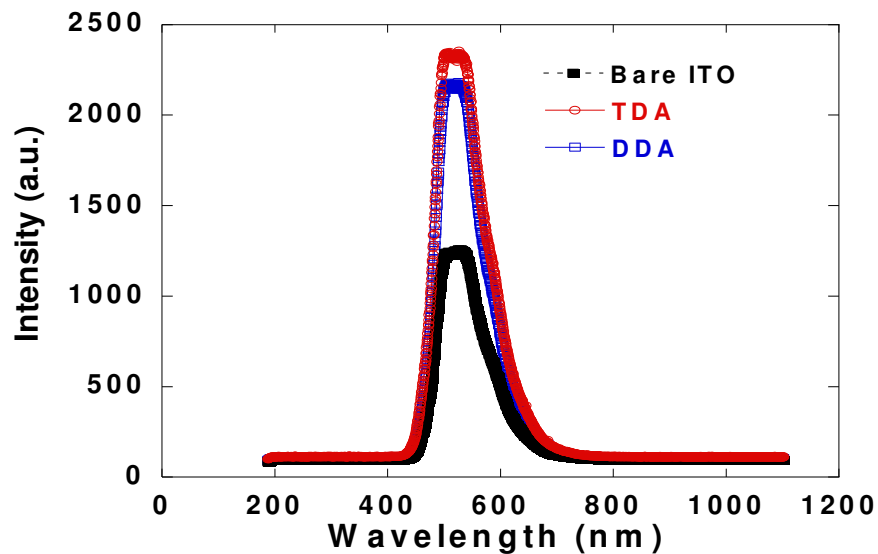


Figure 5.32. EL spectrum of the ITO/SAM (DDA and TDA) modified or unmodified/NPB/Alq<sub>3</sub>/Al OLED devices

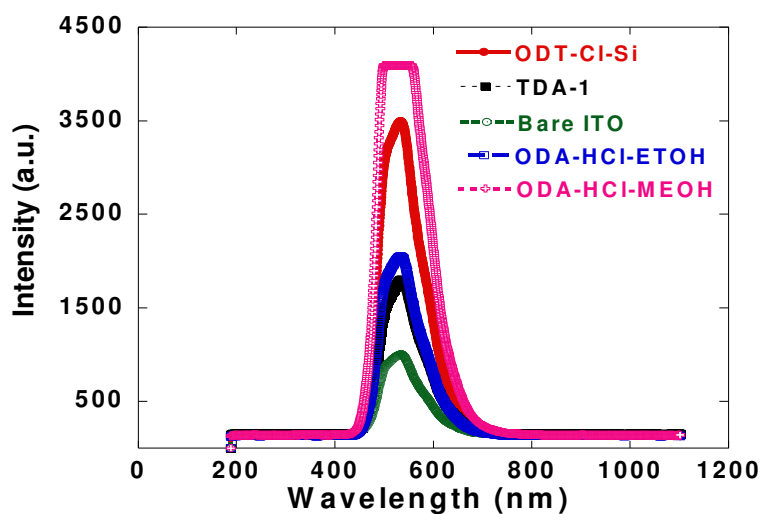


Figure 5.33. EL spectrum of the ITO/SAM (ODA-HCl-ETOH, ODA-HCl-MEOH, TDA-1 and ODT-Cl-Si) modified or unmodified/NPB/Alq<sub>3</sub>/Al OLED devices

It should be noted that all the intensity values obtained with the current of 13 mA. The all devices were radiated at the same wavelength about 530 nm due to the usage of same emissive material, namely Alq<sub>3</sub>. The intensity results of OLEDs with SAM modified ITO and OLED with bare ITO are consistent with I-V characteristic

results. That is to say, the increase in the EL intensity with the SAM modification is the result of the increase in hole injection, namely lower turn-on voltage and higher performance. ITO/K-28/NPB/Alq<sub>3</sub>/Al has an intensity 1.25 times higher than ITO/NPB/Alq<sub>3</sub>/Al as shown in Figure 5.30. In addition, the intensity value of ITO/NPB/Alq<sub>3</sub>/Al is almost same as ITO/K-27/NPB/Alq<sub>3</sub>/Al. The intensity of ITO/MHDA/NPB/Al<sub>3</sub>/Al is approximately 2 times greater than the intensity of ITO/MDA/NPB/Alq<sub>3</sub>/Al and ITO/NPB/Alq<sub>3</sub>/Al as shown in Figure 5.31. ITO/DDA/NPB/Alq<sub>3</sub>/Al and ITO/TDA/NPB/Alq<sub>3</sub>/Al have the intensity approximately 2 times higher than ITO/NPB/Alq<sub>3</sub>/Al as shown in Figure 5.32. And finally, the intensity of ITO/ODA-HCl-MEOH/NPB/Al<sub>3</sub>/Al is approximately 8 times greater than the intensity of ITO/NPB/Alq<sub>3</sub>/Al as shown in Figure 5.33.

Figure 5.34 shows the images of green OLEDs which we achieved during our study.

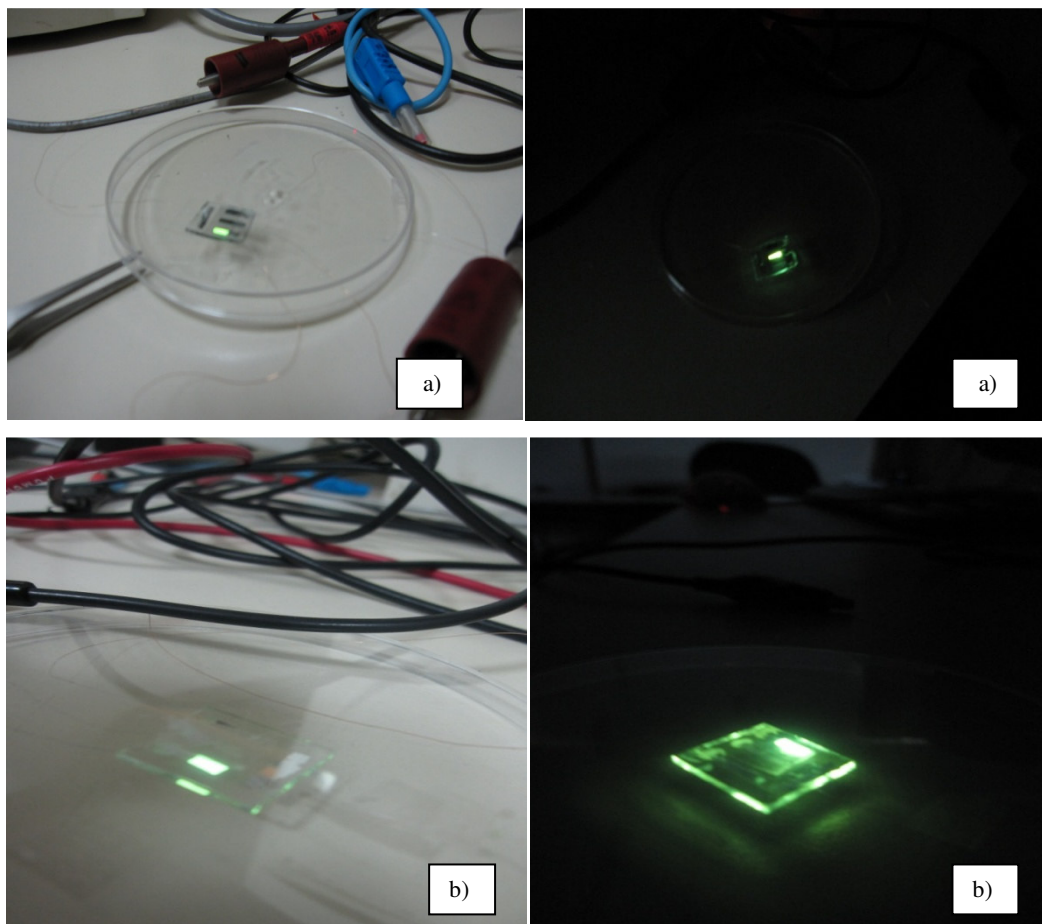


Figure 5.34. Pictures of green OLEDs in operation under the same voltages: a) ITO/NPB/Alq<sub>3</sub>/Al and b) ITO/ODT-Cl-Si/NPB/Alq<sub>3</sub>/Al

## CHAPTER 6

### CONCLUSIONS

The aim of this thesis is using different terminal function group of SAM molecules to modify the ITO surface, not only will affect the surface energy of substrates surface, but also will influence the holes injection from anode in OLED devices. For this purpose, eleven different SAM molecules are used to modify rectangular ITO substrates.

SAM molecules used in this study were classified into four different groups to analyze them easily. Ru complexes which are K-27, K-28 and K-30 are the first group. MDA and MHDA are the second group. DDA and TDA are the third group and finally ODA-HCl (ETOH), ODA-HCl (MEOH), TDA-1 and ODT-Cl-Si are taken as fourth group.

This thesis is organized in three main parts. Briefly, OLEDs, historical perspective of background theory and characterization methods for SAMs have been discussed in Chapter 2 and Chapter 3, respectively. The experimental methods involving fabrication of OLEDs and measurement techniques have been explained in Chapter 4. And finally, the main results on studied devices have been presented in Chapter 5.

After SAM formation, organics (NPB as hole transport layer and Alq<sub>3</sub> as emissive layer) and Aluminum metal cathode were coated respectively using thermal evaporation system. Then in order to obtain current-voltage (I-V) characteristics of our devices, 0.1 mm copper (Cu) lead wires were connected to electrodes by silver paint.

Using I-V characteristics, mobility and Schottky barrier height calculations were done by Space Charge Limited Current (SCLC) and Schottky Thermal Injection models, respectively. For surface characterization, Kelvin Probe Force Microscopy (KPFM) and Atomic Force Microscopy (AFM) were used.

Finally, the whole results of electrical characterization techniques can be summarized with the Table 5.13, Table 5.14, Table 5.15 and Table 5.16, respectively.

Table 5.13. Summary of electrical characterization results of first group with Ru complex

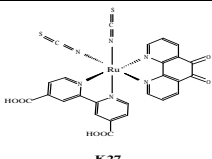
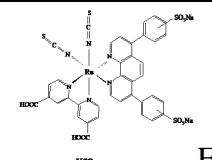
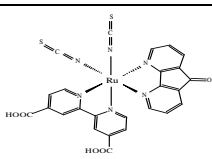
First Group	Chemical structure/Solvent	Turn-on voltage (V)	Intensity (a.u.)	Mobility (cm <sup>2</sup> /Vs) at 1500 (V/cm) <sup>1/2</sup>	Φ <sub>B</sub> Barrier height (eV)
Bare ITO		14.2	3343	4.6×10 <sup>-6</sup>	0.491
K-27	 K 27 Ethanol	13	3356	5.2×10 <sup>-6</sup>	0.465
K-28	 K 28 Ethanol	8.2	4122	2.3×10 <sup>-5</sup>	0.448
K-30	 K 30 Ethanol	16	2222	2.7×10 <sup>-6</sup>	0.458

Table 5.14. Summary of electrical characterization results of second group

Second Group	Chemical structure/Solvent	Turn-on voltage (V)	Intensity (a.u.)	Mobility (cm <sup>2</sup> /Vs) at 1600 (V/cm) <sup>1/2</sup>	Φ <sub>B</sub> Barrier height (eV)
Bare ITO		13.6	1093	2.3×10 <sup>-6</sup>	0.504
Mercaptohexadecanoic acid	$\text{HSCH}_2(\text{CH}_2)_{13}\text{CH}_2\text{COOH}$ Ethanol	7	2180	3.2×10 <sup>-5</sup>	0.418
Mercaptoundecanoic acid	$\text{HSC-CH}_2(\text{CH}_2)_{10}\text{CH}_2\text{COOH}$ Ethanol	9.1	1152	3.0×10 <sup>-6</sup>	0.420

Table 5.15. Summary of electrical characterization results of third group



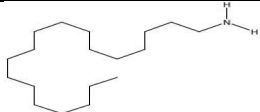
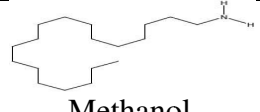
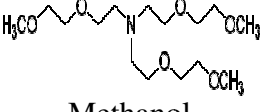
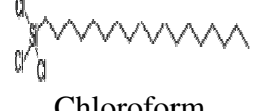
Third Group	Chemical structure/Solvent	Turn-on voltage (V)	Intensity (a.u.)	Mobility (cm <sup>2</sup> /Vs) at 1500 (V/cm) <sup>1/2</sup>	Φ <sub>B</sub> Barrier height (eV)
Bare ITO		13	1235	2.9×10 <sup>-7</sup>	0.521
1,12-Diaminododecane	 DI-Water	9.1	2141	2.1×10 <sup>-6</sup>	0.471
Tridecylamine	 Toluene	8.5	2346	5.1×10 <sup>-6</sup>	0.443

Table 5.16. Summary of electrical characterization results of fourth group

Fourth group	Chemical structure/Solvent	Turn-on voltage (V)	Intensity (a.u.)	Mobility (cm <sup>2</sup> /Vs) at 1500 (V/cm) <sup>1/2</sup>	Φ <sub>B</sub> Barrier height (eV)
Bare ITO		13	1004	3.1×10 <sup>-7</sup>	0.500
ODA-HCl	 Ethanol	9.4	2021	9.3×10 <sup>-6</sup>	0.496
ODA-HCl	 Methanol	7	4131	2.8×10 <sup>-5</sup>	0.469
TDA-1	 Methanol	9.1	1754	1.4×10 <sup>-5</sup>	0.461
ODTCISi	 Chloroform	8.2	3443	2.2×10 <sup>-5</sup>	0.416

The surface morphology of fabricated thin films was observed by AFM in tapping mode. Two dimensional topographic images show that SAM-modified ITO substrates and bare ITO have similar surface features because SAM molecules create very thin monolayer. Additionally, the surface roughness estimated from the AFM images shown differences between bare ITO and SAM-modified ITO morphologies. The results show that bare ITO has a rough surface. All SAM molecules improve the surface roughness and lead to smoother surface. Hence, the interface matching between the anode ITO and the organic HTL have been provided.

Local contact potential difference (CPD) of self-assembled monolayers on ITO substrates and bare ITO was investigated with conductive TiN tip by KPFM. The surface potential values are changed by the presence of SAM molecules. These alterations confirm the monolayer formation on the ITO surface. Except K-30, all SAM molecules are increased the surface potential of ITO. In addition, change in surface potential also means the increments in the work function of the surface. As a result of this, Fermi level of the ITO surface approaches to the HOMO level of the organic layer NPB with SAM modification. Therefore, carrier injection enhanced with decreasing the barrier.

J-V characteristics show two distinct regions at low and high biases such as Schottky thermionic region and SCLC region. At high voltages, J-V characteristics switch to the SCLC. For the electrical characterization, first of all, fabricated organic diodes with the configuration of ITO/SAM (K-27, K-28, K-30, MDA, MHDA, DDA, TDA, ODA-HCl, TDA-1, ODT-Cl-Si)/NPB/Al and ITO/NPB/Al were investigated. To analyze the Schottky barrier characteristics, the organic diodes were examined between -1V and +1V. Electronic properties of Schottky diode depends on its barrier height. Thus, the required calculations were done to determine the Schottky barrier characteristics of organic diodes. Schottky characteristic results show that the barrier height difference between the ITO anode and organic HTL was reduced using SAM molecules, namely ITO modification. The barrier height of bare ITO/NPB/Al, ITO/K-27/NPB/Al, ITO/K-28/NPB/Al and ITO/K-30/NPB/Al were obtained 0.491eV, 0.465eV, 0.448eV and 0.458eV respectively. The barrier height of ITO/NPB/Al, ITO/MDA/NPB/Al and ITO/MHDA/NPB/Al diodes were obtained as 0.500eV, 0.420eV and 0.418eV respectively. The barrier height of bare ITO/NPB/Al,



ITO/DDA/NPB/Al and ITO/TDA/NPB/Al were obtained 0.521eV, 0.471eV and 0.443eV respectively. And finally, the barrier height of bare ITO/NPB/Al, ITO/ODA-HCl-ETOH/NPB/Al, ITO/ODA-HCl-MEOH/NPB/Al, ITO/TDA-1/NPB/Al and ITO/ODT-Cl-Si/NPB/Al were obtained 0.500eV, 0.496eV, 0.469eV, 0.461eV and 0.416eV respectively. SCLC model have been used to evaluate carrier mobility under steady state of current in an organic layer. At high voltages, the carriers eventually fill up all the trap states in the organic film and the device operates in SCLC conduction regime. Hence, the I-V measurements were carried out between -12V and +12V. The SCLC analysis results indicate that the charge mobility of NPB hole transport material on ITO increases using SAM molecules. The hole mobilities of bare ITO/NPB/Al, ITO/K-27/NPB/Al, ITO/K-28/NPB/Al and ITO/K-30/NPB/Al were obtained  $4.6 \times 10^{-6}$  cm<sup>2</sup>/Vs,  $5.2 \times 10^{-6}$  cm<sup>2</sup>/Vs,  $2.3 \times 10^{-5}$  cm<sup>2</sup>/Vs and  $2.7 \times 10^{-6}$  cm<sup>2</sup>/Vs at  $1500 \text{ (V/cm}^2\text{)}^{1/2}$  respectively. The hole mobilities of ITO/NPB/Al, ITO/MDA/NPB/Al and ITO/MHDA/NPB/Al diodes were obtained as  $3.0 \times 10^{-6}$  cm<sup>2</sup>/Vs,  $3.2 \times 10^{-5}$  cm<sup>2</sup>/Vs and  $2.3 \times 10^{-6}$  cm<sup>2</sup>/Vs at  $1600 \text{ (V/cm}^2\text{)}^{1/2}$  respectively. The hole mobility of bare ITO/NPB/Al, ITO/DDA/NPB/Al and ITO/TDA/NPB/Al were obtained  $2.9 \times 10^{-7}$  cm<sup>2</sup>/Vs,  $2.1 \times 10^{-6}$  cm<sup>2</sup>/Vs and  $5.1 \times 10^{-6}$  cm<sup>2</sup>/Vs respectively at  $1500 \text{ (V/cm}^2\text{)}^{1/2}$ . And finally, the hole mobility of bare ITO/NPB/Al, ITO/ODA-HCl-ETOH/NPB/Al, ITO/ODA-HCl-MEOH/NPB/Al, ITO/TDA-1/NPB/Al and ITO/ODT-Cl-Si/NPB/Al were obtained  $3.1 \times 10^{-7}$  cm<sup>2</sup>/Vs,  $9.3 \times 10^{-6}$  cm<sup>2</sup>/Vs,  $2.8 \times 10^{-5}$  cm<sup>2</sup>/Vs,  $1.4 \times 10^{-5}$  cm<sup>2</sup>/Vs and  $2.2 \times 10^{-5}$  cm<sup>2</sup>/Vs respectively at  $1500 \text{ (V/cm}^2\text{)}^{1/2}$ . That means the charge injection from anode to the organic layer increased. Therefore, the surface characteristics of the devices are changed.

Finally, OLED devices with the configuration of ITO/SAM (K-27, K-28, K-30, MDA, MHDA, DDA, TDA, ODA-HCl, TDA-1, ODT-Cl-Si)/NPB/Alq<sub>3</sub>/Al and ITO/NPB/Alq<sub>3</sub>/Al were analyzed. Additionally, the effect of solvent type and length of chain of SAM were investigated. I-V results show that the turn-on voltages of OLEDs reduce using SAM molecules, except K-30. These improvements may be caused due to the decrease of energy barrier for hole injection owing to the dipole moment of molecules or may be attributed to the good adhesion property between the ITO and NBP layer.

In conclusion, using self-assembly monolayer, the ITO surfaces were modified. All of the SAMs except K-30 have enhanced the charge injection in OLED devices and

lowered threshold voltage of charge injection and so applying SAM modification on ITO surface has improved the interfacial contact between the electrode and organic layer. These improvements can be explained with inelastic tunneling mechanism over extra energy levels between HOMO and LUMO of SAM molecules used as tunnel barrier at the interface.

## REFERENCES

- Abkowitz, M., I. Chen, and J.H. Sharp. 1968. Electron Spin Resonance of the Organic Semiconductor, Copper Phthalocyanine. *The Journal of Chemical Physics*. 48:4561.
- Appleyard, S.F.J., S.R. Day, R.D. Pickford, and M.R. Willis. 1999. Organic electroluminescent devices: enhanced carrier injection using SAM derivatized ITO electrodes. *J. Mater. Chem.* 10:169-173.
- Aratani, S., C. Zhang, K. Pakbaz, S. Höger, F. Wudl, and A. Heeger. 1993. Improved efficiency in polymer light-emitting diodes using air-stable electrodes. *Journal of electronic materials*. 22:745-749.
- Bardsley, J.N. 2004. International OLED technology roadmap. *Selected Topics in Quantum Electronics, IEEE Journal of.* 10:3-9.
- Berlin, A., G. Zotti, G. Schianon, and S. Zecchin. 1998. *Journal American Chemical Society*. 120:13453.
- Bernanose, A., M. Comte, and P. Vouaux. 1953. A new method of emission of light by certain organic compounds. *Journal of Chemical Physics*. 50:64-68.
- Bröms, P., J. Birgersson, N. Johansson, M. Lögdlund, and W. Salaneck. 1995. Calcium electrodes in polymer LEDs. *Synthetic metals*. 74:179-181.
- Bruner, E.L., N. Koch, R. Amelia, S.L. Bernasek, A. Kahn, and J. Schwartz. 2002. Controlling the work function of indium tin oxide: differentiating dipolar from local surface effects. *Journal of the American Chemical Society*. 124:3192-3193.
- Bulovic, V., and J.J. Yu. 2008. Improving OLED technology for displays. Massachusetts Institute of Technology.
- Burroughes, J., D. Bradley, A. Brown, R. Marks, K. Mackay, R. Friend, P. Burns, and A. Holmes. 1990. Light-emitting diodes based on conjugated polymers. *Nature*. 347:539-541.
- Burrows, P., Z. Shen, V. Bulovic, D. McCarty, S. Forrest, J. Cronin, and M. Thompson. 1996. Relationship between electroluminescence and current transport in organic heterojunction light emitting devices. *Journal of Applied Physics*. 79:7991-8006.
- Carpick, R.W., and M. Salmeron. 1997. Scratching the surface: Fundamental investigations of tribology with atomic force microscopy. *Chemical reviews*. 97:1163-1194.
- Carrard, M., S. Goncalves-Conto, L. Si-Ahmed, D. Ades, and A. Siove. 1999. Improved stability of interfaces in organic light emitting diodes with high Tg materials and self-assembled monolayers. *Thin Solid Films*. 352:189-194.

- Chen, C.H., J. Shi, and C.W. Tang. 1997. Organic electroluminescent materials and devices *Macromolecular Symposia*. 125.
- Choi, B., J. Rhee, and H.H. Lee. 2001. Tailoring of self-assembled monolayer for polymer light-emitting diodes. *Applied Physics Letters*. 79:2109.
- Chong, L.W., Y.L. Lee, and T.C. Wen. 2007. Surface modification of indium tin oxide anodes by self-assembly monolayers: Effects on interfacial morphology and charge injection in organic light-emitting diodes. *Thin Solid Films*. 515:2833-2841.
- Chu, T.Y., and O.K. Song. 2007. Hole mobility of N, N-bis (naphthalen-1-yl)-N, N-bis (phenyl) benzidine investigated by using space-charge-limited currents. *Applied Physics Letters*. 90:203512.
- Cui, J., Q. Huang, J.G.C. Veinot, H. Yan, and T.J. Marks. 2002. Interfacial Microstructure Function in Organic Light Emitting Diodes: Assembled Tetraaryldiamine and Copper Phthalocyanine Interlayers. *Advanced materials*. 14:565-569.
- Deiries, S., A. Silber, O. Iwert, E. Hummel, and J.L. Lizon. 2005. Plasma Cleaning, A New Method of Ultra-Cleaning Detector Cryostats. *Astrophysics and Space Since Library, Springer*.
- Deng, Z., S. Lee, D. Webb, Y. Chan, and W. Gambling. 1999. Carrier transport in thin films of organic electroluminescent materials. *Synthetic metals*. 107:107-109.
- Diao, P., M. Guo, and R. Tong. 2001. Characterization of defects in the formation process of self-assembled thiol monolayers by electrochemical impedance spectroscopy. *Journal of Electroanalytical Chemistry*. 495:98-105.
- Dimitrakopoulos, C.D., and P.R.L. Malenfant. 2002. Organic thin film transistors for large area electronics. *Advanced materials*. 14:99.
- Forrest, S.R., D.D.C. Bradley, and M.E. Thompson. 2003. Measuring the Efficiency of Organic Light Emitting Devices. *Advanced materials*. 15:1043-1048.
- Forsythe, E., D. Morton, C. Tang, and Y. Gao. 1998. Trap states of tris-8-(hydroxyquinoline) aluminum and naphthyl-substituted benzidine derivative using thermally stimulated luminescence. *Applied Physics Letters*. 73:1457.
- Freeman Jr, D.C., and C.E. White. 1956. The Structure and Characteristics of the Fluorescent Metal Chelates of o, o'-Dihydroxyazo Compounds1. *Journal of the American Chemical Society*. 78:2678-2682.
- Geffroy, B., P. le Roy, and C. Prat. 2006. Organic light-emitting diode (OLED) technology: materials, devices and display technologies. *Polymer International*. 55:572-582.

- Godlewski, J., and M. Obarowska. 2007. Organic light emitting devices. *Opto-Electronics Review*. 15:179-183.
- Greenham, N.C., R.H. Friend, and D.D.C. Bradley. 1994. Angular Dependence of the Emission from a Conjugated Polymer Light Emitting Diode: Implications for efficiency calculations. *Advanced materials*. 6:491-494.
- Gül, S., and S. Okur. 2006. Development of nanopatterns on self assembled monolayer (sam) organic films using scanning probe microscope (spm) nanolithography technique.
- Haddock, N., B. Domercq, and B. Kippelen. 2005. High mobility C60 organic field-effect transistors. *Electronics Letters*. 41:444-446.
- Hartman, W.A., and H.L. Armstrong. 1967. Electroluminescence in organic polymers. *Journal of Applied Physics* 38: 2393-2395
- Hatton, R.A., S.R. Day, M.A. Chesters, and M.R. Willis. 2001. Organic electroluminescent devices: enhanced carrier injection using an organosilane self assembled monolayer (SAM) derivatized ITO electrode. *Thin Solid Films*. 394:291-296.
- Hayashi, S., H. Etoh, and S. Saito. 1986. Electroluminescence of perylene films with a conducting polymer as an anode. *Japanese journal of applied physics*. 25:L773-L775.
- He, G., M. Pfeiffer, K. Leo, M. Hofmann, J. Birnstock, R. Pudzich, and J. Salbeck. 2004. High-efficiency and low-voltage p-i-n electrophosphorescent organic light-emitting diodes with double-emission layers *Applied Physics Letters*. 85:3911-3913.
- Huang, Q., J. Cui, J.G.C. Veinot, H. Yan, and T.J. Marks. 2003. Realization of high-efficiency/high-luminance small-molecule organic light-emitting diodes: synergistic effects of siloxane anode functionalization/hole-injection layers, and hole/exciton-blocking/electron-transport layers. *Applied Physics Letters*. 82:331-333.
- Huang, Q., J. Cui, H. Yan, J.G.C. Veinot, and T.J. Marks. 2002. Small molecule organic light-emitting diodes can exhibit high performance without conventional hole transport layers. *Applied Physics Letters*. 81:3528.
- Ishii, H., K. Sugiyama, E. Ito, and K. Seki. 1999. Energy level alignment and interfacial electronic structures at organic/metal and organic/organic interfaces. *Advanced materials*. 11:605-625.
- Ivanisevic, A., and C.A. Mirkin. 2001. "Dip-Pen" Nanolithography on Semiconductor Surfaces. *Journal of the American Chemical Society*. 123:7887-7889.

- Jee, S.H., S.H. Kim, J.H. Ko, and Y.S. Yoon. 2006. Study on Work Function Change of ITO Modified by Using a Self-Assembled Monolayer for Organic based Devices. *Journal of the Korean Physical Society*. 49:2034-2039.
- Kalinowski, J., and J. Godlewski. 1975. Magnetic field effects on recombination radiation in tetracene crystal\* 1. *Chemical Physics Letters*. 36:345-348.
- Kalinowski, J., J. Godlewski, and R. Signerski. 1983. AC modulation of the recombination electroluminescence in anthracene single crystal. *Applied Physics A: Materials Science & Processing*. 31:215-220.
- Kao, K.C., and W. Hwang. 1981. Electrical transport in solids. Pergamon Press.
- Kelley, T.W., P.F. Baude, C. Gerlach, D.E. Ender, D. Muyres, M.A. Haase, D.E. Vogel, and S.D. Theiss. 2004. Recent progress in organic electronics: Materials, devices, and processes. *Chemistry of materials*. 16:4413-4422.
- Kepler, R.G., P.M. Beeson, S.J. Jacobs, R.A. Anderson, M.B. Sindair, V.S. Valencia, and P.A. Cahill. 1995. Electron and hole mobility in tris(8-hydroxyquinolinolato)-N1,O8) aluminum. *Applied Physics Letters*. 66.
- Khan, M., W. Xu, Y. Bai, X. Jiang, Z. Zhang, and W. Zhu. 2008. Electron mobility of 4, 7-diphenyl-1, 10-phenanthroline estimated by using space-charge-limited currents. *Journal of Applied Physics*. 103:014509.
- Kido, J., K. Nagai, and Y. Ohashi. 1990. Electroluminescence in a terbium complex. *Chemistry Letters*. 19:657-660.
- Kim, J., M. Granström, R. Friend, N. Johansson, W. Salaneck, R. Daik, W. Feast, and F. Cacialli. 1998. Indium-tin oxide treatments for single-and double-layer polymeric light-emitting diodes: The relation between the anode physical, chemical, and morphological properties and the device performance. *Journal of Applied Physics*. 84:6859.
- Kippelen, B., and J.L. Brédas. 2009. Organic photovoltaics. *Energy Environ. Sci*. 2:251-261.
- Koide, Y., Q. Wang, J. Cui, D.D. Benson, and T.J. Marks. 2000. Patterned Luminescence of Organic Light-Emitting Diodes by Hot Microcontact Printing (H CP) of Self-Assembled Monolayers. *Journal of the American Chemical Society*. 122:11266-11267.
- Lee, J., B.J. Jung, J.I. Lee, H.Y. Chu, L.M. Do, and H.K. Shim. 2002. Modification of an ITO anode with a hole-transporting SAM for improved OLED device characteristics. *Journal of Materials Chemistry*. 12:3494-3498.
- Lian, J., Y. Yuan, L. Cao, J. Zhang, H. Pang, Y. Zhou, and X. Zhou. 2007. Improved efficiency in OLEDs with a thin Alq<sub>3</sub> interlayer. *Journal of luminescence*. 122:660-662.

- Love, J.C., L.A. Estroff, J.K. Kriebel, R.G. Nuzzo, and G.M. Whitesides. 2005. Self-assembled monolayers of thiolates on metals as a form of nanotechnology. *Chemical reviews*. 105:1103-1170.
- Lu, H.T., and M. Yokoyama. 2004. Plasma preparation on indium-tin-oxide anode surface for organic light emitting diodes. *Journal of Crystal Growth*. 260:186-190.
- Maboudian, R., and R.T. Howe. 1997. Critical review: adhesion in surface micromechanical structures. *Journal of Vacuum Science & Technology B: Microelectronics and Nanometer Structures*. 15:1.
- Malinsky, J.E., G.E. Jabbour, S.E. Shaheen, J.D. Anderson, A.G. Richter, T.J. Marks, N.R. Armstrong, B. Kippelen, P. Dutta, and N. Peyghambarian. 1999. Self Assembly Processes for Organic LED Electrode Passivation and Charge Injection Balance. *Advanced materials*. 11:227-231.
- Malliaras, G., J. Salem, P. Brock, and C. Scott. 1998. Electrical characteristics and efficiency of single-layer organic light-emitting diodes. *Physical Review B*. 58:13411-13414.
- Meng, H. 2007. Organic light-emitting materials and devices. CRC.
- Mitschke, U., and P. Bäuerle. 2000. The electroluminescence of organic materials. *J. Mater. Chem*. 10:1471-1507.
- Mott, N.F., and R.W. Gurney. 1940. Electronic Processes in Ionic Crystals. *Oxford University Press*.
- Mu, H. 2007. Carriers injection and transport in small molecule organic light emitting diodes(OLED).
- Murgatroyd, P. 1970. Theory of space-charge-limited current enhanced by Frenkel effect. *Journal of Physics D: Applied Physics*. 3:151.
- Nonnenmacher, M., M.P. O'Boyle, and H.K. Wickramasinghe. 1991. Kelvin probe force microscopy. *Applied Physics Letters*. 58:2921.
- Nuzzo, R.G., and D.L. Allara. 1983. Adsorption of bifunctional organic disulfides on gold surfaces. *Journal of the American Chemical Society*. 105:4481-4483.
- Ocakoglu, K., C. Zafer, B. Cetinkaya, and S. Icli. 2007. Synthesis, characterization, electrochemical and spectroscopic studies of two new heteroleptic Ru (II) polypyridyl complexes. *Dyes and pigments*. 75:385-394.
- Okutan, M., E. Basaran, and F. Yakuphanoglu. 2005. Electronic and interface state density distribution properties of Ag/p-Si Schottky diode. *Applied surface science*. 252:1966-1973.

- Oxtoby, D.W., W.A. Freeman, and T.F. Block. 1998. Chemistry: Science of change. Saunders College Pub.
- Patel, N., S. Cina, and J. Burroughes. 2002. High-efficiency organic light-emitting diodes. *Selected Topics in Quantum Electronics, IEEE Journal of.* 8:346-361.
- Pauli, W. 1947. Exclusion principle and quantum mechanics. Éds. du Griffon.
- Pfeiffer, M., K. Leo, X. Zhou, J. Huang, M. Hofmann, A. Werner, and J. Blochwitz-Nimoth. 2003. Doped organic semiconductors: Physics and application in light emitting diodes. *Organic Electronics.* 4:89-103.
- Pope, M., H. Kallmann, and P. Magnante. 1963. Electroluminescence in organic crystals. *Journal of Chemical Physics.* 38:2042-2043.
- Pope, M., and C.E. Swenberg. 1999. Electronic processes in organic crystals and polymers. Oxford University Press New York.
- Poulsen, D.A. 2011. Functional polymer architectures for solution processed organic light emitting diodes. UNIVERSITY OF CALIFORNIA, BERKELEY.
- Rhoderick, E., and R. Williams. Metal-Semiconductor Contacts, (Clarendon, Oxford, 1988). *Appendix E:226-231.*
- Sberveglieri, G., P. Benussi, G. Coccoli, S. Groppelli, and P. Nelli. 1990. Reactively sputtered indium tin oxide polycrystalline thin films as NO and NO<sub>2</sub> gas sensors. *Thin Solid Films.* 186:349-360.
- Schaffel, M., A. Hunze, J. Birnstock, J. Blassing, W. Rogler, G. Wittmann, and A. Winnacker. 2001. *Proc. Eur. Conf. on Organic Electronics:158-160.*
- Schreiber, F. 2000. Structure and growth of self-assembling monolayers. *Progress in surface science.* 65:151-257.
- Schwartz, J., E.L. Bruner, N. Koch, A.R. Span, S.L. Bernasek, and A. Kahn. 2003. Controlling the work function of indium tin oxide: differentiating dipolar from local surface effects. *Synthetic metals.* 138:223-227.
- Selamet, Y., and Ö. Tuna. 2009. Applications of transparent conductive indium tin oxide films in automotive and vitrifications industries.
- Shinar, J. 2004. Organic light-emitting devices: a survey. Springer Verlag.
- Shipway, A., M. Lahav, and I. Willner. 2000. Nanostructured gold colloid electrodes. *Advanced materials.* 12:993-998.
- Shirakawa, H., E.J. Louis, A.G. MacDiarmid, C.K. Chiang, and A.J. Heeger. 1977. Synthesis of electrically conducting organic polymers: halogen derivatives of polyacetylene,(CH)<sub>x</sub>. *Journal of the Chemical Society, Chemical Communications.* 1977:578-580.



- Stolka, M., J. Yanus, and D. Pai. 1984. Hole transport in solid solutions of a diamine in polycarbonate. *The Journal of Physical Chemistry*. 88:4707-4714.
- Subramanian, V., E. Wolf, and P.V. Kamat. 2001. Semiconductor-metal composite nanostructures. To what extent do metal nanoparticles improve the photocatalytic activity of TiO<sub>2</sub> films? *The Journal of Physical Chemistry B*. 105:11439-11446.
- Sutcu, S.M. 2010. The effects of ITO surface modification on lifetime in organic photovoltaic devices and a test setup for measuring lifetime.
- Sze, S. 1981. *Physics of semiconductor devices*. 1981. Wiley, New York.
- Tamada, K., J. Nagasawa, F. Nakanishi, K. Abe, M. Hara, W. Knoll, T. Ishida, H. Fukushima, S. Miyashita, and T. Usui. 1998. Structure of SAMs generated from functionalized thiols on gold. *Thin Solid Films*. 327:150-155.
- Ulman, A. 1991. *An introduction to ultrathin organic films: from Langmuir-Blodgett to self-assembly*. Academic Press New York.
- Ulman, A. 1996. Formation and structure of self-assembled monolayers. *Chemical reviews*. 96:1533-1554.
- Ulman, A. 1998. *Self-assembled monolayers of thiols*. Academic Pr.
- Uvu, Utah Valley University, Organic Chemistry, Hybridization, <http://science.uvu.edu/ochem/index.php/alphabetical/g-h/hybridization/>, 2011
- VanSlyke, S., and C. Tang. 1987. Organic electroluminescent diodes. *Appl. Phys. Lett.* 51:913.
- Vincett, P., W. Barlow, R. Hann, and G. Roberts. 1982. Electrical conduction and low voltage blue electroluminescence in vacuum-deposited organic films. *Thin Solid Films*. 94:171-183.
- Vyavahare, O. 2009. *Fabrication and Characterization of Organic Light Emitting Diodes for Display Applications*. Rochester Institute of Technology.
- Weill, A. 1986. In: Kelly MJ, Weisbuch C (eds) *The Physics and Fabrication of Microstructures and Microdevices*. Springer Verlag Berlin, Heidelberg, New York.
- Werner, A., J. Blochwitz, M. Pfeiffer, and K. Leo. 2001. Field dependence of thermally stimulated currents in Alq. *Journal of Applied Physics*. 90:123.
- Wong, W.Y. 2009. Challenges in organometallic research-Great opportunity for solar cells and OLEDs. *Journal of Organometallic Chemistry*. 694:2644-2647.
- Wu, C., C. Wu, J. Sturm, and A. Kahn. 1997. Surface modification of indium tin oxide by plasma treatment: An effective method to improve the efficiency, brightness,

and reliability of organic light emitting devices. *Applied Physics Letters*. 70:1348.

Xu, X., G. Yu, Y. Liu, and D. Zhu. 2006. Electrode modification in organic light-emitting diodes. *Displays*. 27:24-34.

Yakuphanoglu, F. 2007. Electrical characterization and interface state density properties of the ITO/C70/Au Schottky diode. *The Journal of Physical Chemistry C*. 111:1505-1507.

Yan, H., P. Lee, N.R. Armstrong, A. Graham, G.A. Evmenenko, P. Dutta, and T.J. Marks. 2005. High-performance hole-transport layers for polymer light-emitting diodes. Implementation of organosiloxane cross-linking chemistry in polymeric electroluminescent devices. *Journal of the American Chemical Society*. 127:3172-3183.

Zhu, L., H. Tang, Y. Harima, K. Yamashita, Y. Aso, and T. Otsubo. 2002. Enhanced hole injection in organic light-emitting diodes consisting of self-assembled monolayer of tripod-shaped  $\pi$ -conjugated thiols. *J. Mater. Chem.* 12:2250-2254.